

COLLISION FREE AUTONOMOUS NAVIGATION AND  
FORMATION BUILDING FOR NON-HOLONOMIC GROUND  
ROBOTS

Chao Wang

## Abstract

The primary objective of a safe navigation algorithm is to guide the object from its current position to the target position while avoiding any collision with the en-route obstacles, and the appropriate obstacle avoidance strategies are the key factors to ensure safe navigation tasks in dynamic environments. The basic requirement for an appropriate obstacle avoidance strategy is to sense or detect obstacles and make proper decisions when the obstacles are nearby. By fulfilling the basic requirement, the more advanced obstacle algorithms should have other additional features.

In this report, three different obstacle avoidance strategies for safe navigation in dynamic environments have been presented. All of them are applicable in the non-holonomic systems by which motions of many objects can be described. The biologically-inspired navigation algorithm (BINA) is efficient in terms of avoidance time, it is also simple and easy to compute. The equidistant based navigation algorithm (ENA) is able to achieve navigation task with in uncertain dynamic environments, and it is suitable for a variety of situations due to its flexibility. The navigation algorithm based on an integrated environment representation (NAIER) allows the object to seek a safe path through obstacles in unknown dynamic environment in a human-like fashion and it is very efficient in numerous particular scenarios where other algorithm are found inefficient or even impossible to solve. The performances and features of the proposed navigation algorithms are confirmed by extensive simulation results and experiments with a real non-holonomic mobile robot. Furthermore, the performance of these algorithms are compared with each other in various aspects.

The algorithms have been implemented on two real control systems: intelligent wheelchair and robotic hospital bed. The performance of the proposed algorithms with SAM and Flexbed demonstrate their capabilities to achieve navigation tasks in complicated real time scenarios. The proposed algorithms are easy to be implemented in real time and costly efficient.

An extra study on networked multi-robots formation building algorithm is pre-

sented in this paper. A constructive and easy-to-implement decentralised control is proposed for a formation building of a group of random positioned objects. Furthermore, the problem of formation building with anonymous objects is addressed. This randomised decentralised navigation algorithm achieves the convergence to a desired configuration with probability 1.

# Contents

<b>Contents</b>	<b>iii</b>
<b>List of Figures</b>	<b>vii</b>
<b>List of Tables</b>	<b>xiii</b>
<b>1 Introduction</b>	<b>1</b>
1.1 Obstacle Avoidance Strategies for Safe Navigation Algorithm . . . . .	3
1.1.1 BUG Algorithms . . . . .	4
1.1.2 Model Predictive Control . . . . .	5
1.1.3 Velocity Obstacle Approach . . . . .	6
1.1.4 Other Navigation Algorithms . . . . .	7
1.2 Formation Building Control Strategies . . . . .	8
1.3 Main Contributions of This report . . . . .	10
1.4 Chapter Outline . . . . .	12
<b>2 Biologically-Inspired Obstacle Avoidance Strategy for Safe Navigation</b>	<b>13</b>
2.1 Problem Description . . . . .	13
2.2 Biologically-Inspired Reactive Navigation Algorithm . . . . .	16
2.3 Computer Simulation Results . . . . .	21
2.4 ActivMedia Pioneer 3-DX Wheeled Mobile Robot . . . . .	27
2.5 Experiments with Real Mobile Robot . . . . .	28

2.6	Summary . . . . .	30
<b>3</b>	<b>Range-only Based Obstacle Avoidance Strategy for Safe Navigation in Uncertain Dynamic Environments</b>	<b>35</b>
3.1	Problem Description . . . . .	36
3.2	Reactive Navigation Algorithm . . . . .	38
3.3	Computer Simulation Results . . . . .	40
3.4	Experiments with Real Mobile Robot . . . . .	47
3.5	Summary . . . . .	52
<b>4</b>	<b>Navigation Algorithm Based on an Integrated Environment Rep- resentation</b>	<b>53</b>
4.1	Problem Description . . . . .	54
4.2	Navigation Algorithm . . . . .	58
4.3	Computer Simulation Results . . . . .	61
4.4	Experiments with Real Mobile Robot . . . . .	64
4.5	Summary . . . . .	67
<b>5</b>	<b>Comparison Between the Navigation Algorithms</b>	<b>73</b>
5.1	Essential Measurements . . . . .	73
5.2	Computation Complexity . . . . .	74
5.3	Performance Comparison . . . . .	76
5.3.1	Stationary Obstacles . . . . .	76
5.3.2	Dynamic Obstacles . . . . .	80
5.3.3	Section Summary . . . . .	86
5.4	Summary . . . . .	87
<b>6</b>	<b>The Implementations on an Intelligent Wheelchair Control System</b>	<b>91</b>
6.1	Background and Motivation . . . . .	92
6.2	System Model . . . . .	94
6.3	Wheelchair System Description . . . . .	95

6.4	Implementation and Experiments of Biologically-Inspired Navigation Algorithm (BINA) . . . . .	97
6.4.1	Parameter Measurements . . . . .	97
6.4.2	Experiments Results with a SAM Wheelchair . . . . .	99
6.5	Implementation and Experiments of Equidistant Navigation Algorithm (ENA) . . . . .	103
6.5.1	Parameter Measurement . . . . .	103
6.5.2	Experiment Results with SAM Wheelchair . . . . .	103
6.6	Summary . . . . .	107
<b>7</b>	<b>The Implementations on an Autonomous Intelligent Hospital Bed</b>	<b>109</b>
7.1	Background and Motivation . . . . .	110
7.2	System Model . . . . .	111
7.3	Hospital Bed System Description . . . . .	112
7.4	Experiments of Flexbed with Biologically-Inspired Navigation Algorithm (BINA) . . . . .	115
7.5	Experiments of Flexbed with Equidistant Navigation Algorithm (ENA)	119
7.6	Summary . . . . .	122
<b>8</b>	<b>Decentralised Formation Building Algorithm for Groups of Mobile Robots</b>	<b>127</b>
8.1	Multi-Robots System Description . . . . .	128
8.2	General Formation Building . . . . .	132
8.3	Formation Building with Anonymous Robots . . . . .	137
8.4	Computer Simulation Results . . . . .	139
8.4.1	General Formation Building . . . . .	139
8.4.2	Formation Building with Anonymous Robots . . . . .	141
8.5	Experiments with Group of Real Robots . . . . .	144
8.6	Summary . . . . .	146

<b>9 Conclusion</b>	<b>153</b>
9.1 Future Research Directions . . . . .	155
<b>Bibliography</b>	<b>157</b>

# List of Figures

2.1	Coordinate and orientation of the mobile robot and its minimal turning radius $R$ . . . . .	15
2.2	(a)Minimum distance $d_i(t)$ and angular difference $H(t)$ ; (b) the Vision cone $\alpha_i^{(1)}$ and $\alpha_i^{(2)}$ . . . . .	16
2.3	The enlarged vision cone . . . . .	17
2.4	(a)Illustrative example; (b)Two possible angle differences . . . . .	18
2.5	Illustration of the proposed navigation algorithm with one obstacle scenario . . . . .	22
2.6	Mobile robot navigating in a cluttered environment with multiple moving obstacle . . . . .	23
2.7	Mobile robot avoids an obstacle moving along an arc . . . . .	24
2.8	Mobile robot avoids an obstacle in a sinusoidal path . . . . .	24
2.9	Mobile robot avoids an obstacle with dynamically changing radius . .	25
2.10	Proposed navigation algorithm (upper row) versus VOA (lower row) .	26
2.11	Pioneer 3-DX wheeled mobile robot with SICK laser range finder . .	28
2.12	Robot navigating in an open area . . . . .	29
2.13	Robot navigating in a corridor with stationary and moving obstacles case 1 . . . . .	31
2.14	Robot navigating in a corridor with stationary and moving obstacles case 2 . . . . .	32
2.15	Robot avoiding obstacle with non-linear velocity case 1 . . . . .	33
2.16	Robot avoiding obstacle with non-linear velocity case 2 . . . . .	33



3.1	(a)Coordinates and orientation of the mobile robot and its minimal turning radius $R$ ; (b)Moving domain $D(t)$ and heading to target $H(t)$	37
3.2	Linear function with saturation . . . . .	38
3.3	(a)Sliding mode maneuver; (b)linear mode maneuver . . . . .	40
3.4	Execution of the proposed navigation algorithm in a simple scenario .	41
3.5	Mobile robot navigating in uncertain dynamic environments . . . . .	42
3.6	Mobile robot avoids moving and rotating obstacles . . . . .	43
3.7	The implementation of interpolation technique with the proposed navigation algorithm . . . . .	44
3.8	Mobile robot avoids dynamic deforming obstacle . . . . .	45
3.9	Proposed navigation algorithm (upper row) versus VOA (lower row) .	46
3.10	Robot avoids U-shape obstacle . . . . .	47
3.11	Robot navigating in an environment with stationary and dynamic obstacles . . . . .	48
3.12	The implementation of the proposed navigation algorithm with the interpolation technique . . . . .	49
3.13	Robot avoids tight clusters of obstacles with dynamical changing radii	50
3.14	Robot avoids deforming obstacle . . . . .	51
4.1	The environment (interior darker region) $\mathcal{E}(t)$ , The enlarged environment (the gray larger region covers $\mathcal{E}(t)$ ) $\hat{\mathcal{E}}(t)$ and the $d_{safe}$ -neighbourhood	55
4.2	Illustration of the binary function $M(\alpha, t)$ . . . . .	56
4.3	The disc $D(t)$ of diameter $D_s$ . . . . .	57
4.4	Robot navigating in unknown static environment with irregular obstacles . . . . .	62
4.5	Robot navigating in a unknown dynamic environments with multiple moving obstacles . . . . .	63
4.6	Performance comparison: two square obstacles moving side by side . .	64
4.7	Performance comparison 2: chains of obstacles . . . . .	65
4.8	Performance comparison 3: robot navigating in a crowded environment	66

4.9	Illustration of obstacle detection . . . . .	67
4.10	Robot avoids static obstacles . . . . .	68
4.11	Robot avoids obstacles in ambiguous scenario . . . . .	69
4.12	Robot navigating in complicated unknown environment with station- ary and dynamic obstacles case 1 . . . . .	70
4.13	Robot navigating in complicated unknown environment with station- ary and dynamic obstacles case 2 . . . . .	71
4.14	Robot navigating in complicated unknown environment with station- ary and dynamic obstacles case 3 . . . . .	72
5.1	(a)Essential measurements for BINA (b)Essential measurements for ENA (c)Essential measurements for NAIER . . . . .	74
5.2	(a)Flowchart for BINA (b)Flowchart for ENA (c)Flowchart for NAIER	75
5.3	Performance comparison: single stationary obstacle for (a) BINA (b)ENA (C)NAIER . . . . .	78
5.4	Performance comparison: single rectangular obstacle for (a) BINA (b)ENA (C)NAIER . . . . .	79
5.5	Performance comparison: single obstacle with irregular shape for (a) BINA (b)ENA (C)NAIER . . . . .	80
5.6	Performance comparison: a crowd of obstacles with irregular shapes for (a) BINA (b)ENA (C)NAIER . . . . .	81
5.7	Performance comparison: dynamic environment with single moving obstacle for (a) BINA (b)ENA (C)NAIER . . . . .	82
5.8	Performance comparison: dynamic environment with three moving obstacles for (a) BINA (b)ENA (C)NAIER . . . . .	83
5.9	Performance comparison: dynamic environment with six moving ob- stacles for (a) BINA (b)ENA (C)NAIER . . . . .	84
5.10	Performance comparison: obstacle with non-linear velocity for (a) BINA (b)ENA (C)NAIER . . . . .	85

5.11	Performance comparison: navigation in a extremely cluttered dynamic environments for (a) BINA (b)ENA (C)NAIER . . . . .	86
6.1	(a)Front view of the wheelchair; (b)Rear view of the wheelchair . . .	96
6.2	Interconnections between hardwares of wheelchair control system . . .	97
6.3	Graphic Illustration of the received data . . . . .	98
6.4	Wheelchair navigating in a dynamic environment with two moving obstacles . . . . .	100
6.5	Wheelchair avoiding static and moving obstacles . . . . .	101
6.6	Wheelchair navigating in a cluttered corridor with moving pedestrians	102
6.7	Wheelchair performs basic navigation tasks . . . . .	104
6.8	Wheelchair avoids random obstacles . . . . .	105
6.9	Wheelchair navigating among stationary and dynamic obstacles . . .	106
6.10	Wheelchair avoids multiple moving obstacles . . . . .	108
7.1	Key components in Flexbed . . . . .	113
7.2	Schematic for the motor control system of Flexbed . . . . .	114
7.3	safety measurements during obstacle avoidance maneuver . . . . .	116
7.4	Flexbed avoids static and dynamic obstacles . . . . .	117
7.5	Flexbed avoids multiple dynamic obstacles . . . . .	118
7.6	Flexbed avoids obstacle with dynamic changing radius . . . . .	119
7.7	Flexbed keeps a constant distance to the obstacle . . . . .	120
7.8	Flexbed avoids the stationary obstacle (long bench) and the dynamic obstacle (the experimenter) . . . . .	121
7.9	Flexbed navigating in dynamic environment with moving obstacles .	123
7.10	Flexbed avoids group of obstacles . . . . .	124
7.11	Flexbed avoids obstacle with dynamic dyforming shape . . . . .	125
8.1	Multi-robots system . . . . .	129
8.2	Connected undirected graph $\mathcal{G}(k)$ . . . . .	130

8.3	(a) Initial state (robots with arbitrary $\tilde{\theta}_i(0)$ , $\tilde{x}_i(0)$ , $\tilde{y}_i(0)$ and $\tilde{v}_i(0)$ )	
	(b) Final state (robots move in the same speed and direction with a desired square formation) . . . . .	134
8.4	Graph $\mathcal{P}$ . . . . .	138
8.5	Straight line formation with equal separation between two consecutive robots . . . . .	140
8.6	Equilateral Triangle formation . . . . .	141
8.7	Robots form a square shape . . . . .	141
8.8	Robots form an arc . . . . .	142
8.9	Robots form regular pentagon . . . . .	142
8.10	Straight line formation with anonymous robots, permutation applied .	143
8.11	Square formation with anonymous robots, permutation applied . . . .	145
8.12	Regular pentagon formation with anonymous robots, permutation ap- plied . . . . .	145
8.13	Random shape formation with anonymous robots, permutation applied	146
8.14	Robots form a regular triangle . . . . .	148
8.15	Robots form a straight line . . . . .	149
8.16	Robots form a rectangle . . . . .	150
8.17	Robots form a kite . . . . .	151



# List of Tables

5.1	Navigation time (in <i>sec</i> ) for BINA, ENA and NAIER over 25 experiment runs (obstacles moving with constant speeds) . . . . .	88
5.2	Navigation time (in <i>sec</i> ) for BINA, ENA and NAIER over 20 experiment runs (obstacles moving with non-linear velocities) . . . . .	89
6.1	Fragment of data from URG-04LX laser range finder . . . . .	97
6.2	Wheelchair and controller parameters . . . . .	99
6.3	Fragment of data from URG-04LX laser range finder . . . . .	103
8.1	Experiment Results over ten experiment runs (x coordinate) . . . . .	143
8.2	Experiment Results over ten experiment runs (y coordinate) . . . . .	144
8.3	Indices assigned to all the robots . . . . .	144

# Chapter 1

## Introduction

A safe navigation is defined as the process of ascertaining the object's current position and planning its route from this current position to the target position on the premise of the safety of the object. An appropriate obstacle avoidance strategy is the key factor to ensure a safe navigation process. Numerous existing researches are focused on the development of navigation algorithms in static environments (see e.g. [61,104,115,163]), which have limited applications in many real world scenarios where the obstacle are dynamically moving. The problem of safe navigation in dynamic environments poses a serious challenge in the field of mobile robotics. This challenge is further extended when the informations about the dynamic obstacles are scarce, especially some basic prior informations which are assumed to be available in many researches. These prior informations include the complete map of the environments, the position and the orientation of the obstacles in the map, the nature of the obstacles (whether the shape of the obstacles are consistent or deforming over time) and the motion of the obstacles (whether the obstacle is moving with a constant or time-varying velocity) etc.

The basic requirement for an appropriate obstacle avoidance strategy is to sense or detect obstacles and make proper decisions when the obstacles are nearby. By fulfilling the basic requirement, the more advanced obstacle algorithms should have one or more additional features such as: obstacle avoidance with minimum effort,

optimum obstacle avoidance time, avoidance with limited information, and computational efficiency. Although most of the existing obstacle avoidance algorithms achieve the basic requirement, few of them have the additional features necessary to be considered as more advanced algorithms.

In this report, three advanced obstacle avoidance strategies for safe navigation in dynamic environments have been presented. The proposed navigation algorithms are based on controller switching. Mathematical analysis of such switched controller systems including global stability analysis can be found in [97, 148, 153, 171]. All of the proposed algorithms are applicable for the non-holonomic unicycle mobile systems with bounded speed and angular velocity. It is well-known that the motion of many wheeled robots, missiles and unmanned aerial vehicles can be described by this model; see e.g. [91, 93, 179] and references therein. Each of the proposed strategies has more than one additional feature besides the basic requirement for an appropriate obstacle avoidance strategy.

The detailed description of the proposed navigation algorithms are provided. Their features are shown in extensive computer simulations. The implementation of the proposed navigation algorithms on different platforms, including ActivMedia Pioneer 3-DX mobile robot, a electric-powered wheelchair and a hospital bed control system, are presented to demonstrate their applicability in a wide range of real world scenarios. Furthermore, the performance of three obstacle avoidance strategies are compared with each other across various scenarios, which gives the insight to the merits and advantages of each of the algorithm.

The problem of networked multi-robots formation building, another interesting challenge in the field of navigation, is also investigated. A constructive and easy-to-implement decentralised navigation algorithm is proposed for a group of randomly positioned objects. Furthermore, we present a randomised decentralised navigation algorithm that achieves the convergence to a desired configuration with probability of 1. Its performance is confirmed by the simulations results and the implementation on the ActivMedia Pioneer 3-Dx mobile robots.



The following section presents a literature review on the relevant topics in this report.

## 1.1 Obstacle Avoidance Strategies for Safe Navigation Algorithm

The concept of safe navigation has been reflected in different aspects of our life, for example, pedestrians avoid colliding each other in the street, vehicles follow traffic rules in the driving lanes, animals use simple motion control rules that result in remarkable intelligent behaviors. The implementation of navigation algorithms can also be found various applications such as agricultural applications [95], GPS navigation systems [118], auto-pilot function [162], missile guidance [83, 84], robots designed for specific purposes (rescue [50], multiple robot navigation [42] and explore [195], etc). Therefore, it is hardly surprising that safe navigation in dynamic environments has become one of the most interesting and attractive research topics, and has already generated a large number of successful results.

The existing navigation approaches fall into two main categories: global and local (reactive) navigation approaches.

Global navigation algorithms [5, 52, 53, 78, 164, 186] assume that a complete set of priori information about the environment, i.e. "map", is known, so that optimal theoretical solutions based on different policies can be computed. Within this framework, several techniques (surveyed in e.g., [63, 68]) have been developed for dynamic scenes, including nonholonomic planners [129] and state-time space [31, 132] approaches. One major problem of the global navigation algorithms is that they are computationally expensive which makes them inapplicable in many real time implementations. Also, their performance can be easily plagued by incomplete or erroneous data, so that in many applications, the paths computed by the global navigation algorithm need to be revised and evaluated online, which is time consuming and cost inefficient. Furthermore, the performances of these algorithms are

very likely to be ruined by the unexpected "changes" in the environments, such as an unexpected obstacle appearing in the environment.

Local navigation algorithms [20, 67, 91, 149, 179], on the other hand, use sensory systems to observe a small fraction of an unknown environment. The best decisions are made iteratively each time using the information available. These algorithms are more realistic in real time implementation where the sensory systems have finite detection range. These navigation algorithms are more computationally efficient when compared to global navigation algorithms as relatively less information needs to be processed each time. However, many of the researches only focus themselves on static environments, approaches such as dynamic window [30, 161], the curvature velocity [167], and the lane curvature [106] approaches, consider only the simple problem of navigation in static environments. The obstacle avoidance with moving obstacles is much harder because the object only has finite time and limited options to avoid the obstacles when they are detected within a certain range. Some approaches are proposed to deal with obstacle avoidance with moving obstacles, for example, velocity obstacles [26, 68], collision cones [8], or inevitable collision states [33, 117]. These approaches require the deterministic knowledges about the obstacles' velocity and a moderate rate of its change. Finally, many of these papers [52, 53, 78, 164] do not take into account non-holonomic constraints on robot's motion which is a severe limitation in practice.

The following subsections briefly discuss some of the well-know navigation algorithms.

### 1.1.1 BUG Algorithms

The family of BUG algorithms are examples of biologically-inspired algorithms. The concept of first two members, Bug1 and Bug2, of the Bug algorithm family is introduced in [81]. The maneuver of BUG algorithms are inspired from animals (i.e. rats) unidirectionally following the obstacle (i.e. walls) boundary to the target location in a known environment. In general, Bug2 is more "aggressive" than Bug1

in terms of finding the possible paths to the target, and work in many scenarios where BUG are found impossible to accomplish. The advantage of the Bug algorithms is that it allows the object to navigate in an environment with obstacles whose shapes and coordination are not known, which is the primary assumption for many approaches. However, the problem with these algorithms is that they do not guarantee global convergence to the target, i.e. the object may be "looping" around the same obstacle infinitely. This is partially because the BUG algorithms are often proposed as pseudo codes. The obstacle boundary following methods and the leave conditions are not specifically defined which makes the implementations of the BUG algorithms inconsistent for different types of control systems. Also, these algorithm are only investigated in the static environments where the obstacles are stationary, which is not applicable in many real world scenarios where the obstacles are dynamically moving. The later varieties of the BUG algorithms includes: Alg1 and Alg2 [141, 142], DistBug [54], RoveerBug [71], Rev1 and Rev2 [111], TangentBug [55], and others [82, 112]. The performance of the BUG algorithms varies in different environments (as investigated in [107]), for example, TangentBug [55] works best in the environments with wider spaces that allow the equipped range sensors to be used efficiently. A detailed performance comparison of most of the BUG algorithm family is carried out in [107].

### 1.1.2 Model Predictive Control

Model Predictive Control (MPC) is an iterative computation process which computes a set of future control signals which minimises some cost functions at every time instant, only the first control signal is applied to the control system. This process is repeated at next time instant until the control objective is achieved. The concept of (MPC) can be employed to solve the problems of safe robot navigation. In case of robot navigation, the robot computes a set of future control signals for  $t \in [t, t + T)$  based on the feedbacks from sensory systems at time  $t$  and the control signal at time  $t$  is applied. This control scheme is more flexible than global naviga-

tion algorithm because the robot has access to the updated information from sensory systems at every time instant, any changes in the environments can be adapted according to the control strategies. The final convergence achieved when the robot arrived at the target location.

There are a number of varieties of MPC being proposed in different literatures. The robust Model Predictive Control is favourable for the implementation of navigation algorithms on real control systems. There are three main approaches to robust Model Predictive Control: 1) Min-Max MPC [160] 2) Constraint Tightening MPC [65, 137] and 3) Tube MPC [66]. The common features of these robust Model Predictive Control is demonstrated by their performances in the presence of set bounded disturbance which is a desired property in real robotic applications. The general MPC is applicable for vehicles with simple linear models. However, many of the vehicle exhibits more complicated non-holonomic characteristics with bounded speed and angular velocity. The non-linear MPC is a more suitable control approach to these non-linear vehicle types.

### 1.1.3 Velocity Obstacle Approach

The problem of safe navigation in dynamic environments is much more challenging. A number of approaches have been proposed to solve the problem. Velocity Obstacle Approach ([27, 28]) is one of the most well-known approaches which achieves navigation tasks in dynamic environments by computing a set of potential collision velocities, any velocity within this set will cause a collision in future time. The primary objective is to choose a velocity that is outside of the collision velocities set to guarantee the safety of the object, and then find the optimal velocity (depending on different criteria) among these safe velocities. This approach has the merit of taking into account the velocities of the obstacles, predicting potential collision velocities in the future, allowing various motion planning options and guaranteeing the safety of the object in dynamic environments. This approach has proven its successfulness in theoretical basis, however, since the approach does not consider

the non-holonomic constraints of the real robot, it may not be suitable for many of the real time implementations. Moreover, the set of collision velocities are computed based on the assumption that the obstacles maintain their velocities in the future time. For obstacles moving with non-linear velocities, a more advanced Non-Linear Velocity Obstacles [69, 70, 165] has to be estimated which is computationally expensive. Many other navigation approaches are inspired by the concept of Velocity Obstacle Approach, including Reciprocal Velocity Obstacle Approach [184], Probabilistic Velocity Obstacle [35], Generalised Velocity Obstacle [191] etc.

In [116, 117], an approach similar to velocity obstacle is proposed, which computes the collision velocities in Velocity Space. This approach takes into account the non-holonomic constraints of the object during computation. Due to the nature of the computation method, this approach can only apply to obstacles that are moving in straight lines or other paths consisting of segments of short straight lines. Furthermore, this approach assumes the shapes of the obstacles to be either circles or polygons. The Collision Cone Approach [9] is one of a few approaches which allows the objects to avoid moving obstacles regardless of the shapes of the obstacle. Once again, the non-holonomic constraints are not considered in [9]. Examples concerning nonholonomic robots include artificial potential approach, combined with sliding-mode control for gradient climbing [24, 76], and kinematic control based on polar coordinates and Lyapunov-like analysis [17].

#### 1.1.4 Other Navigation Algorithms

The Artificial Potential Field (APF) [57] approach treats the robot as a point in a potential field. The robot is influenced by two forces: the repulsive force from the obstacles and the attractive force from the target. The advantage of APF is that the approach is able to generate a safe path to the target with little computational effort. However, the robot can be trapped in local minima when APF is employed which leads to failure of navigation task. This problem has been investigated by many researchers and possible solutions have been proposed (see e.g. [87, 88]). The

APF is also improved to adapt robots of unicycle model in [134] .

Sliding Mode Control (SMC) is a non-linear control scheme which offers a number of benefits in robotic navigation. The most well-known advantage of SMC is its robustness against external disturbance and internal state uncertainties. This is critically important in the cases of noisy sensory measurements or uncertain state estimations [95]. Since the execution of SMC involves simply switching between several states (usually two or three), it is generally simple to be implemented in a wide range of dynamic systems. A number of sliding mode controller has been designed for robot navigation: in [91, 96], a sliding mode controller is proposed for the problem of border patrolling (boundary following) and obstacle avoidance; the environmental extremum seeking problem in an unknown environment is investigated in [92]; a navigation algorithm based on range-only measurements is proposed in [179]; navigation problems in maze-like environment [94] and environmental level tracking problem is considered in [101]

The motion safety for robotic systems are studies on [32,33,122]. In these papers, three safety criteria which assess the safety state of an object in a risky environment. These three criteria are summarised as: 1) robotic system's dynamic 2) environment obstacle's future behavior and 3) time horizon. The safety of the robotic systems are not guaranteed if any of these criteria is violated. Based on the criteria, the authors propose a state in which robotic systems will always collide with the obstacles regardless of the future motion of the robotic system is, namely Inevitable Collision State. A survey regarding other recent navigation algorithms can be found in [43].

## 1.2 Formation Building Control Strategies

Formation building control strategies focus on the coordinated control of a group of mobile robots, which is another topic in the field of autonomous navigation. The formation building control strategies allow the groups of mobile robots to move in a desired pattern, which is found particularly useful in a wide range of applications

including robotic sensing networks [18, 113], rescue robot teams [56, 174], research and explore operation in unknown environments [172] etc. The employ of formation building strategies in these applications has advantages of increasing system efficiency and robustness and reducing the system cost and operation effort [10].

Numerous formation building control strategies have been proposed in recent years. The leader-follower approach [21, 187, 188] is simple to understand: one of the robots in the group is assigned as the leader which has the group formation information to guide the movements of the followers. This centralised formation approach is easy to implement in a group of real mobile robots. However, the formation group is not efficient as the leader is responsible for most of the computation tasks, and the performance of the group relies heavily on the leader. Moreover, the group is not robust as any failure on the leader (e.g. communication error, computation error) will cause the whole group to collapse. Finally, as surveyed in [135], the typically leader-follower approach is lack of inter-vehicle feedback throughout the group.

The study of decentralised control laws for groups of autonomous mobile robots has emerged as a challenging new research area in recent years (see, e.g., [15, 22, 34, 39, 40, 48, 89, 144, 145, 194]). Broadly speaking, this problem falls within the domain of decentralised control, but the unique aspect of it is that groups of mobile robots are dynamically decoupled, meaning that the motion of one robot does not directly affect that of the others. In decentralised formation control schemes, each member in the group is responsible for deciding its own motion based on the state of itself and its neighbors. The group's objective can still be achieved even when failure of any members in the group occurs.

A discrete time model of a system consisting of several autonomous agents is presented in [185]. This model can be viewed as a special case of a computer model proposed in [136] for the computer animation industry and mimicking animal aggregation. This model proves that control of the motion of multiple autonomous agents can be achieved in decentralised fashion. A modification of the model in [185]

is presented in [48], and a mathematical analysis of the model is presented. The main results of [48] are sufficient conditions for coordination of the system of agents that are given in terms of a family of graphs characterizing all possible neighbouring relationships among agents. In behavior-based approach [3, 73, 85], a set of desired behaviors are prescribed for each member in the group. These desired behavior may includes: collision avoidance to other members in the group, avoidance of exterior obstacles, formation building, and formation keeping. The motion of each member is based on the weighting of these behaviors. The performance of the behavior-based approach under the influence of member failure is studied in [133]. Other types of formation control strategies can be found in e.g. [10, 36, 59, 193].

It should be pointed out that many papers in this area consider simplest first- or second-order linear models for the motion of each robot; see, e.g., [114, 175] and [176]. Therefore, the obtained results are heavily based on tools and methods from linear system theory, such as stochastic matrices or graph Laplacians. It is known that there are examples of unrealistic physically embodied behaviour that would be possible under such simplified models. In particular, the robot motion in such linear models does not satisfy the standard hard constraint on either robot speed or angular velocity. Furthermore, it can be shown that the models proposed in [144] and many other papers will result in arbitrarily large robot angular velocity and arbitrarily small robot turning radius, which is impossible on actual wheeled robots.

### 1.3 Main Contributions of This report

The main contributions of this report are described as follows:

1. Three novel obstacle avoidance strategies are proposed for safe navigation of mobile robots of non-holonomic unicycle model. The detailed descriptions of the proposed navigation algorithms are presented.
2. The computer simulation results and experiment results with real P-3 mobile



robot are presented with detailed descriptions and explanations. The results demonstrate the features of the proposed algorithms and their performance with a real non-holonomic systems.

3. These navigation algorithms are compared with each other across various aspects including measurements required for computation, computation complexity and performance comparison in different scenarios. Each of the proposed algorithm has unique characteristics over the others which make itself more efficient in one or more of the mentioned aspects.
4. The algorithms have been implemented on two real control systems: intelligent wheelchair (SAM) and autonomous hospital bed (Flexbed). The objective is to show the applicabilities of the algorithms with real control systems. The performance of the proposed navigation algorithms with the SAM and Flexbed demonstrate their capabilities to achieve navigation tasks in complicated real time scenarios. The applications of the proposed algorithms are not limited to these two control systems, but can be easily implemented into many other control systems.
5. The problem of formation building for a group of mobile robots is considered. We propose a robust decentralised formation building algorithm for a group of mobile robots to move in the defined geometric configurations. Furthermore, we consider a more complicated formation problem with a group of anonymous robots, these robots are not aware of their position in the final configuration and have to reach a consensus during the formation process. We propose a randomized algorithm for the anonymous robots which achieves the convergence to a desired configuration with probability 1. The performance and applicability of the proposed algorithm is confirmed by the computer simulation result as well as the experiments with a group of real mobile robots.

## 1.4 Chapter Outline

This report is organised as follows: the detailed descriptions of the navigation algorithms Biologically-Inspired Navigation Algorithm (BINA), Equidistant Navigation Algorithm (ENA) and Navigation Algorithm based on Integrated Environment Representation (NAIER) are presented in Chapter 2, 3 and 4, respectively. We also present the simulation results and the experimental results with the real robots for each of the proposed navigation algorithms in the corresponding chapters. These results demonstrate the features, effectiveness and applicability of the proposed navigation algorithms. These three navigation algorithms are compared with each other across various aspects to give a deeper insight to the merits of each of the proposed algorithm in Chapter 5. The implementation of the proposed algorithms on two real control systems, wheelchair and hospital bed, are shown in Chapter 6 and Chapter 7. The performance and applicability of the algorithms are confirmed by real life experimental results. We proposed a decentralised control strategy for formation building of a group of mobile robots and a randomised algorithm for formation building with anonymous robots in Chapter 8. Finally, Chapter 9 states the conclusion of this report.

## Chapter 2

# Biologically-Inspired Obstacle Avoidance Strategy for Safe Navigation

Researchers in the area of robot navigation are finding much inspiration from biology, where the problem of controlled animal motion is a central one. Animals, such as insects, birds, or mammals, are believed to use simple, local motion control rules that result in remarkable and complex intelligent behaviours. The algorithm proposed in this paper also belongs to the class of biologically inspired or biomimetic navigation algorithms. In biology, a similar obstacle avoidance strategy is called negotiating obstacles with constant curvatures (see e.g. [72]). An example of such a movement is a squirrel running around a tree. We confirm the performance of our real-time navigation strategy with extensive computer simulations and experiments with a Pioneer P3-DX mobile wheeled robot.

### 2.1 Problem Description

We consider a wheeled mobile robot, modeled as unicycle, travels in a two dimensional plane. The position of the wheeled mobile robot is represented by the absolute

## 14Biologically-Inspired Obstacle Avoidance Strategy for Safe Navigation

Cartesian coordinates as  $(x, y)$  of the reference point, which is the center of mass of the mobile robot. The orientation of the mobile robot, measured in counterclockwise direction from the reference axis, is give by  $\theta$ , see Fig. 2.1. The motion of the mobile robot exhibits non-holonomic characteristics with hard constraints on its speed and angular velocity. The mathematical model of the mobile robot is as follows:

$$\begin{aligned}\dot{x} &= v(t) \cos \theta, & x(0) &= x_0, \\ \dot{y} &= v(t) \sin \theta, & y(0) &= y_0, \\ \dot{\theta} &= u & \theta(0) &= \theta_0\end{aligned}\tag{2.1}$$

where

$$u \in [-U_{max}, U_{max}], \quad v(t) \in [0, V_{max}].\tag{2.2}$$

here  $v(t)$  and  $u(t)$  are the speed and angular velocity of the mobile robot, respectively.  $V_{max}$  and  $U_{max}$  are the non-holonomic constraints. This is the standard non-holonomic model with hard constraints on the angular and linear velocities. It is well-known that the motion of many wheeled robots, missiles and unmanned aerial vehicles can be described by this model; see e.g. [79, 91, 93, 179] and references therein. The non-holonomic constraints establish restrictions on the forward and rotational movements of the mobile robot, see Fig. 2.1; in particular, for given  $v$ , they limit the turning radius of the mobile robot from below by

$$R = v/U_{max}.\tag{2.3}$$

There are also a steady point-wise target  $\mathbf{T}$  and several moving obstacles. These obstacles are moving in random directions with various speeds. Each of the obstacles at time  $t$  occupies a certain domain  $D_i(t)$  for  $i = 1, 2, \dots, n$ , each of the domain  $D_i(t)$  is assumed to be a closed bounded planar set.

The objective for safe navigation of the mobile robot in the cluttered dynamic environment is to avoid the enroute obstacles with a safety distance  $d_{safe} > 0$  and drive the mobile robot to the target location at time  $t_f > 0$ , i.e,  $c(t_f) = \mathbf{T}$  and  $d_i(t) \geq d_{safe} \forall i = 1, 2, \dots, k, \quad \forall t \in [0, t_f]$ .

To achieve the navigation task, the following information is required:

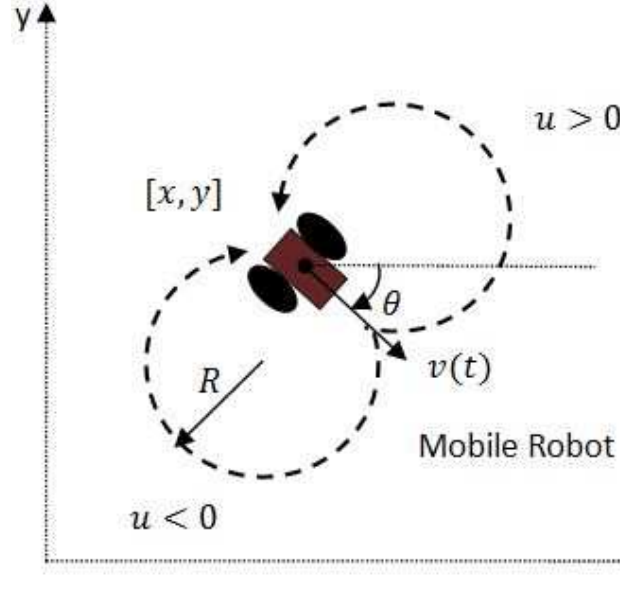


Figure 2.1: Coordinate and orientation of the mobile robot and its minimal turning radius  $R$

1. The minimum distance  $d_i(t)$  between the mobile robot and the border of the obstacle  $i$ , see Fig. 2.2(a)

$$d_i(t) := \min_{r \in D_i(t)} \|r - c(t)\|.$$

where  $c(t) := [x(t), y(t)]$  is vector of the the mobile robot's Cartesian coordinate. Note that  $\|\cdot\|$  denotes the standard Euclidean vector norm. And  $\dot{d}_i(t)$  is also accessible.

2. The velocity  $v_i(t)$  of the moving obstacle. We assume that any obstacle  $i$  bounded and moving in the plane without rotations with the time-varying velocity  $v_i(t)$ . and the velocities  $v_i(t)$  satisfy the following constraint:

$$\|v_i(t)\| \leq V < V_{max} \quad (2.4)$$

for all times  $t$  and for all obstacles  $i$ . It is obvious that if the constraint (2.4) does not hold, the safe navigation of the mobile robot is impossible.

3. The mobile robot measures  $\alpha_i^{(1)}$  and  $\alpha_i^{(2)}$  with respect to the reference axis, see

Fig. 2.2(b), these are the boundaries of the vision cone from the mobile robot to obstacle  $i$ .

4. The angular difference  $H(t)$  between its current orientation and the direction of the target, see Fig. 2.2(a)

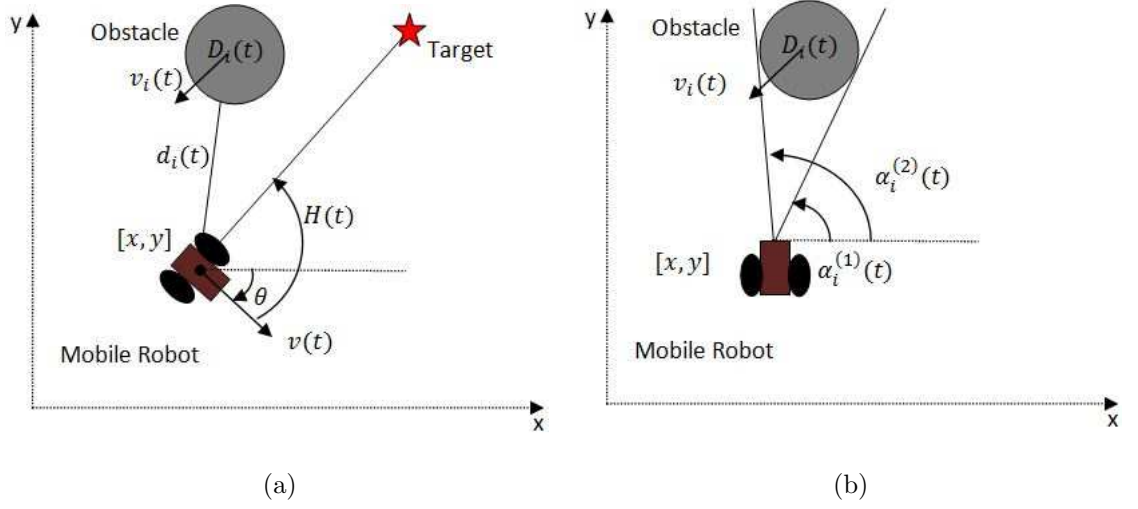


Figure 2.2: (a) Minimum distance  $d_i(t)$  and angular difference  $H(t)$ ; (b) the Vision cone  $\alpha_i^{(1)}$  and  $\alpha_i^{(2)}$

## 2.2 Biologically-Inspired Reactive Navigation Algorithm

In this section, we present the description of the biologically-inspired or biomimetic navigation algorithm.

We first enlarge the vision cone  $\alpha_i^{(1)}$  and  $\alpha_i^{(2)}$  measured from the mobile robot to the obstacle  $i$  by a given angle  $\alpha_0$ .  $0 < \alpha_0 < \pi$ , we denote the boundaries of the enlarged vision cone for obstacle  $i$  as:

$$\beta_i^{(1)}(t) := \alpha_i^{(1)}(t) - \alpha_0, \quad \beta_i^{(2)}(t) := \alpha_i^{(2)}(t) + \alpha_0; \quad (2.5)$$

see Fig. 2.3, we also introduce the following vectors  $l_i^{(1)}$  and  $l_i^{(2)}$  ( $l_i^{(1)}, l_i^{(2)} \in \mathbb{R}^2$ ) as:

$$l_i^{(j)}(t) := (V_{max} - V)[\cos(\beta_i^{(j)}(t)), \sin(\beta_i^{(j)}(t))] \quad \forall j = 1, 2 \quad (2.6)$$

where  $V_{max}$  and  $V$  are the constants from (2.2) and (2.4). A geometric interpretation of (2.6) is straightforward. The equations (2.6) define the two lines which are the boundaries of an enlarged vision cone of the obstacle. These lines are also known as occlusion lines.

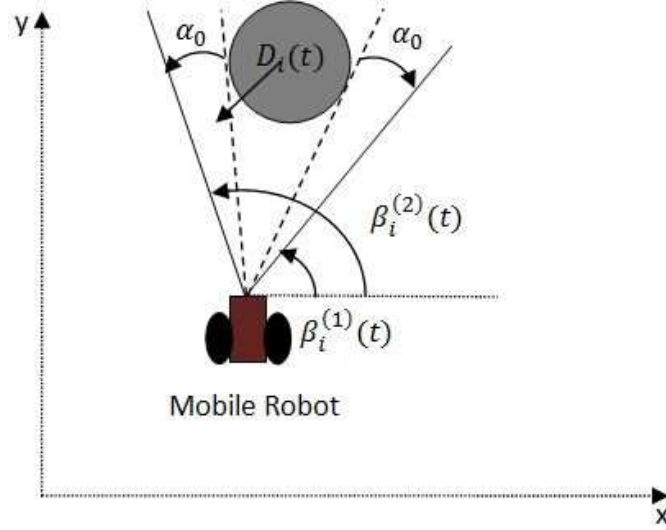


Figure 2.3: The enlarged vision cone

Let  $r_1$  and  $r_2$  be non-zero two-dimensional vectors. We use  $\gamma(r_1, r_2)$  to represent the relative angular difference measured from  $r_1$  to  $r_2$  in counterclockwise direction. We need the following  $f$  function to assign different values depending on  $\gamma(r_1, r_2)$ :

$$f(r_1, r_2) := \begin{cases} 0 & \gamma(r_1, r_2) = 0 \\ 1 & 0 < \gamma(r_1, r_2) \leq \pi \\ -1 & -\pi < \gamma(r_1, r_2) < 0, \end{cases} \quad (2.7)$$

where  $r_1, r_2 \in \mathbb{R}^2$ ,  $\gamma(r_1, r_2) \in (-\pi, \pi]$ .

Furthermore, let  $C > 0$  be the switching distance.

When the distance between the mobile robot and the obstacle  $i$  is reduced below  $C$  at  $t_0$ , the robot measures the vision cone  $(\alpha_i^{(1)}, \alpha_i^{(2)})$  and calculates the vector  $l_i^{(1)}$

and  $l_i^{(2)}$  by (2.6).

The velocity of the obstacle  $v_i(t)$  is added to both  $l_i^{(1)}$  and  $l_i^{(2)}$ , and we want to find the one which makes the smallest angle between itself and the mobile robot's current velocity vector  $v(t)$ , i.e, the minimum condition in (2.8) is satisfied, for all time  $t$  during the process of avoiding obstacle  $i$  and  $t \geq t_0$ .

$$\min_{j=1,2} |\gamma(v_i(t) + l_i^{(j)}(t), v(t))| \quad (2.8)$$

An illustrative example of (2.8) is given in Fig. 2.4(a). The angular difference between  $v(t)$  and  $v_i(t) + l_i^{(j)}(t)$  for  $j = 1, 2$  is shown in curved arrows. It can be observed from Fig. 2.4(b) that the vector  $v_i(t) + l_i^{(1)}(t)$  is closer to the robot's current moving direction  $v(t)$ .

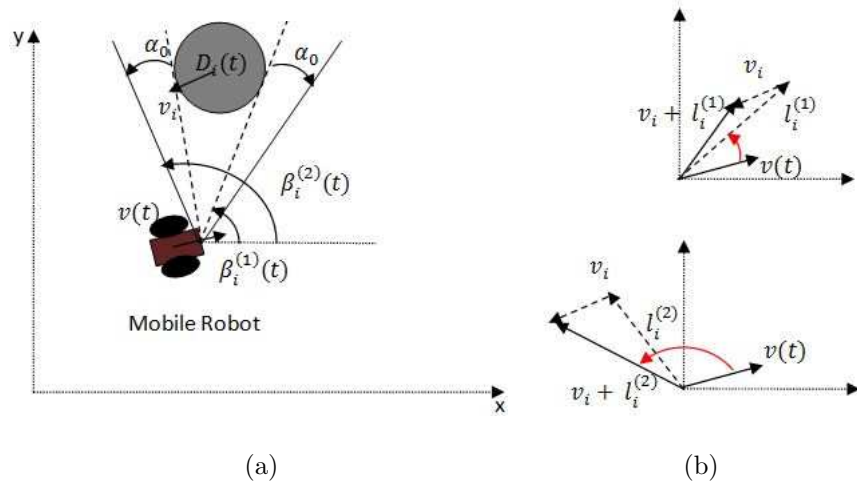


Figure 2.4: (a)Illustrative example; (b)Two possible angle differences

Let  $h$  be the index for which (2.8) is achieved, we proposed the following obstacle avoidance law:

$$\begin{aligned} u(t) &= U_{max} f(v_i(t) + l_i^{(h)}(t), v(t)); \\ V(t) &= \|v_i(t) + l_i^{(h)}(t)\|. \end{aligned} \quad (2.9)$$

Notice that the control inputs defined in (2.9) satisfy the constraints (2.2). (2.7) implies that the non-holonomic constraint on the angular velocity is satisfied, i.e.



$|u(t)| \leq U_{max}$ . Furthermore, (2.9), (2.4) and (2.6) imply that

$$\begin{aligned} V(t) &= \|v_i(t) + l_i^{(h)}(t)\| \leq \|v_i(t)\| + \|l_i^{(h)}(t)\| \\ &\leq V + (V_{max} - V) = V_{max}. \end{aligned}$$

Therefore the second constraint (2.2) on the linear velocity holds as well.

The intuition behind the obstacle avoidance strategy (2.9) can be explained as follows: The law (2.9) belongs to the class of sliding mode control laws; see e.g. [183]. The closed-loop system (2.1), (2.9) is a system of ordinary differential equations with a discontinuous right-hand side. The control law (2.9) steers the velocity vector  $v_R(t)$  of the robot to a switching surface on which the robot's velocity becomes equal to the vector  $v_i(t) + l_i^{(h)}(t)$ . Now consider a coordinates system moving with the velocity  $v_i(t)$ . In these coordinates, the obstacle  $i$  becomes stationary, and the robot is moving with the velocity  $l_i^{(h)}(t)$ . Furthermore, the motion with the velocity  $l_i^{(h)}(t)$  is an obstacle avoidance strategy which keeps a constant avoiding angle  $\alpha_0$  between the instantaneous moving direction of the robot and one of the two boundary rays of the vision cone of the obstacle  $i$  from the robot. In other words, the control law consists of steering toward the closer of the two edges of the enlarged obstacle vision cone defined by (2.6). The idea of this obstacle avoidance strategy originates from biology where it was called negotiating obstacles with constant curvatures (see e.g. [72]). An example of such a movement is a squirrel running around a tree. A similar strategy for avoiding stationary obstacles was proposed and studied in [44].

The complete navigation algorithm combines the obstacle avoidance law (2.9) with the target pursuit law (2.10).

$$\begin{aligned} u(t) &= 0; \\ v(t) &= V_{max}. \end{aligned} \tag{2.10}$$

Introduce the following constants  $\alpha_i > 0$ :

$$a_i := \frac{R_i}{\cos \alpha_0} - R_i \quad \forall i = 1, 2, \dots, k. \tag{2.11}$$

The execution of the navigation algorithm requires proper switching between the obstacle avoidance law (2.9) and the target pursuit law (2.10) obeys the following rules:

**R1:** (2.10)→(2.9) when the distance between the mobile robot and the obstacle  $i$  reduced below trigger distance  $C$  at time  $t_0$ .i.e,  $d_i(t_0) = C$  and  $\dot{d}_i(t_0) < 0$

**R1:** (2.9)→(2.10) when the distance is greater than certain values  $1.1\alpha_i$  and the mobile robot is oriented towards the target at time  $t_*$ . i.e,  $\dot{d}_i(t_*) \leq 1.1\alpha_i$  and  $\theta(t_*) = H(t_*)$

Our main theoretical result requires a number of assumptions.

**Assumption 2.2.1.** We assume that every obstacles  $i$  can be covered by a circular disk of radius  $R_i > 0$ . moving with the constant velocity  $v_i \neq 0$ . Furthermore,  $V_i < V_{max} \quad \forall i = 1, 2, \dots, k$  where  $V_i := \|v_i\|$ , and the vectors  $v_i$  and  $v_j$  are not collinear for all  $i \neq j$ .

**Assumption 2.2.2.** The maximum angular velocity of the mobile robot  $U_{max}$  satisfies:

$$U_{max} > F_i \quad (2.12)$$

where  $F_i$  is defined as

$$F_i := \frac{(V_i + V_{max})R_i}{(R_i + d_{safe})^2 \sqrt{1 - \frac{R_i^2}{(R_i + d_{safe})^2}}} \quad \forall i = 1, 2, \dots, k. \quad (2.13)$$

**Assumption 2.2.3.** The switching distance  $C$  for which the obstacle avoidance law to be activated satisfies the following constraint:

$$C \geq \frac{\pi V_{max}}{U_{max} - F_i} + 1.1a_i \quad \forall i = 1, 2, \dots, k. \quad (2.14)$$

**Assumption 2.2.4.** The avoiding angle  $\alpha_0$  in (2.5) satisfies the following condition:

$$\alpha_0 \geq \arccos \left( \frac{R_i}{R_i + d_{safe}} \right). \quad (2.15)$$

It is obviously follows from Assumption 2.2.4 and (2.11) that  $a_i \geq d_{safe}$  for all  $i$ .

**Assumption 2.2.5.** We assume the distance between different obstacle  $i$  and obstacle  $j$  satisfies:

$$Dist_{ij}(t) \geq 2C + \frac{\pi V_{max}}{U_{max} - F_i}; \quad (2.16)$$

and the distance between obstacle  $i$  and the target  $\mathbf{T}$  satisfies:

$$Dist_i \geq 1.1a_i$$

**Theorem 2.2.1.** *Let  $d_{safe} > 0$ ,  $0 < \alpha_0 < \frac{\pi}{2}$  and  $C > 0$  be given and suppose that Assumptions 2.2.1 – 2.2.5 hold. Then the control rule **R1**, **R2** provides a target reaching strategy with collision avoidance.*

The mathematical proof of Theorem 2.2.1 is proposed in [155]

## 2.3 Computer Simulation Results

In this section, we present the computer simulation results for the proposed navigation algorithm. With these simulation results, we demonstrate the capability of the proposed navigation algorithm to guide the mobile robot to the target position in cluttered dynamic environments.

In the following simulation results, we give figures for each simulation and provide simulation data to explain the features of the proposed navigation algorithm when necessary. In these figures, The mobile robot, the obstacles and the target are depicted by gray dick, black circles and red star, respectively, and the instantaneous moving direction of the mobile robot and the obstacles are shown in black arrows.

In Fig. 2.5, we demonstrate the execution of the proposed navigation algorithm with a simple scenario. The mobile robot measures the vision cone  $(\alpha_i^{(1)}, \alpha_i^{(2)})$  from itself to the obstacle, calculates the necessary parameters  $(\beta_i^{(1)}, \beta_i^{(2)}, l_i^{(h)})$  by (2.5), (2.6), (2.8) and the control signal by (2.9), see Fig. 2.5(a). The mobile robot safely arrives the target location while avoiding the moving obstacle with the proper switching between (2.9) and (2.10), the indication of different maneuvers taken by the mobile robot during its path to the target location are shown in Fig. 2.5(b).

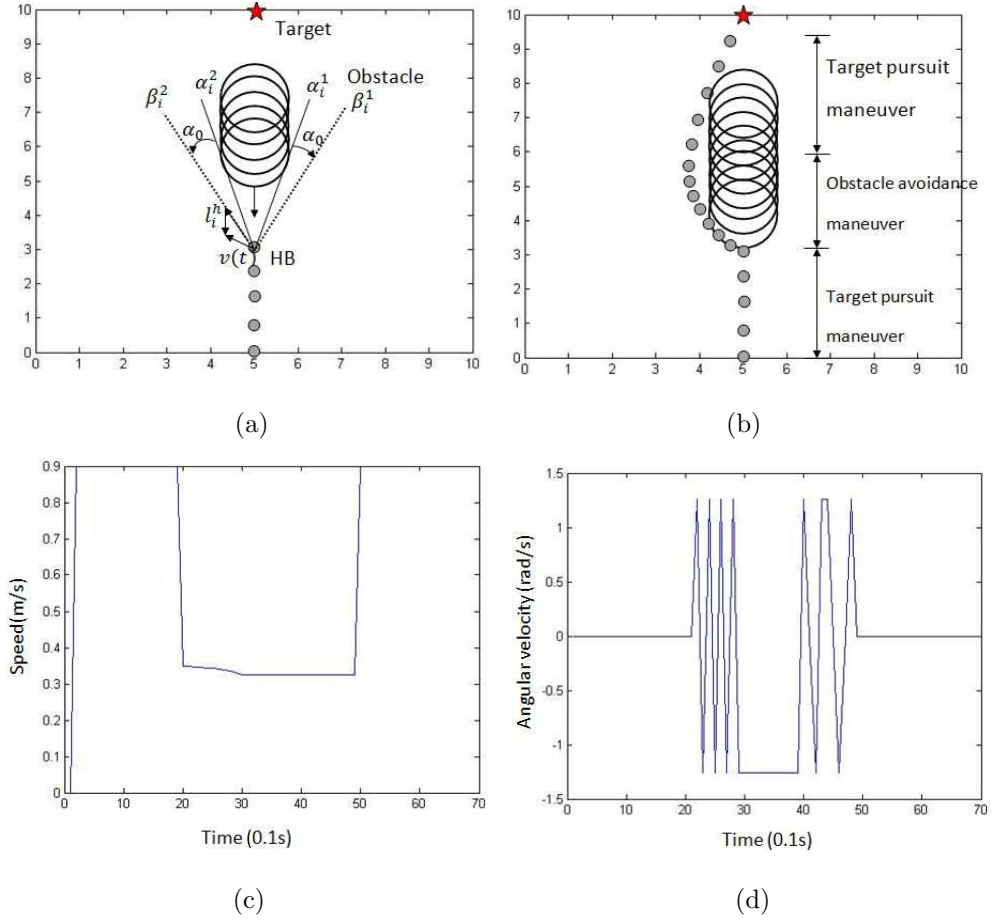


Figure 2.5: Illustration of the proposed navigation algorithm with one obstacle scenario

The speed and angular velocity of the mobile robot is shown in Fig. 2.5(c) and Fig. 2.5(d), respectively.

The next simulation shows the performance of the proposed navigation algorithm in a cluttered dynamic environment. This scenario can be treated as an extension of the simple scenario shown in Fig. 2.5. In Fig. 2.6, the obstacles of different radii are moving at various velocities, the mobile robot treats and bypasses each of these obstacles with a similar fashion shown in Fig. 2.5. The proposed navigation algorithm ensures the safety of the mobile robot in this cluttered dynamic environment, and delivers it to the target position. The crucial moments for the mobile robot to avoid each of the obstacles with the proposed obstacle avoidance law (2.9) are shown in

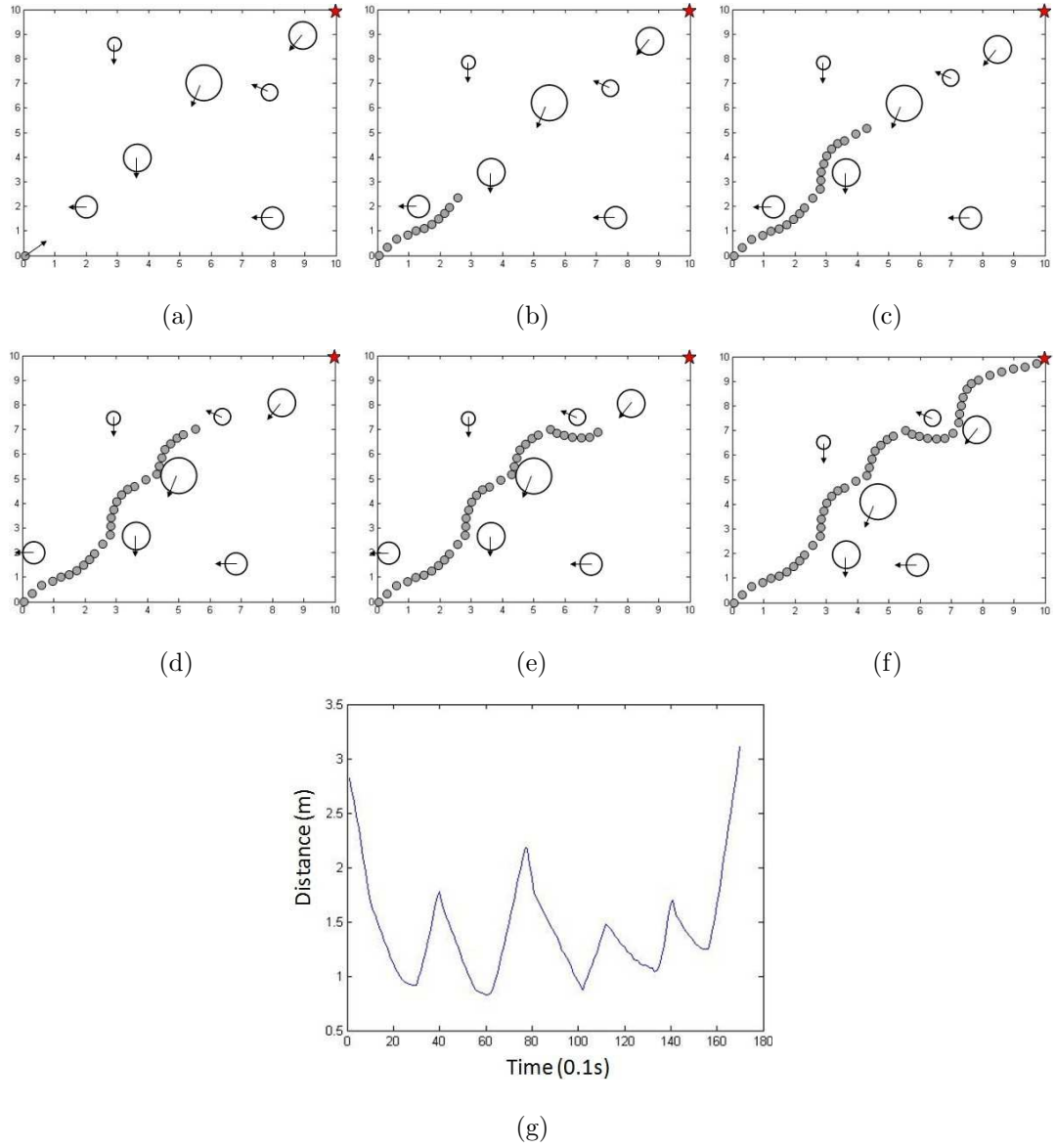


Figure 2.6: Mobile robot navigating in a cluttered environment with multiple moving obstacle

Fig. 2.6(b), Fig. 2.6(c), Fig. 2.6(d), Fig. 2.6(e), and the overall path taken by the mobile robot is shown in Fig. 2.6(f). The safety of the mobile robot is confirmed by the distance between itself and the closest obstacle which is shown in Fig. 2.6(g). The minimum value ( $d_{safe}$ ) of the distance in this simulation is  $0.832m$ .

In many real life scenarios, the movements of the obstacles are usually more complicated than simple straight motion. Fig. 2.7 and Fig. 2.8 show the avoidance of the

obstacles with non-linear velocities by the proposed navigation algorithm. The path taken by the obstacle are depicted in dashed lines, see Fig. 2.7(a) and Fig. 2.8(a). The proposed navigation algorithm takes account of the non-linear velocity  $v_i(t)$  in (2.8) and (2.9), it always steers the mobile robot so that the orientation of mobile robot is  $\alpha_0$  degree away from the  $l_i^{(h)}$ . The overall path taken by the mobile robot is shown in Fig.2.7(b) and Fig.2.8(b).

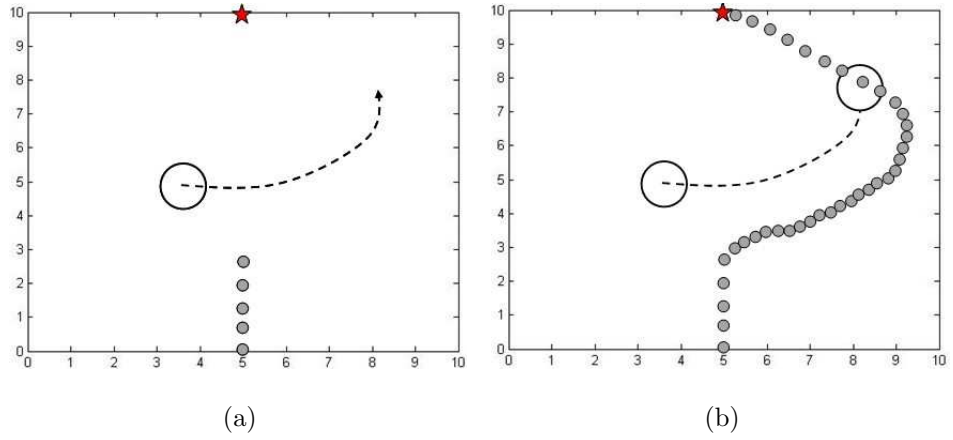


Figure 2.7: Mobile robot avoids an obstacle moving along an arc

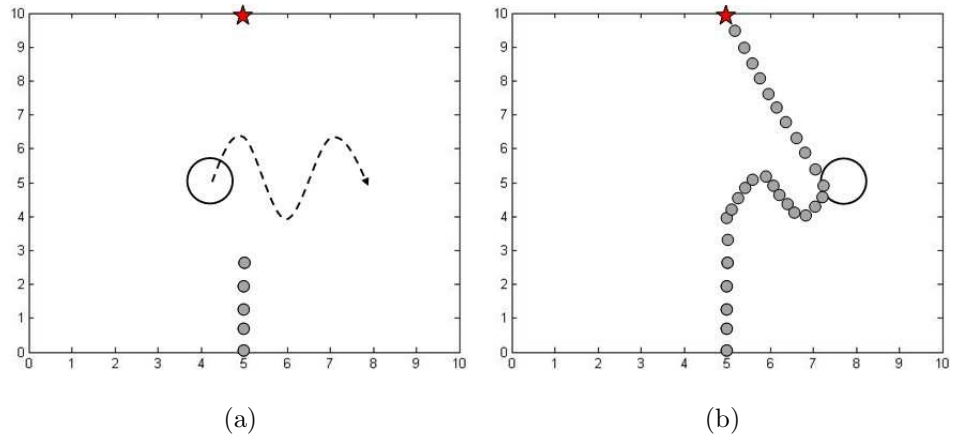


Figure 2.8: Mobile robot avoids an obstacle in a sinusoidal path

We investigate the performance of the proposed navigation algorithm when the radius of the obstacle are dynamically changing. This is a common behavior especially in workspaces or other populated places, for example, when the mobile robot sensors one obstacle within the switching distance  $C$  and starts to avoid it, at the

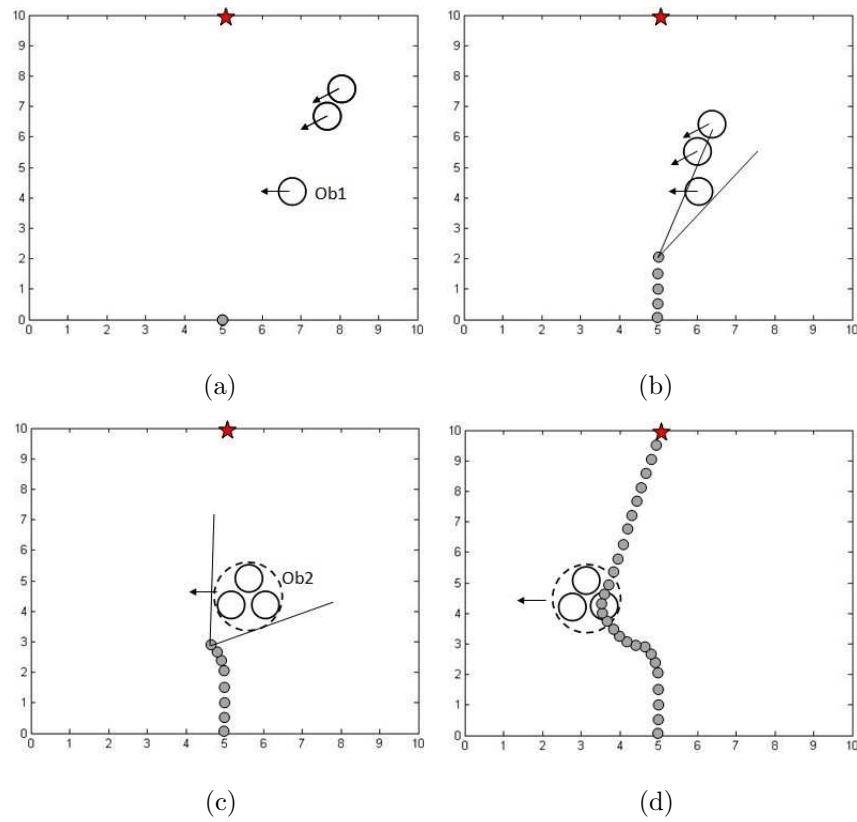


Figure 2.9: Mobile robot avoids an obstacle with dynamically changing radius

meantime, two other obstacles approaches the first obstacle and forms a group of three obstacles with larger radius. Fig. 2.9 shows a simulation of such scenario where the radius of the obstacle are dynamically changing. The change of radius of the obstacle "seen" by the mobile robot are shown in Fig. 2.9(b) and Fig. 2.9(c). The mobile robot arrives the target location safely in Fig.2.9(d) and its path is depicted.

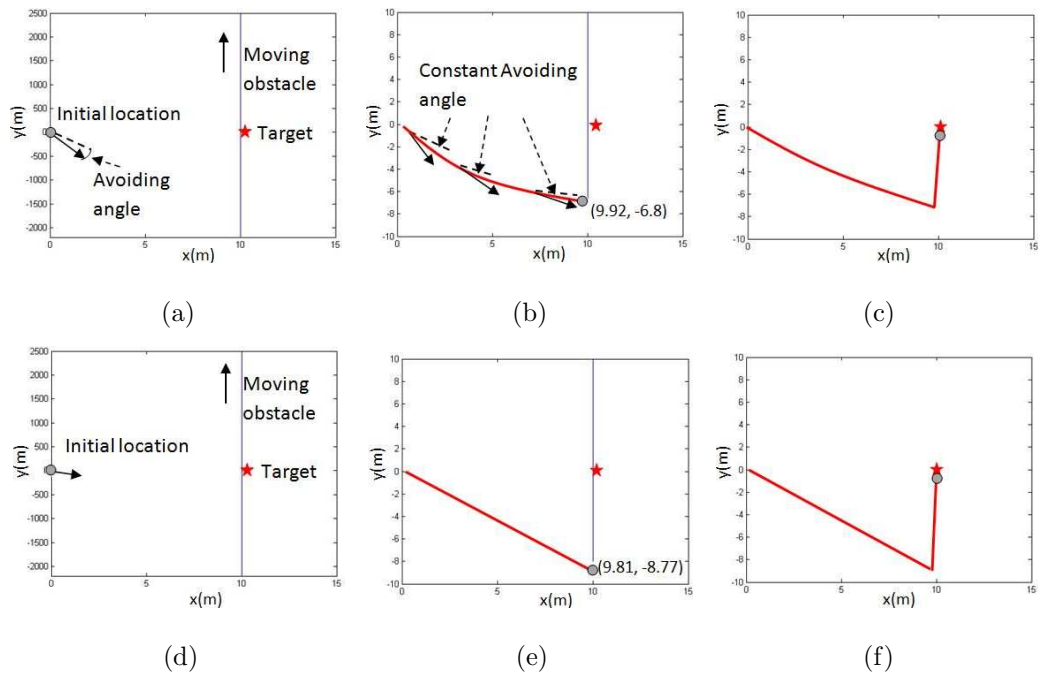


Figure 2.10: Proposed navigation algorithm (upper row) versus VOA (lower row)

The performance of our biologically-inspired algorithm was compared with that of other well-known navigation algorithms. Fig. 2.10 shows the comparison between our algorithm and the Velocity Obstacle Approach (VOA) [26, 68]. In Fig. 2.10(a) and 2.10(b), a long obstacle is moving perpendicularly to the path between the mobile robot and the target. Fig. 2.10(c) and 2.10(d) show the moment when the mobile robot is about to pass the lower end of the obstacle. As it can be observed, the biomimetic algorithm avoids the obstacle by keeping a constant avoiding angle between the mobile robot's moving direction and the lower end of the obstacle. On the other hand, VOA drives the mobile robot towards the lower end of the obstacle in a straight line and then move towards the target position. The complete paths for mobile robot to reach the target are shown in Fig. 2.10(e) and Fig. 2.10(f). The overall maneuver time for the biomimetic algorithm is 17.3s and for VOA is 18.7s. Hence, the biomimetic algorithm outperforms VOA in this scenario in terms of maneuver time.



## 2.4 ActivMedia Pioneer 3-DX Wheeled Mobile Robot

The navigation algorithms proposed in this report are implemented on ActivMedia Pioneer 3-DX wheeled mobile robot to demonstrate their performance and features. The description of Pioneer 3-DX mobile robot is presented in this section, Pioneer 3-DX (abbreviated as P3) is one of the most commonly used testbeds in a robotic laboratory (see e.g. [86, 120]) due to its versatility, reliability and durability, manufactured by ActivMedia Robotics.

The base of P3 contains onboard computer, swappable batteries (8-10 hours run-time with 3 batteries) and other circuitries. The body of the base is made of tough (1.6mm) aluminum which protects these important internal components from physical damages. It is a two-wheeled differential driven robot. The tire of P3 is made of foam-filled rubber which provides sufficient traction on various types of floor. The encoders are attached to the motors of both wheels. There are 8 front and 8 rear ultrasonic sensors equipped around the sides of P3. Furthermore, P3 has a wide range of accessories and extensions, such as Laser sensor and navigation package, manipulator arms and gripper, color stereo camera etc.

The following components are closely related to the implementation of the proposed navigation algorithm, thus their specification and functions should be emphasised:

- An onboard computer or an internal notebook with wireless capability with the proposed navigation algorithm is the centre piece of the P3 control system. All data are sent to the computer, where the corresponding control signals are computed and sent to the motor of P3.
- The differential driven motor system allows P3 to drive forward and backward at maximum speed of  $1.2m/s$ , and rotation speed of  $300degree/s$ .
- The 500-tick encoders are attached to the motors so that the relative position



Figure 2.11: Pioneer 3-DX wheeled mobile robot with SICK laser range finder

and the orientation of P3 regarding to the reference point can be estimated.

- the sensory system is consisted of a SICK laser range finder which provides only  $190\text{degree}$  field of view, and totally 16 ultrasonic sensors which provide  $360\text{degree}$  field of view. In general, the SICK range finder is more robust to noise ( $1\text{mm}$  distance resolution and  $0.25\text{degree}$  angular resolution with  $\pm 0.25\text{mm}$  measurement error) and has a further detection range (maximum  $80\text{m}$ ). On the other hand, the sets of ultrasonic sensor is able to provide  $360\text{degree}$  field of view. Therefore, a better utilisation of the laser range finder and the ultrasonic sensors will optimise the performance of sensory system.

The more detailed description and specification of P3 system can be found in [1, 2].

## 2.5 Experiments with Real Mobile Robot

The proposed navigation algorithm is implemented and experiments are carried out on an ActivMedia Pioneer 3-DX (P3) robot (see detailed description and speci-

cation in Section 2.4) to demonstrate its applicability and performance on a real non-holonomic system.

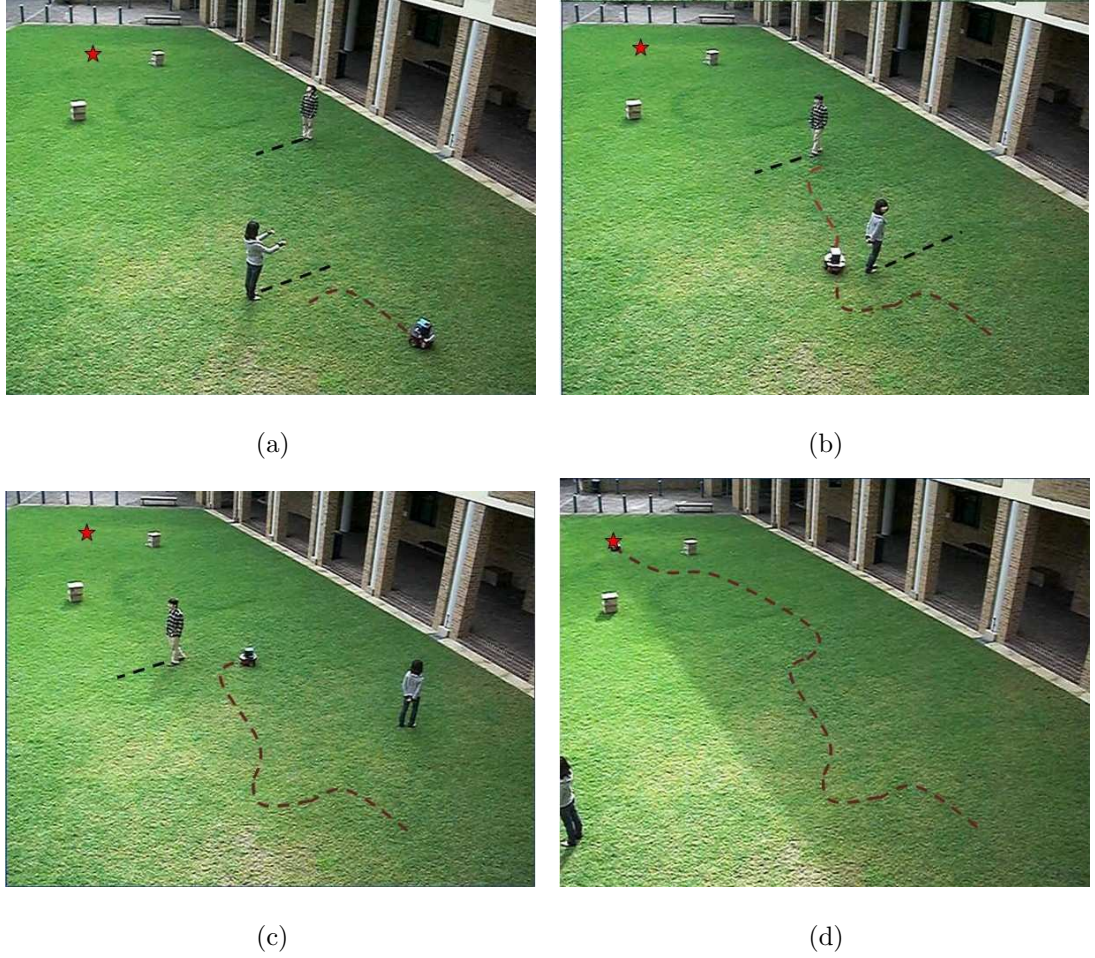


Figure 2.12: Robot navigating in an open area

In these experiments, the distance ( $d_i(t)$ ) and the vision cone ( $\alpha_i^{(1)}, \alpha_i^{(2)}$ ) from P3 to the closest obstacle are measured by SICK laser range finder (for the front area) and ultrasonic sensors (for the rear area). The position ( $x(t), y(t)$ ) and orientation ( $\theta(t)$ ) of P3 are fed back from encoders attached to the motors of both wheels. The target position ( $T_x, T_y$ ) is prescribed to P3 and the heading ( $H(t)$ ) can be calculated by simple geometry. These information is sent to a notebook where the appropriate control signals are computed.

The first experiment is carried out in a general open area. The movements of the robot is governed by our biologically-inspired navigation algorithm. The proper

switching between the obstacle avoidance law (2.9) and the target pursuit law (2.10) allows the robot to efficiently avoid the obstacles (see Fig. 2.12(a), Fig. 2.12(b) and Fig. 2.12(c)) and safely arrive at the target location (see Fig. 2.12(d)).

In the next experiments, we examine the performance of the proposed navigation algorithm in a corridor with stationary and moving obstacles. The robot needs to avoid these obstacles while not colliding into the walls. Note that in the experiments, the vision cone to the obstacles are finite. In particular, the vision cone of a wall consists of straight lines connecting the robot and points of the wall at the distance less than value  $D$ . In Fig. 2.13, the robot avoids two stationary obstacle in Fig. 2.13(a), Fig. 2.13(b) and a moving obstacle in Fig. 2.13(c). During the avoidance maneuver, the robot is able to keep a certain distance to the obstacles and the walls. The complete path taken by the robot is shown in Fig. 2.13(d). A similar experiment is presented in Fig. 2.14, in this experiment, one more moving obstacle is brought into the scene and the stationary obstacles are moved close to the center of the corridor which restricts the maneuver area for the robot.

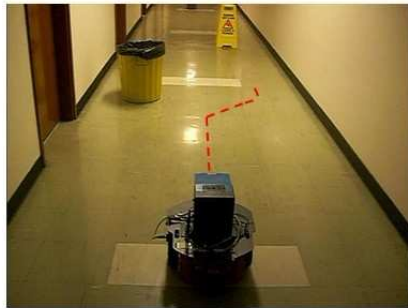
The last experiment shows the ability of the proposed navigation algorithm to avoid obstacles with non-linear velocities. The avoidance of obstacles with non-linear velocities is much more difficult since the future trajectory of the obstacles is more unpredictable and the non-linear velocities are much difficult to estimate (possible solution can be found in [47,173,197]). In this experiment, we use another P3 robot as the obstacle, the maneuver of this obstacle is limited by non-holonomic constraints and its angular velocity is severely limited for the obstacle avoidance to be possible. Fig. 2.15 and Fig. 2.16 show two examples of avoidance of obstacle with non-linear velocity.

## 2.6 Summary

In this section, we present a biologically-inspired navigation algorithm for non-holonomic mobile robots. The proper switching between the obstacle avoidance



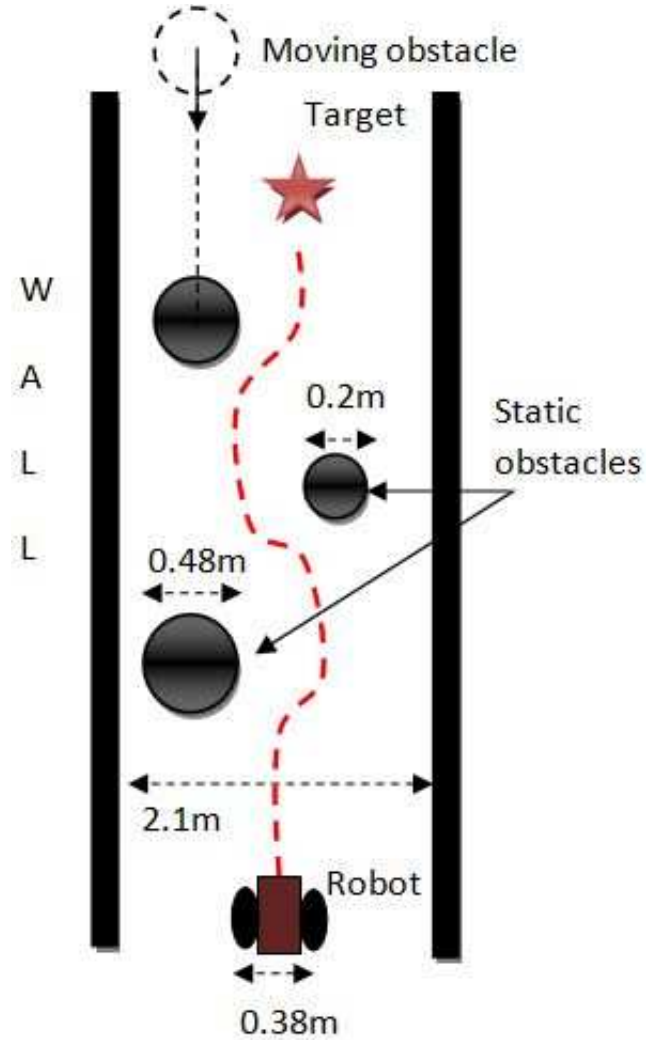
(a)



(b)



(c)

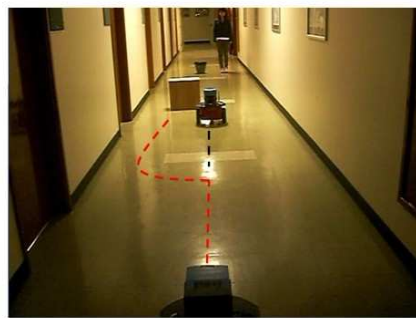


(d)

Figure 2.13: Robot navigating in a corridor with stationary and moving obstacles case 1

law and the target pursuit law guarantees the safety of the mobile robot in cluttered dynamic environment, and safely drives the mobile robot to the target position. The performance of our real-time navigation strategy is confirmed by extensive computer simulations and experiments with a Pioneer 3-DX mobile robot.





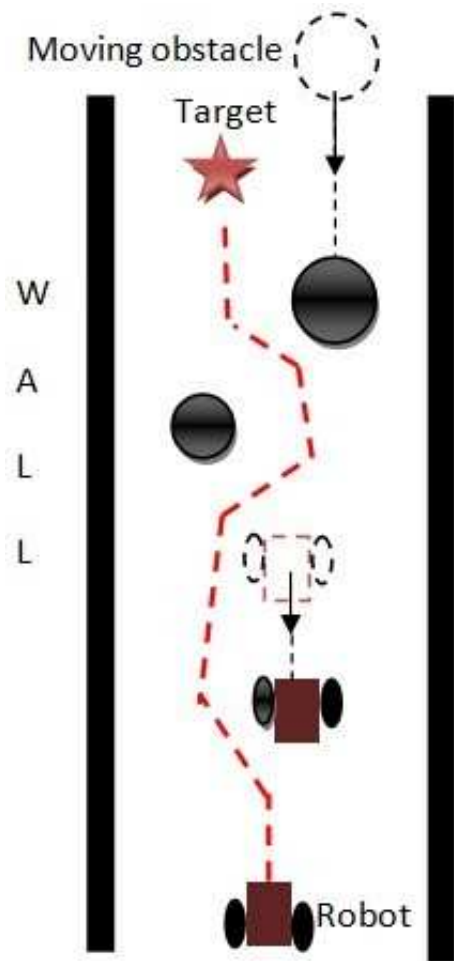
(a)



(b)



(c)



(d)

Figure 2.14: Robot navigating in a corridor with stationary and moving obstacles case 2

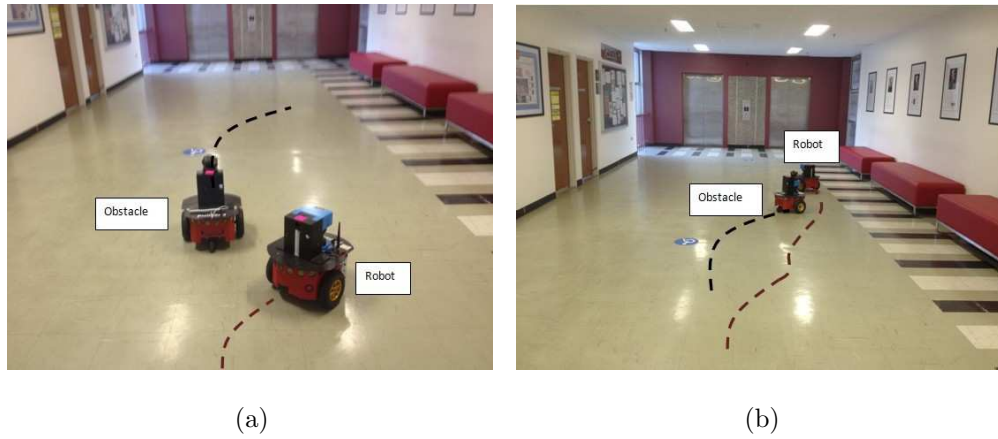


Figure 2.15: Robot avoiding obstacle with non-linear velocity case 1

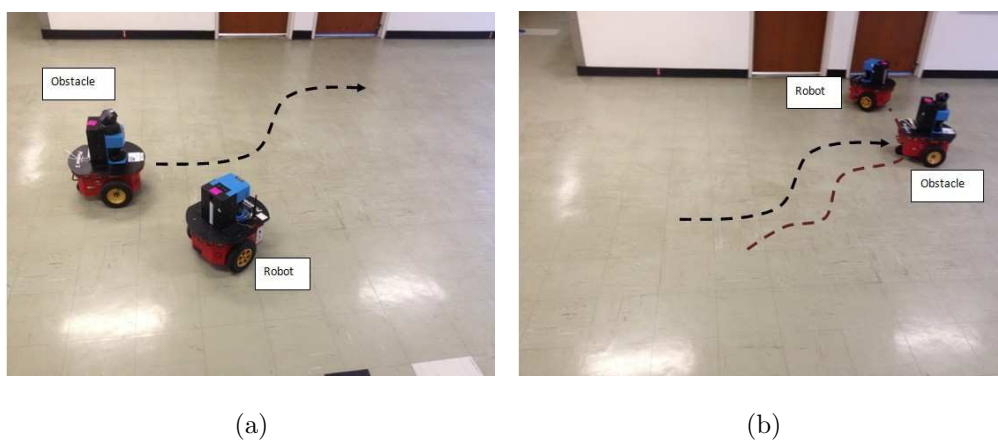


Figure 2.16: Robot avoiding obstacle with non-linear velocity case 2

## 34Biologically-Inspired Obstacle Avoidance Strategy for Safe Navigation



## Chapter 3

# Range-only Based Obstacle Avoidance Strategy for Safe Navigation in Uncertain Dynamic Environments

The navigation of mobile robot in uncertain dynamic environments is a very challenging topic in robotics due to limited information available. The term uncertain implies the mobile robot may observe only a small part of the obstacle, may not distinguish between its points, and so may be unable to estimate many of its parameters, especially the size, center, edge and full velocity etc. In this section, we present a reactive navigation algorithm for non-holonomic mobile robot. Unlike the previous researches on navigation in uncertain environments, such as BUG algorithm [81], the obstacles are assumed stationary in the environment, our proposed navigation algorithm deals with dynamic obstacles in uncertain environments. The proposed navigation algorithm does not need to build a complete map for the environment or to recognise individual obstacle in the scene, it does not require data, either exact or estimated, about the obstacle' size, position, orientation and velocities, which is required by many other existing algorithms such as Velocity Obstacle

Approach [27, 28]. Additionally, the obstacles are not assumed to be rigid or even solid. They are continuums of arbitrary and time-varying that may rotate, twist, wring, skew, wriggle or be deformed in any other way. The only information available is the minimum distance from the mobile robot to the nearest obstacle.

### 3.1 Problem Description

We consider a mobile robot which travels in a plane. Its motion is controlled by its speed  $v$  and angular velocity  $u$  both limited by given constants  $V$  and  $\bar{u}$ . The position of mobile robot is represented by the absolute Cartesian coordinate  $(x, y)$  of the reference point, which is the center of axle connecting the two driving wheels. Its orientation is given by the angle  $\theta$  between the mobile robot centerline and the abscissa axis. The mathematical model of the mobile robot is described by the following equations:

$$\begin{aligned} \dot{x} &= v \cos \theta, & x(0) &= x_0, \\ \dot{y} &= v \sin \theta, & y(0) &= y_0, \\ \dot{\theta} &= u & \theta(0) &= \theta_0 \end{aligned} \tag{3.1}$$

where

$$u \in [-U_{max}, U_{max}], \quad v \in [0, V]. \tag{3.2}$$

These equations describes the ability of the mobile robot to move forward with a certain speed in the forward direction along planar curves whose curvature radius exceeds a given threshold. In this case, this minimal turning radius equals

$$R = v/\bar{u} \tag{3.3}$$

There are multiple unknown disjoint static and moving obstacles in the same plane as the mobile robot. At time  $t$ , each of them occupies a certain domain  $D_i$ , where  $i = 1, 2, \dots, n$  is the serial number of the obstacle. The information regarding to these obstacle is scarce: the positions of them are not known in advance and they may undergo arbitrary motions. Furthermore, there is no specifications on the shapes of the obstacles and the obstacles are not necessarily a rigid body: they may

perpetually change their shapes and undergo any displacements and deformations, including stretches, bends, twists, etc. We do not limit ourselves to a particular type of the obstacle kinematics and do not specify whether the obstacles are rigid, elastic, or plastic solid or fluid.

The only information that is available to the mobile robot is the current distance  $d(t) := \mathbf{dist}_{D(t)}[r(t)]$  to the closest obstacle  $D(t)$  and the rate  $\dot{d}(t)$  at which this measurement evolves over time. Here  $r := [x, y]^\top$  is the vector of the coordinates of the mobile robot and

$$\mathbf{dist}_D(r) := \min_{r' \in D} \|r - r'\| \quad (3.4)$$

(see Fig.3.1(b)), where  $\|\cdot\|$  denotes the standard Euclidean vector norm and the minimum is achieved if  $D$  is closed.

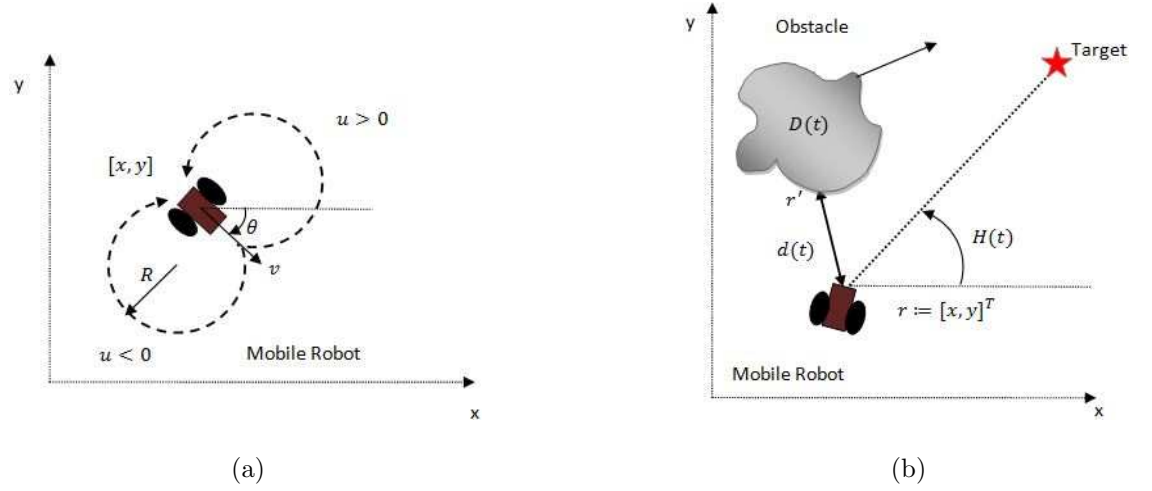


Figure 3.1: (a)Coordinates and orientation of the mobile robot and its minimal turning radius  $R$ ; (b)Moving domain  $D(t)$  and heading to target  $H(t)$

Finally, there is a steady point-wise target  $\mathbf{T}$  in the plane and the mobile robot is able to measure the heading  $H(t)$  towards the target, see Fig.3.1(b). The objective is to guide the mobile robot through the obstacle-free part of the plane and reach the target  $\mathbf{T}$  at a certain time  $t_f > 0$ :

$$r(t_f) = \mathbf{T}; \quad r(t) \notin \bigcup_{i=1}^n D_i(t) \quad \forall t \in [0, t_f].$$

Moreover, the distance between the mobile robot and any obstacle should constantly exceed a given safety margin  $d_{\text{safe}} > 0$ :

$$\text{dist}_{D_i(t)}[r(t)] \geq d_{\text{safe}} \quad \forall t \in [0, t_f], i = 1, \dots, n. \quad (3.5)$$

## 3.2 Reactive Navigation Algorithm

In this section, we present a description of the proposed navigation algorithm, which combines a sliding mode obstacle avoidance strategy and a target reaching strategy. The obstacle avoidance strategy is activated when an obstacle is nearby and the target reaching strategy is put to use when there is no threat of collision.

We first examine the obstacle avoidance strategy:

$$u(t) = U_{\max} \cdot \text{sgn}\{\dot{d}(t) + \chi[d(t) - d_0]\}, \quad \text{where} \quad (3.6)$$

$$\chi(z) := \begin{cases} \gamma z & \text{if } |z| \leq \delta \\ v_* \text{sgn}(z) & \text{if } |z| > \delta \end{cases} \quad (v_* := \gamma\delta) \quad (3.7)$$

is the linear function with saturation, see Fig.3.2, whereas  $\gamma > 0, \delta > 0$ , and  $d_0 > d_{\text{safe}}$  are the controller parameters, with the last of them  $d_0$  being the desired distance to the obstacle when bypassing it.

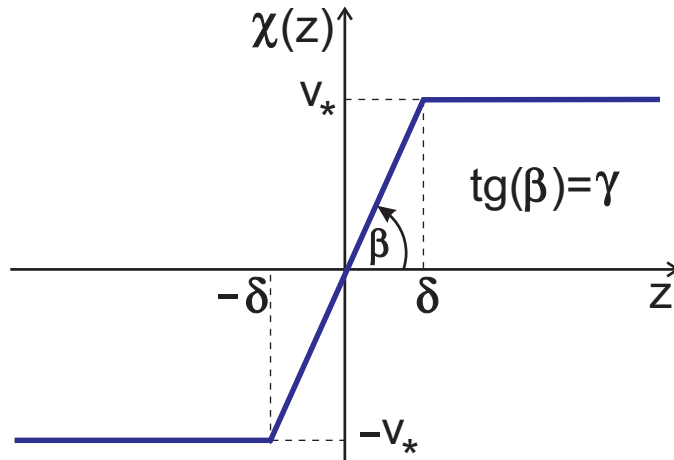


Figure 3.2: Linear function with saturation

The proposed obstacle avoidance strategy belongs to the class of sliding mode control algorithms; see e.g. [183]. The intuition behind this strategy is that in the sliding mode, the equation  $\dot{d} + \chi(d - d_0) = 0$  of the sliding surface is satisfied, according to which the mobile robot is steered towards the desired distance  $d_0$  to the obstacle. For this to take effect, the sliding mode maneuver should be at least realistic. Since the derivative  $\dot{d}$  does not exceed  $|\dot{d}| \leq v_r$  the relative speed  $v_r$  of the mobile robot with respect to the obstacle, this means that in (3.7), the saturation level  $v_*$  should not exceed this speed. This can be achieved by proper tuning of the controller parameters  $\gamma$  and  $\delta$  based on available estimates of the speeds of the obstacles. If initially the mobile robot is not on the sliding surface, the control law (3.6) quickly drives it to this surface after a short initial turn with the maximal steering actuation, see [102] for details. So sliding motion is the main part of the obstacle avoidance maneuver.

In more details, this motion looks as follows. The equation  $\dot{d} + \chi(d - d_0) = 0$  means that the angle  $\alpha$  between the relative velocity of the mobile robot  $\vec{v}_r$  and the line of sight at the nearest point of the obstacle equals  $\alpha = \arccos \frac{\chi(d-d_0)}{v_r}$ . It follows that the angle  $\alpha$  is obtuse for  $d < d_0$  and acute for  $d > d_0$ , and so the mobile robot is driven towards the desired distance  $d_0$  to the obstacle. In doing so, the angle  $\alpha$  is kept constant  $\alpha = \arccos[\frac{v_*}{v_r} \text{sgn}\chi(d - d_0)]$  in the saturation zone  $|d - d_0| > \delta$ . As  $d$  leaves this zone and approaches  $d_0$ , the angle goes to  $\frac{\pi}{2}$ . In the limit where  $d = d_0$ , the mobile robot is oriented parallel to the border of the obstacle  $\alpha = \pi/2$ , which means traveling along the  $d_0$ -equidistant curve, see Fig.3.3(b).

The above control law (3.6) is activated in a close vicinity of an en-route obstacle. Whenever the mobile robot is far away from them, it is driven towards the target in a straight line and so

$$u(t) = 0; \tag{3.8}$$

Switching between two control laws (3.6) and (3.8) is based on two parameters:  $C > 0$  — the threshold distance at which the obstacle avoidance maneuver is activated, and  $\epsilon > 0$  — the mismatch between the current and desired  $d_0$  distances to the



Figure 3.3: (a)Sliding mode maneuver; (b)linear mode maneuver

obstacle with which termination of the obstacle avoidance maneuver is permitted. Specifically, the switching rules are as follows. Switching from (3.8) to (3.6) occurs whenever the distance to the nearest obstacle reduces to  $C$ ; switching from (3.6) to (3.8) occurs when  $d \leq d_0 + \epsilon$  and the mobile robot is oriented towards the target. This switching strategy allows the mobile robot to keep a safe distance to the obstacles and reach the target position in a dynamic environment [102].

An example of its execution in a simple scenario is depicted in Fig. 3.4.

Mathematically rigorous analysis of the presented algorithm under some technical assumptions was given in [102].

### 3.3 Computer Simulation Results

In this section, the performance and features of the proposed navigation algorithm in uncertain dynamic environments are demonstrated by computer simulations performed in Matlab. In the following simulation figures presented, we depict the mobile robot gray disk and obstacles by black circle/block, the paths taken by the mobile robot to avoid the obstacles are shown by a series of gray disk and its current heading is presented by an arrow.

We first demonstrate the performance of the proposed navigation algorithm in

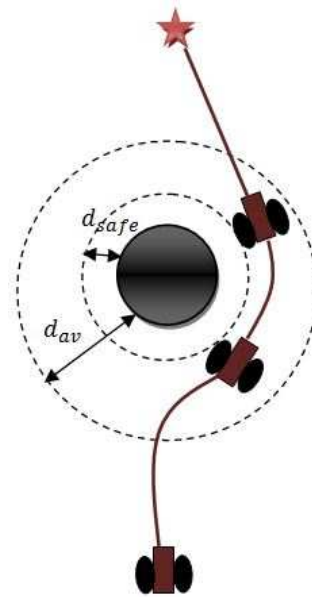


Figure 3.4: Execution of the proposed navigation algorithm in a simple scenario

uncertain dynamic environment, see Fig. 3.5. Notice that the robot does not require any information about the properties of the obstacles in advance. In Fig. 3.5(a), it can be observed that the two different types of obstacles are shown: one single obstacle and a chain of obstacles (this group is treated as one obstacle). The initial position and moving direction of these obstacles are also shown. In Fig. 3.5(b) and Fig. 3.5(c), the robot tracks the  $d_0$ -equidistant curves (dashed lines around the obstacles) of the obstacles regardless the shape of the obstacle when the obstacle avoidance mode is activated. The complete path taken by the robot to the target location while avoiding en-route obstacles are shown in Fig. 3.5(d). During the whole simulation, the only data measurable by the robot is the minimum distance between itself and the closest obstacle, this data is shown in Fig. 3.5(e). It can be seen that the robot maintains a constant distance ( $1.5m$ ) to the closest obstacle during its obstacle avoidance maneuver.

We enhance the mobility of the obstacle in the next simulation. In Fig. 3.6, the obstacles (crosses) are not only moving in straight line but also rotating slowly around their center points, the direction of their movement and rotation are depicted

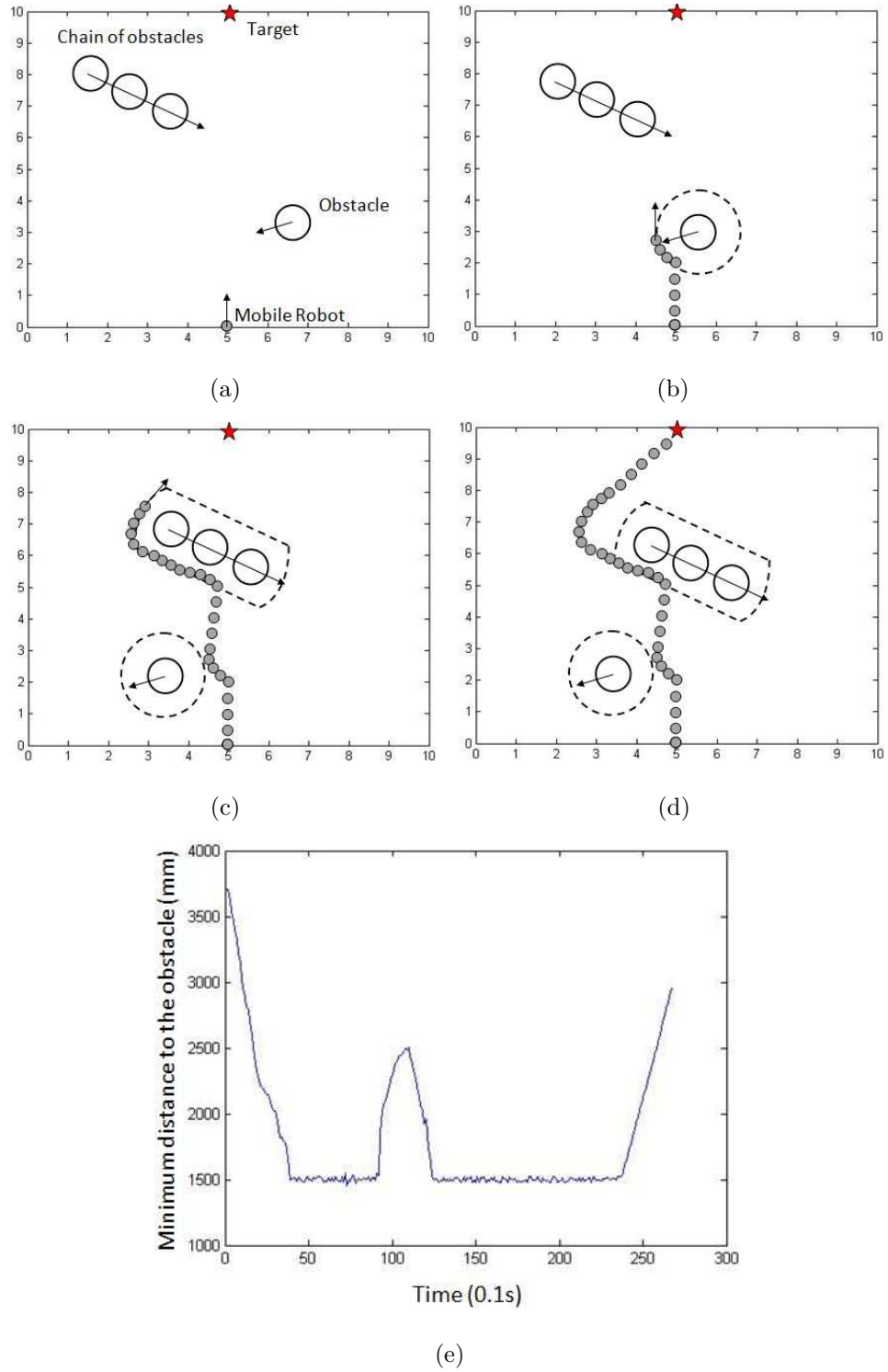


Figure 3.5: Mobile robot navigating in uncertain dynamic environments



in Fig. 3.6(a). In order to avoid these obstacles, the proposed navigation algorithm is able to adapt the rotational movement of the obstacle and keep itself away from any part of the obstacle, especially the "wings" of the crosses. The robot successfully avoids the obstacles and arrives the target position in Fig. 3.6(b), Fig. 3.6(c) and Fig. 3.6(d). This simulation shows that the proposed navigation algorithm can cope with obstacles undergoing complex motions.

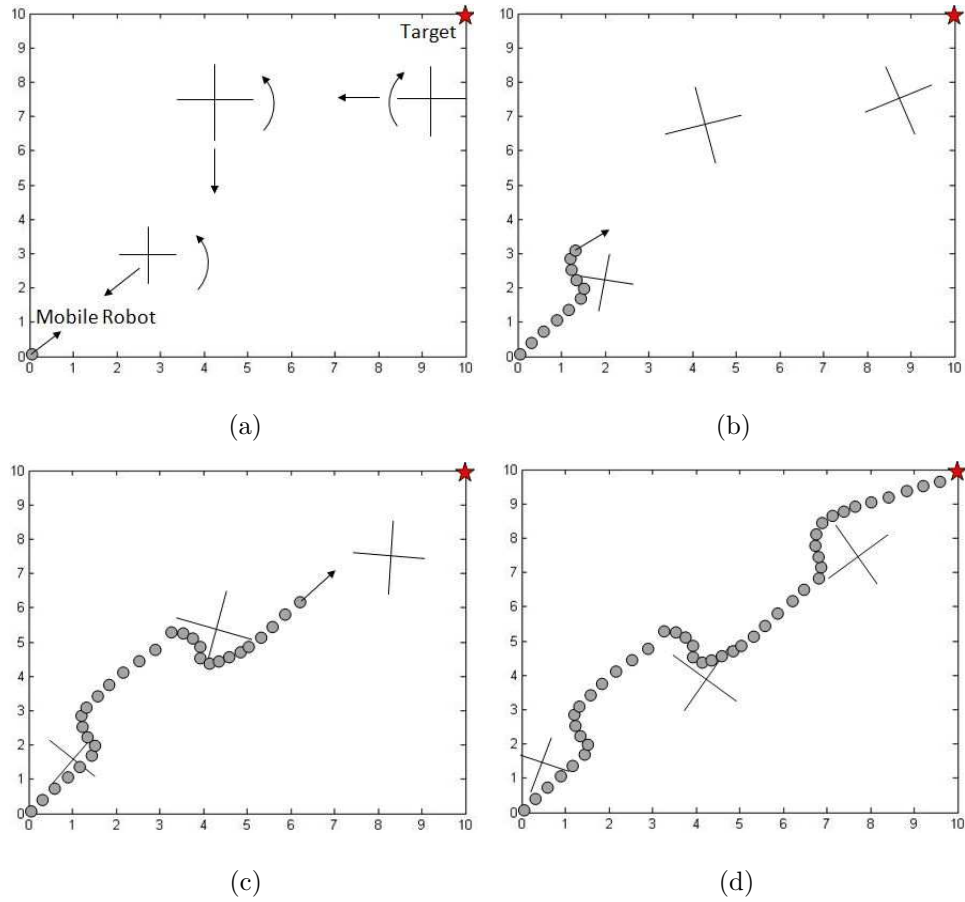


Figure 3.6: Mobile robot avoids moving and rotating obstacles

The performance of our proposed navigation algorithm can be improved by the on-the-fly interpolation technique, which treats several closely positioned obstacles one single deformed object. This technique gives the proposed algorithm extra flexibility in the scenes with multiple stationary and moving obstacles, such as corridor with multiple pedestrians and train stations with many passengers. The utilisation of the interpolation technique together with the proposed navigation is presented

in Fig. 3.7, where the mobile robot is facing one moving obstacle which travels towards a stationary block obstacle. In Fig. 3.7(a), the mobile robot treats these two obstacles as one single obstacle and avoids it in a path shown in Fig. 3.7(b). If the interpolation technique is not put to use in this case, the robot will avoid the moving obstacle once the distance between them is reduced below threshold distance  $C$ , and ignore the existence of the static obstacle, which will result a collision as shown in Fig. 3.7(c).

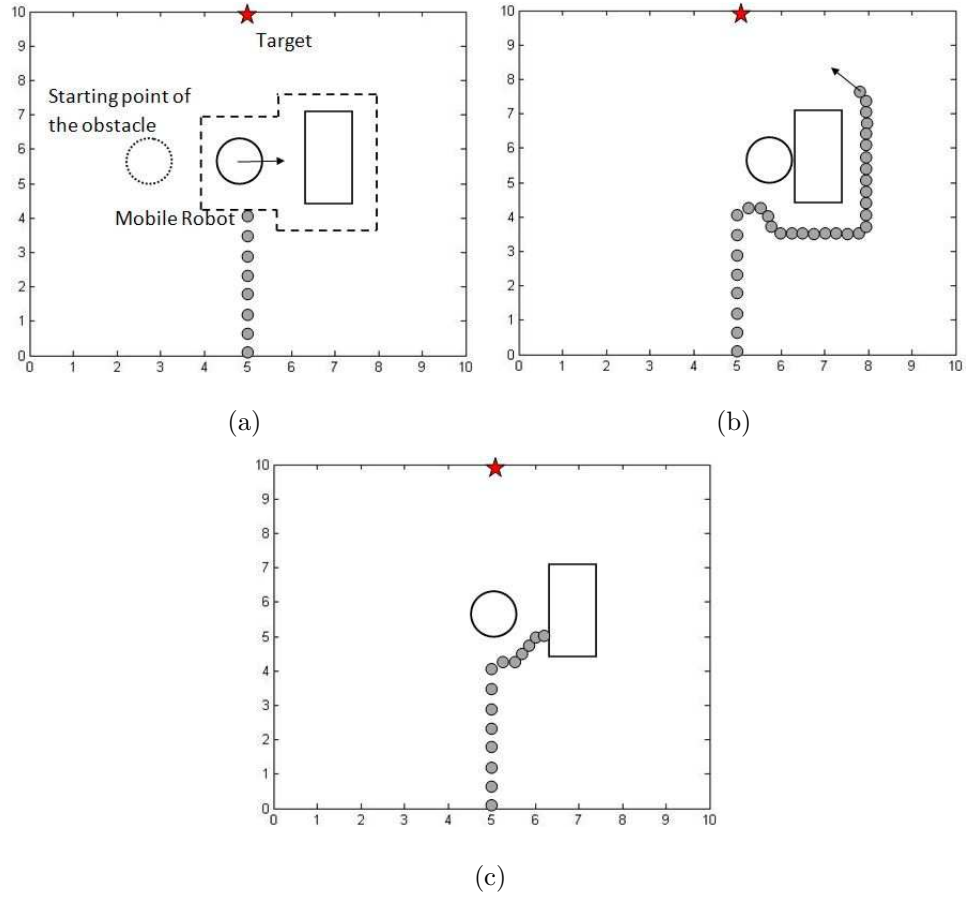


Figure 3.7: The implementation of interpolation technique with the proposed navigation algorithm

The next simulation result demonstrate the ability of the proposed navigation algorithm to avoid dynamic deforming obstacles. The dynamic deforming obstacles with time-varying shapes covers many complex real life scenarios. For example, scenarios with reconfigurable rigid obstacles, rigid obstacles with large moving parts,

forbidden zones between moving obstacles, like inter-vehicle those in a dense platoon, flexible underwater obstacles, like fishing nets, schools of big fish, bunches of cables, etc., and virtual obstacles, like areas corrupted with hazardous chemicals, vapor, radiation, high turbulence etc. or on-line estimated areas of operation of a hostile agent.

In Fig. 3.8, a group of three obstacles are interpolated as one obstacle, and its movement is led by the first obstacle (the leader), the obstacle moves in a sinusoidal fashion as shown in Fig. 3.8(a). Fig.3.8(b) and Fig.3.8(c) show the moments for which the mobile robot avoids this dynamic deforming obstacle, notice that the shape of the obstacle is different from each other in each of the figures.

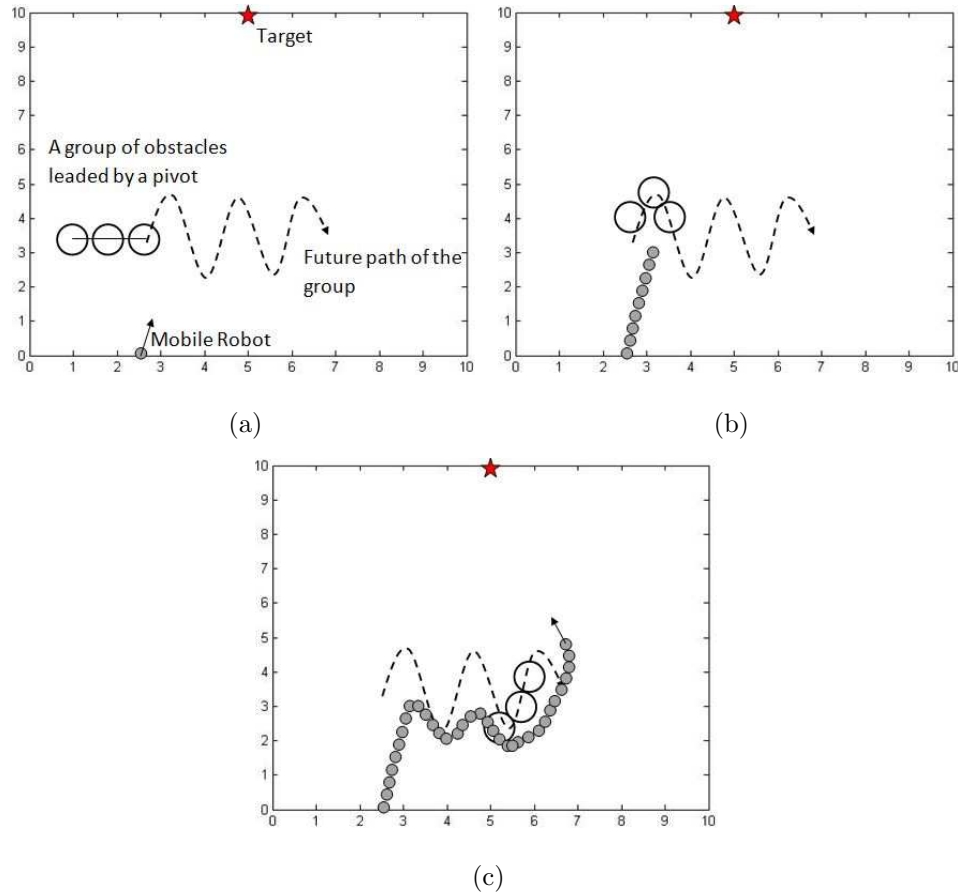


Figure 3.8: Mobile robot avoids dynamic deforming obstacle

The last simulation result presents the comparison between the performance of the proposed navigation algorithm with that of Velocity Obstacle Approach (VOA)

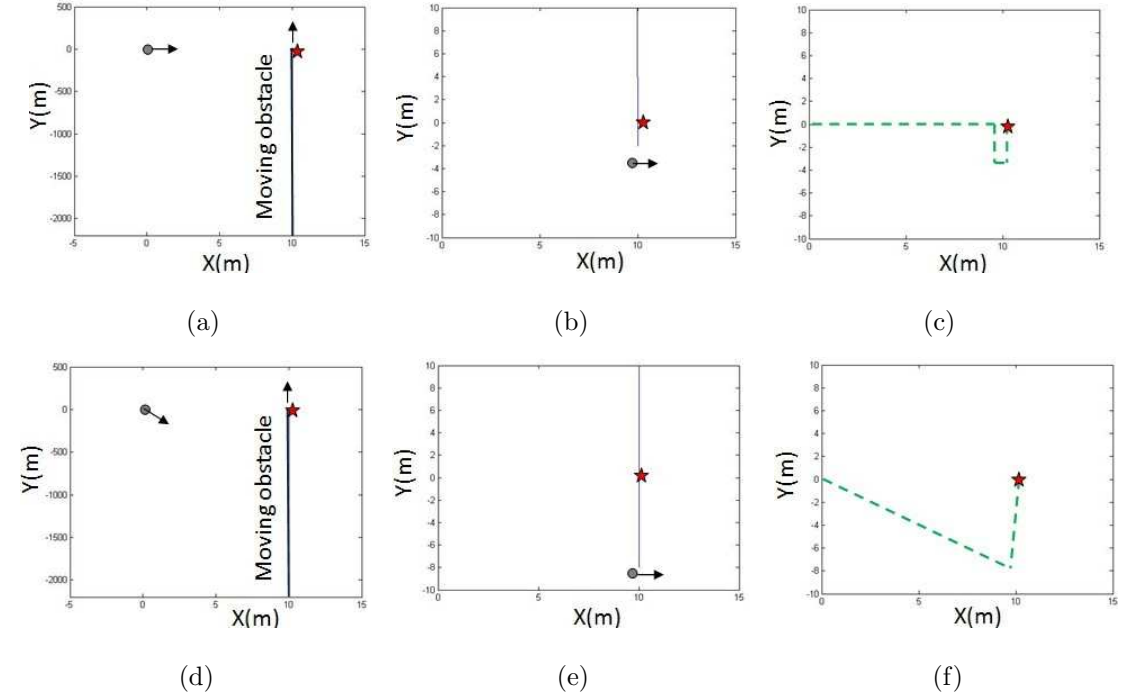


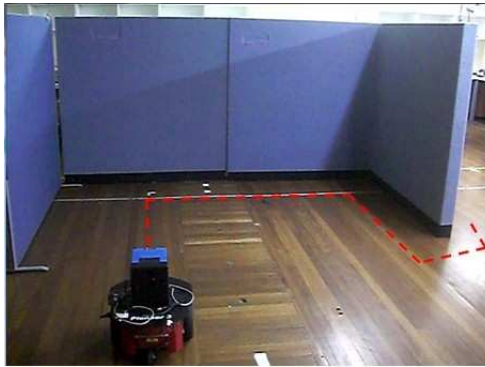
Figure 3.9: Proposed navigation algorithm (upper row) versus VOA (lower row)

[26,68] in the scenario where a long obstacle perpendicularly intervenes between the robot and the target, which is hidden just behind the obstacle, see Fig. 3.9(a) and Fig. 3.9(d). Fig. 3.9(b) and Fig. 3.9(e) display the situations at the moments when the robot transverses the path of the obstacle. The entire paths of the robot during target reaching with obstacle avoidance are depicted in Fig. 3.9(c) and Fig. 3.9(f). (We considered VOA with two choices of velocity per maneuver, with the second choice being made at the favorable moment of bypassing the obstacle.) The proposed navigation algorithm first drives the robot directly to the target in a straight line until the trigger threshold is trespassed and then undertakes a relatively small detour by following the obstacle boundary. VOA basically drives the robot to the target along two straight lines with bypass of the obstacle in a close range at the rear. Thus the both guidance laws do drive the robot to the target. However PGL does this faster: the ratio of the maneuver times is as follows  $\frac{T_{\text{Proposed}}}{T_{\text{VOA}}} = \frac{14.51}{18.61} \approx 0.78$ . Thus in this experiment, the proposed navigation algorithm outperforms VOA.

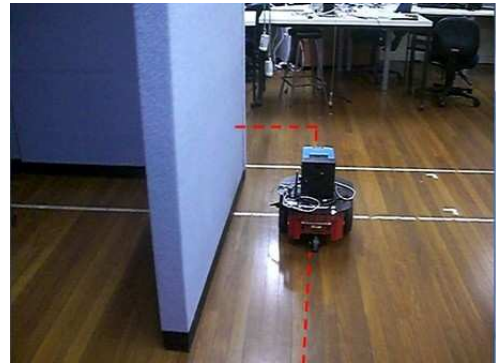
### 3.4 Experiments with Real Mobile Robot

The performance and applicability of the proposed navigation algorithm is examined on ActivMedia Pioneer 3-DX (P3) robot.

In these experiments, the only information available to the mobile robot P3, which is the distance between itself and the closest obstacle, is measured by the SICK laser range (for the front area) finder and ultrasonic sensors (for the rear area). Any other information about the obstacles is not known to P3 prior and during the experiments.



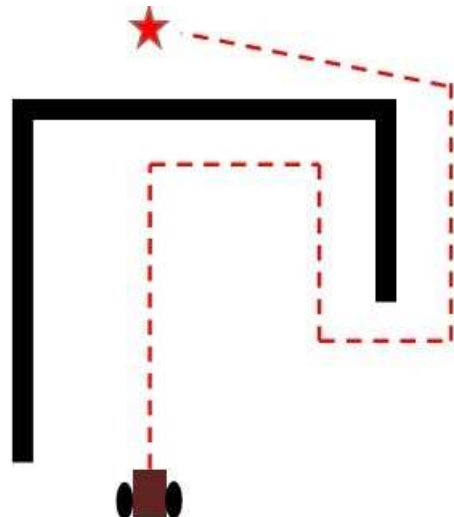
(a)



(b)



(c)



(d)

Figure 3.10: Robot avoids U-shape obstacle

The first experiment shows the avoidance of a U-shape obstacle using the pro-

posed navigation algorithm. the robot move straight towards the target location, which is behind the obstacle, until it senses the obstacle within the threshold distance. The robot starts to avoid the obstacle by keeping constant distance to it, see Fig. 3.10(a) and Fig. 3.10(b). In Fig. 3.10(c), the robot is oriented towards the target and safely move towards it. The complete path is depicted in Fig. 3.10(d).

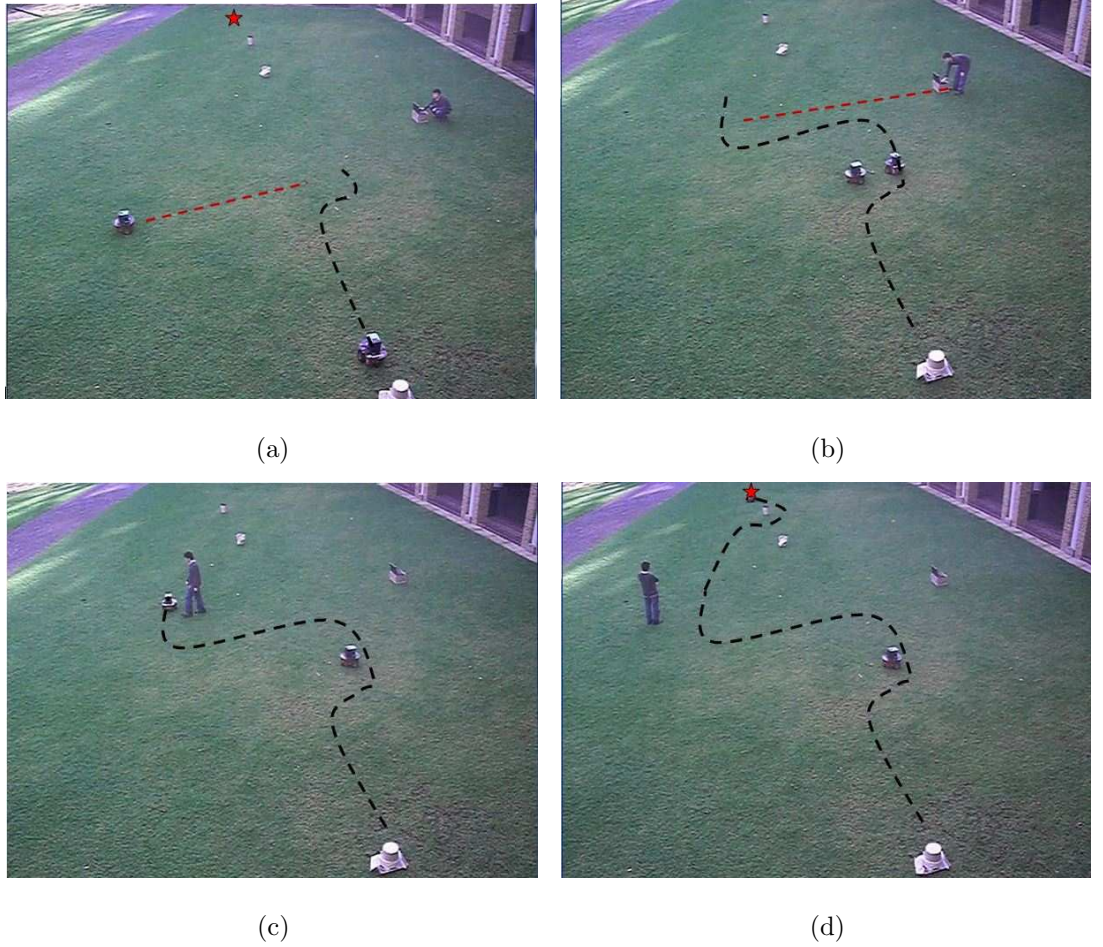


Figure 3.11: Robot navigating in an environment with stationary and dynamic obstacles

The next experiment demonstrate the basic ability of the proposed navigation algorithm to guide the mobile robot in an environment with stationary and dynamic obstacles. At the beginning of the experiment, the mobile robot moves towards the target because there is no threat of collision. When there is an obstacle detected within the threshold distance  $C$ , the mobile robot avoid colliding into the obstacle



by keeping a constant distance between itself and the obstacle, i.e. tracking the  $d_0$ -equidistant curve, the mobile robot continues to pursuit the target when  $d \leq d_0 + \epsilon$  and the robot is oriented towards the target. see Fig. 3.11(a), Fig. 3.11(b) and Fig. 3.11(c). The complete path is shown in Fig. 3.11(d).

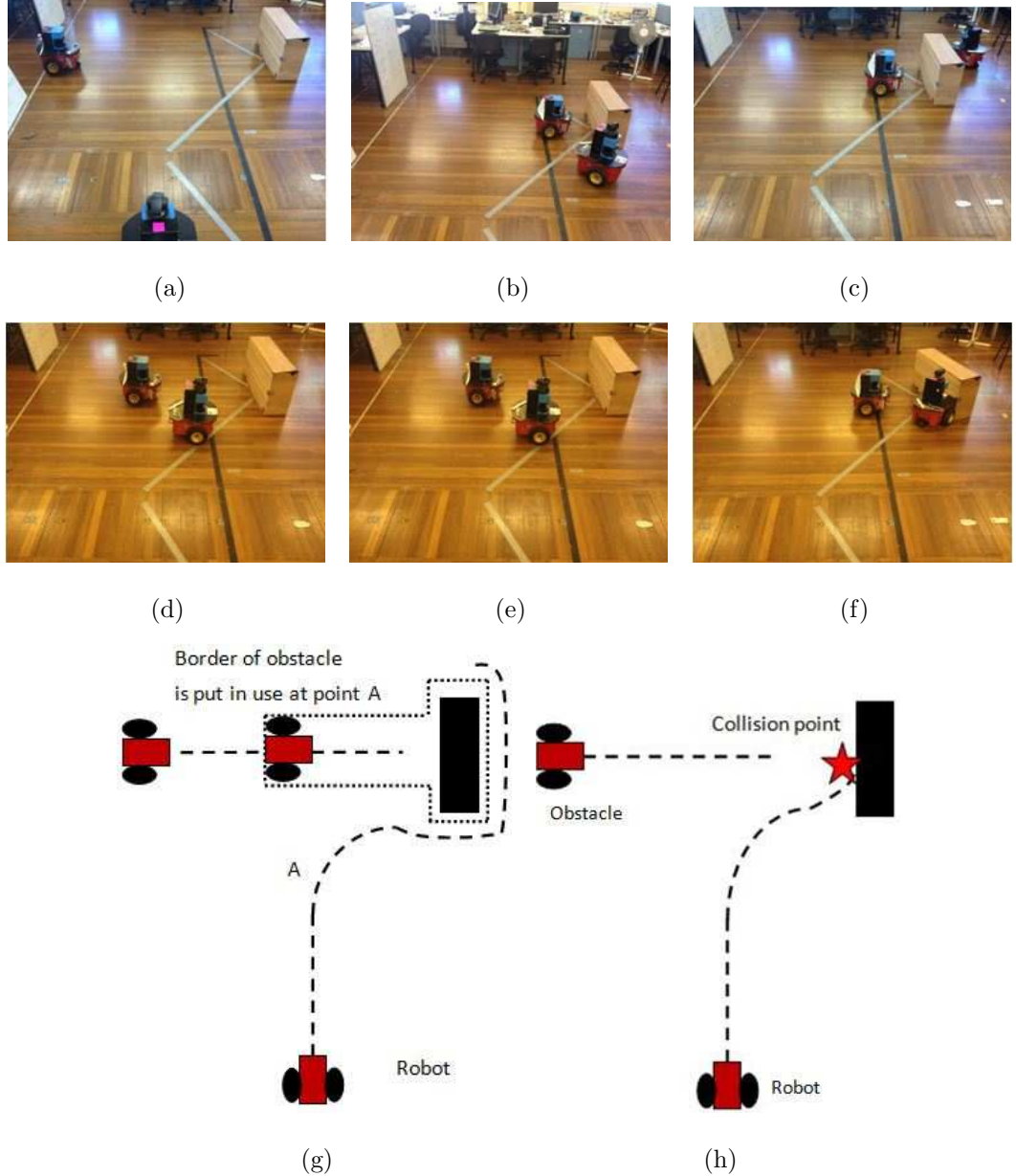


Figure 3.12: The implementation of the proposed navigation algorithm with the interpolation technique

In Fig. 3.12, the implementation of the proposed navigation algorithm with the

interpolation technique (as discussed in Fig. 3.7) is shown. In this scenario, the robot successfully avoid the moving obstacle and the stationary obstacle by considering them as one obstacle using interpolation technique, see Fig. 3.12(a), Fig. 3.12(b) and Fig. 3.12(c) . Note that the interpolation technique is put in use when the obstacles are closely positioned, for example, as shown in Fig. 3.12(g), the interpolation is put in use at point A rather than at the beginning of the experiment, which otherwise would create a very large obstacle with spacious maneuverable gap in between them. However, the robot collides into the box while avoiding the moving obstacle if the interpolation technique is not put in use, as seen in Fig. 3.12(d), Fig. 3.12(e) and Fig. 3.12(f). The comparison of the overall paths taken by the robot for these two cases are present in Fig. 3.12(g) and Fig. 3.12(h).

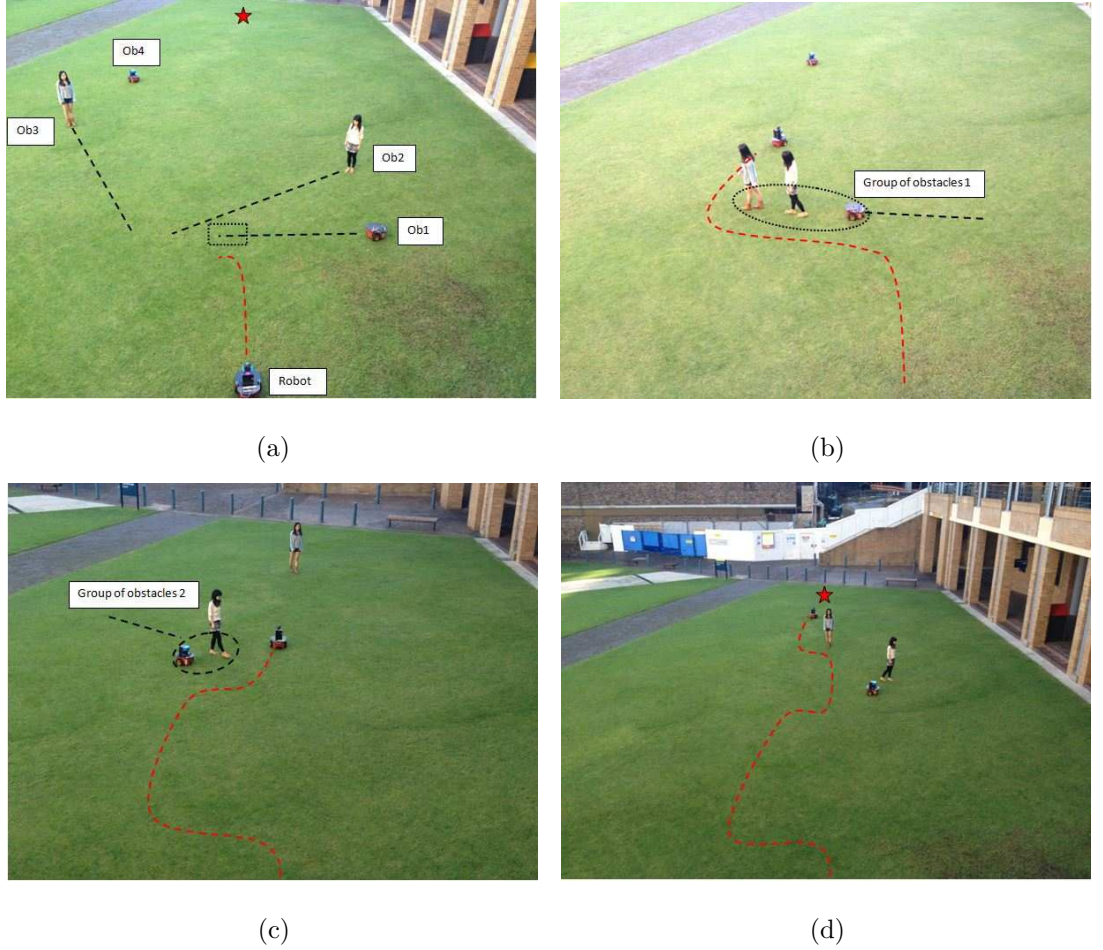


Figure 3.13: Robot avoids tight clusters of obstacles with dynamical changing radii



The proposed navigation algorithm with interpolation technique can be used to deal with more complicated real life scenario such as obstacles with dynamical changing radii and tight clusters of obstacles. Fig. 3.13 shows an example of such scenario. In Fig. 3.13(a), the robot starts to bypass obstacle 1 (ob1), the obstacles ob2 and ob3 approach ob1, see Fig. 3.13(a), thus forming a tight cluster (group of obstacles) which move in a common direction of ob1. The imaginary border of this group of obstacles is indicated by the dashed line. The robot is able to keep a constant distance to the imaginary border of the group and avoid the group as a whole, see Fig. 3.13(b). After this, the robot encounters the second group of obstacle 2 and one single obstacle with different radii, the robot is able to avoid both of them and safely arrive the target location, see Fig. 3.13(c) and Fig. 3.13(d).

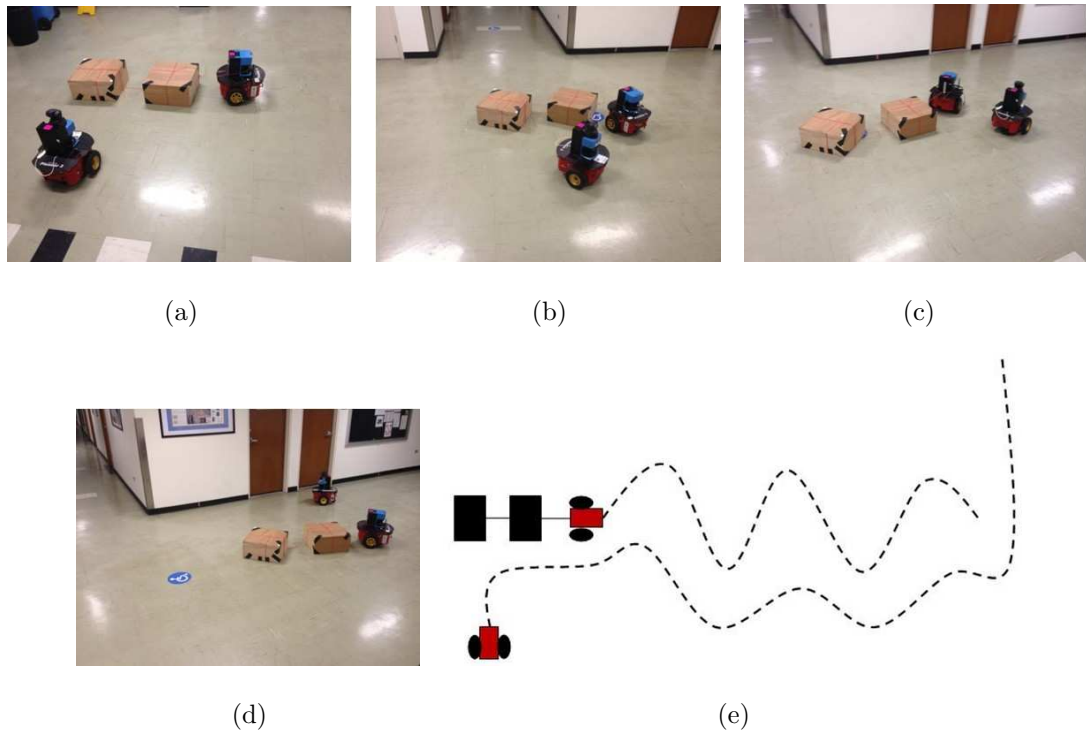


Figure 3.14: Robot avoids deforming obstacle

In the last experiment, the robot faces an obstacle with deforming shape. This obstacle consists of a P3 robot towing two boxes forming a chain of interconnected obstacles. The inter-element free spaces in the chain are interpolated so that the robot has to avoid the resultant snake-like obstacle. The towing robot moves in

a sinusoidal fashion so that the obstacle "snake" squirms. The challenge is that the robot needs to keep a constant distance to the border of the obstacle which is time-varying, see Fig. 3.14(a), Fig. 3.14(b), Fig. 3.14(c) and Fig. 3.14(d). The complete path for the robot to avoid this obstacle with deforming shape is depicted in Fig. 3.14(e)

### 3.5 Summary

A sliding mode based navigation algorithm for non-holonomic mobile robots has been proposed. The proposed navigation algorithm is safe and implement cost-efficient, which guarantees the safety of the mobile robots in uncertain dynamic environments. The efficiency of the proposed algorithm are illustrated by extensive computer simulations. The applicability of the proposed algorithm in many challenging real life scenario are demonstrated by experiments with P3 mobile robot.

## Chapter 4

# Navigation Algorithm Based on an Integrated Environment Representation

A typical obstacle avoidance strategy, when performing navigation tasks in complex environments, avoids "the closest" or "the most dangerous" obstacle and continues to move in a desired direction until another dangerous obstacle is detected. The strategy of this kind raises several issues, e.g, the concept of "dangerous" is hard to be defined and may vary in different scenarios, difficulties in dealing with obstacles which are hidden or outside the sensing range, and the ambiguous case where two or more dangerous obstacles presented at the same time. In this section, we propose instead a novel reactive navigation approach based on an integrated environment representation which overcomes the above problems. This approach is partially inspired by the paradigm shift from binary interaction models to an integrated treatment of multiple interactions which are typical for social interactions in human crowds or animal swarms suggested in [105] for analysis of pedestrian behaviour in crowds. Our approach is based on an integrated representation of the information about the environment in which the combined effect of close multiple stationary and moving obstacles is implicitly included in the representation of a sensing field of the

robot. An advantage of our approach is that we do not have to separate obstacles and approximate their shapes by discs or polygons. Moreover, our algorithm does not require any information on the obstacle's velocities or any other derivatives of measurements. Our approach results in a very efficient and intelligent robotic behaviour. Instead of being repelled by a crowd of obstacles, as it happens for many other navigation algorithms, the robot seeks a path through this crowd.

## 4.1 Problem Description

Consider a non-holonomic mobile robot with hard constraints on its angular velocity. It travels in a two-dimensional plane. The vector of the robot's Cartesian coordinate in this plane is presented by  $[x(t), y(t)]$ , and its heading is given by  $\theta(t)$ . The movement of this mobile robot is controlled by both its speed  $V > 0$  and its angular velocity  $u(t)$ . The mathematical model of the robot is as follows:

$$\begin{aligned} \dot{x}(t) &= V \cos \theta(t), \\ \dot{y}(t) &= V \sin \theta(t), \\ \dot{\theta}(t) &= u(t) \end{aligned} \tag{4.1}$$

where

$$u \in [-U_{max}, U_{max}]. \tag{4.2}$$

Here  $U_{max}$  is the non-holonomic constraint on the angular velocity which is given. The angle  $\theta(t) \in (-\pi, \pi]$  is measured in the counterclockwise direction from the  $x$ -axis.

Let  $\delta > 0$  be the sampling period. The robot updates its angular velocity  $u(t)$  at discrete times  $0, \delta, 2\delta, 3\delta, \dots$ . Also, let

$$c_R(t) := [x(t), y(t)] \tag{4.3}$$

be the vector of the robot's coordinates, and

$$v_R : (t) = \dot{c}_R(t) \tag{4.4}$$

be the robot's velocity vector.

We assume that there exists an unknown dynamic environment, which consists of any number of stationary or moving obstacles which can be deformable. In other words, the environment is described by a time-varying planar subset  $\mathcal{E}(t)$  which is not known to the robot. The current distance  $d(t)$  from the robot to the environment  $\mathcal{E}(t)$  is defined as

$$d(t) := \min_{r \in \mathcal{E}(t)} \|r - c_R(t)\|.$$

Here  $\|\cdot\|$  denotes the standard Euclidean vector norm.

Let  $\theta_0 \in (-\pi, \pi)$  be a given desired direction and  $d_{safe} > 0$  be a given distance. The objective of our proposed navigation algorithm is to navigate the robot in the direction  $\theta_0$  while satisfying the safety constraints  $d(t) \geq d_{safe}$  for all  $t$ , i.e.  $d(t) \geq d_{safe}$  for all  $t \geq 0$

To further ensure the safety of the robot, we define the  $d_{safe}$ -neighborhood of  $\mathcal{E}(t)$  as the enlarged environment  $\hat{\mathcal{E}}(t)$ , see Fig. 4.1. If the robot can avoid colliding into the enlarged environment  $\hat{\mathcal{E}}(t)$ , the robot is considered as safe with respect to the environment  $\mathcal{E}(t)$ .

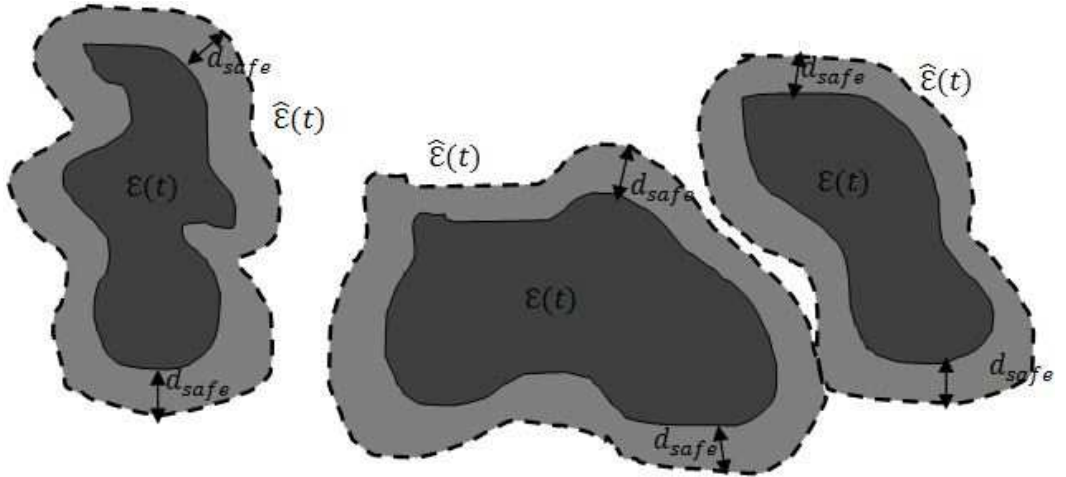


Figure 4.1: The environment (interior darker region)  $\mathcal{E}(t)$ , The enlarged environment (the gray larger region covers  $\mathcal{E}(t)$ )  $\hat{\mathcal{E}}(t)$  and the  $d_{safe}$ -neighbourhood

**Assumption 4.1.1.** The set  $\hat{\mathcal{E}}(t)$  is closed with piecewise analytic boundary.

Let  $D_s > 0$  be the sensing range of the robot. Introduce the binary function  $M(\alpha, t) \in \{0, 1\}$  defined for all  $t \geq 0$  and all  $\alpha \in (\theta(t) - \pi, \theta(t) + \pi)$  as follows:  $M(\alpha, t) = 1$  in the direction defined by the angle  $\alpha$  and the robot's position at time  $t$ , there is a point  $P$  of an enlarged environment  $\hat{\mathcal{E}}(t)$  at the distance  $d_P(t)$  such that

$$d_P(t) \leq D_s \cos \alpha; \quad (4.5)$$

and  $M(\alpha, t) = 0$  otherwise; see Fig. 4.2(a).

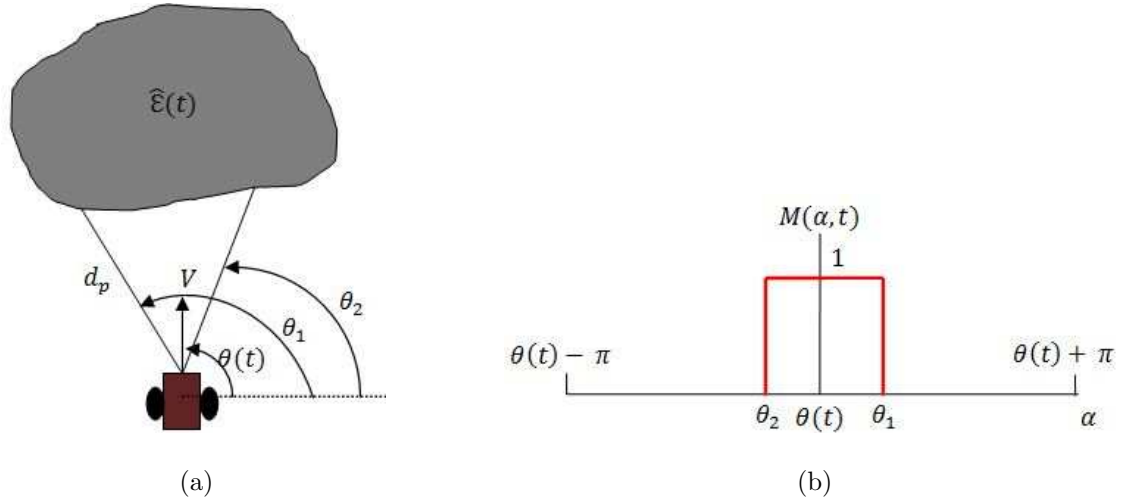
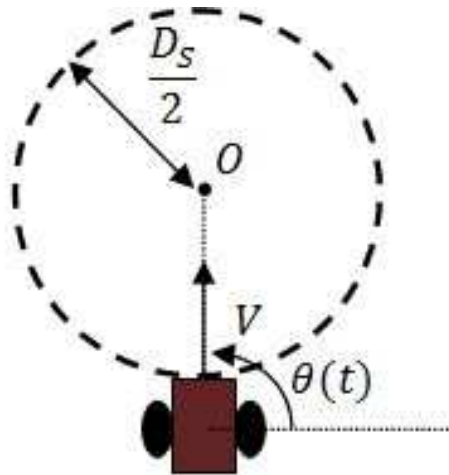


Figure 4.2: Illustration of the binary function  $M(\alpha, t)$

The equation in (4.5) defines a disc  $D$  with diameter  $D_s$  centered at point  $O$  that is  $D_s/2$  ahead of the robot's position at time  $t$  in the direction of its current heading  $\theta(t)$ , see Fig. 4.3. It is straight forward that the binary function  $M(\alpha, t)$  indicate whether the boundary of the area  $D$  has been invaded by some points of the unknown dynamic environments in the direction defined by the angle  $\alpha$ .

In fact, the binary function  $M(\alpha, t)$  about the environment  $\mathcal{E}(t)$  is the only available measurement to the unknown dynamic environment for our algorithm. This measurement is relatively easy to be obtained in practice comparing to that required by other existing approaches. Our algorithm may not require any additional information about the obstacles, these obstacles are not necessarily be rigid and their shapes can be time-varying or deformable. Moreover, our algorithm does not

Figure 4.3: The disc  $D(t)$  of diameter  $D_s$ 

required the exact information or estimation about the velocities of the obstacles and their derivatives.

Finally, the robot has the knowledge of its own heading  $\theta(t)$  and the desired direction  $\theta_0$ .

Now we wish to illustrate a geometric sense of our choice of the disc  $D(t)$  and the related inequality (4.5) as the core of the measurement available to the robot.

Suppose that  $\mathcal{T}$  is a point-wise obstacle moving with an arbitrary time-varying velocity  $v_T(t)$  satisfying the only constraint

$$\|v_T(t)\| \leq V. \quad (4.6)$$

It is obvious that if (4.6) does not hold, it is impossible for the robot to surely avoid collisions with  $\mathcal{T}$  for any navigation strategy.

Now we are in a position to state the following proposition.

**Proposition 4.1.1.** Let  $t_0 > 0$  be a given time and let  $[x_T(0), y_T(0)]$  be the initial condition of the obstacle  $\mathcal{T}$ . Suppose that the robot moves ahead with the control input  $u(t) = 0$  for  $t \in [0, t_0]$ . Then the obstacle  $\mathcal{T}$  does not collide with the robot over time interval  $t \in [0, t_0]$  for any obstacle's satisfying (4.6) if and only if the initial condition  $[x_T(0), y_T(0)]$  does not belong to the disc  $D(0)$  shown in Fig. 4.3 with the diameter  $D_s = 2Vt_0$ .

The proof of Proposition 4.1.1 is presented in [156].

## 4.2 Navigation Algorithm

In this section, we present a description of the proposed navigation algorithm. We start with the necessary assumptions:

**Assumption 4.2.1.** The initial condition of the robot satisfies  $\theta(t) = \theta_0$  and  $M(\alpha, 0) = 0$  for all  $\alpha \in (\theta_0 - \pi, \theta_0 + \pi)$ .

Furthermore, introduce the function  $m(t)$  as follows:

$$\begin{aligned} m(t) : &= 0 \quad \text{if} \quad M(\alpha, 0) = 0 \quad \forall \alpha \in (\theta_0 - \pi, \theta_0 + \pi); \\ m(t) : &= 1 \quad \text{otherwise.} \end{aligned} \tag{4.7}$$

The value  $m(t) = 1$  indicates that there are finite number of open intervals  $(\theta_0 - \pi, \theta_0 + \pi)$  in the set  $\alpha \in (\theta_0 - \pi, \theta_0 + \pi)$ . These intervals are sets of direction that are considered safe to the robot in the sense that they are far enough from the robot's current position.

Let  $j(t)$  be the index of the interval that is closest to the robot's current heading  $\theta(t)$ , which has two possible results: if  $M(t, \theta(t)) = 0$  meaning that the robot's current heading  $\theta(t)$  is safe, thus  $\theta(t) \in (A_i^-, A_i^+)$  for some  $i$ , then  $j(t) := i$ . If  $M(t, \theta(t)) = 1$ , meaning that the enlarged environment has crossed  $D$  in the direction of robot's current heading, thus  $\theta(t) \notin (A_i^-, A_i^+)$ , then

$$j(t) := \operatorname{arccmin}\{|A_i^-|, |A_i^+|\} \tag{4.8}$$

over all  $i$ . In other words,  $j(t)$  is the index  $i$  for which the minimum over numbers  $\{|A_i^-|, |A_i^+|\}$  is achieved. Finally, we define the direction  $C(t)$  as the middle of the interval closest to  $\theta(t)$ , i.e.

$$C(t) := \frac{A_{j(t)}^- + A_{j(t)}^+}{2}. \tag{4.9}$$

Our navigation algorithm law for controlling the robot's angular velocity  $u(t)$  as discrete times  $0, \delta, 2\delta, 3\delta, \dots$  is as follows:



**if**  $m(k\delta) = 0$  **then**  $u(t) := U_{max} \text{sign}(\theta_0 - \theta(t)) \quad \forall t \in [k\delta, (k+1)\delta);$   
**if**  $m(k\delta) = 1$  **then**  $u(t) := U_{max} \text{sign}(C(t) - \theta(t)) \quad \forall t \in [k\delta, (k+1)\delta);$

Here  $C(t)$  is defined by (4.9) and  $\text{sign}(\cdot)$  is the standard sign function

$$\text{sign}(x) := \begin{cases} -1 & \text{if } x < 0 \\ 0 & \text{if } x = 0 \\ 1 & \text{if } x > 0 \end{cases}$$

The idea behind the navigation law (4.10) is to make the robot's heading as close as possible to the closest safe interval  $C(t)$  when it senses unknown environments inside  $D(t)$ , on the other hand, when the robot does not sense any environment inside  $D(t)$ , the navigation law (4.10) makes the robot's heading as close as possible to the desired direction  $\theta_0$ .

We state the assumptions for the proofs of the proposed navigation algorithms as follows"

We now suppose that the environment  $\mathcal{E}(t)$  consists of several disjoint stationary or moving obstacles  $D_1(t), \dots, D_n(t)$  in the plane. These can be deformable. Moreover, consider the enlarged obstacles  $\hat{D}_1(t), \dots, \hat{D}_n(t)$  that are defined as the  $d_{safe}$ -neighbourhood of  $D_1(t), \dots, D_n(t)$ .

**Assumption 4.2.2.** The enlarged obstacles  $\hat{D}_1(t), \dots, \hat{D}_n(t)$  are convex closed sets with piecewise analytical boundary.

Furthermore, we define the maximum displacement of the set  $\hat{D}_i(t)$  over time interval  $[t_1, t_2)$  as

$$\rho_i(t_1, t_2) := \max_{r \in \hat{D}_i(t_2)} \min_{h \in \hat{D}_i(t_1)} \|r - h\|.$$

Moreover, introduce the following upper bound on the environment displacement speed:

$$V_E := \max_{i=1, \dots, n} \sup_{t_2 > t_1 \geq 0} \frac{\rho_i(t_1, t_2)}{(t_2 - t_1)}. \quad (4.11)$$

**Assumption 4.2.3.** The following inequalities hold:

$$\frac{V \sin(U_{max}\delta)}{U_{max}} > V_E\delta, \quad (4.12)$$

$$D_s > 2(V + V_E)\delta, \quad (4.13)$$

$$(D_s - 2V\delta) \sin(U_{max}\delta) > 2V_E\delta, \quad (4.14)$$

$$(D_s - 2V\delta)(1 - \cos(U_{max}\delta)) > 2V_E\delta. \quad (4.15)$$

*Remark 4.2.1.* It should be noticed that Assumption 4.2.3 is not very restrictive. Indeed, for small  $\delta$ ,  $\sin(U_{max}\delta)$  is close to  $U_{max}\delta$ , therefore the requirement (4.12) becomes close to the inequality  $V > V_E$ . It is obvious that if this inequality does not hold, it is impossible for the robot to surely avoid collisions for any navigation strategy. Furthermore, the requirements (4.13), (4.14) and (4.15) can be satisfied by taking a large enough sensing parameter  $D_s$ .

We define the distance between enlarged obstacles  $\hat{D}_i(t)$  and  $\hat{D}_j(t)$ ,  $i \neq j$  as

$$d_{ij}(t) := \min_{r \in \hat{D}_i(t), h \in \hat{D}_j(t)} \|r - h\|.$$

**Assumption 4.2.4.** For all  $i \neq j, t \geq 0$  the following inequality  $d_{ij}(t) > D_s + 2V\delta$  holds.

**Assumption 4.2.5.** We also assume that for any time  $t$ , there is no a point of the enlarged environment  $\hat{\mathcal{E}}(t)$  in the direction that is opposite to the robot's current velocity vector and at the distance less than  $2V\delta$  from the robot's current position. holds.

**Theorem 4.2.1.** *Suppose that Assumptions 4.2.1–4.2.5 hold. Then the robot navigation strategy (4.10) is safe collision free.*

The mathematical proof of the theorem 4.2.1 is presented in [156].

## 4.3 Computer Simulation Results

In this section, we present computer simulation results for a wheeled mobile robot navigating in unknown environments. The movement of the mobile robot is guided by the proposed navigation algorithm. The simulations are performed using Mobot-Sim and Matlab. The desired direction is same as the initial direction of the robot, i.e.  $\theta_0 = \theta(0)$ .

We start with a simple scenario of navigating a mobile robot in an unknown static environment. The mobile robot does not have the information about the position of the obstacle in advance, more importantly, unlike many of the existing navigation algorithms which restrict the shapes of the obstacles for computational simplicity, the shapes of the obstacles are random and irregular in this simulation as shown in Fig. 4.4. The proposed navigation algorithm guides the mobile robot through the vacancy between the static obstacles as shown in Fig. 4.4

In the following simulations performed in Matlab, we depict the mobile robot as a gray disk, we also indicate the current heading of the robot as black arrow and the intended direction (middle of vacancy) as a red arrow. Furthermore, the sensing range of the robot is represented by a dashed circle around it.

In Fig. 4.5, the robot is navigating in a dynamic environment with four obstacles. Once the robot sense one (Fig. 4.5(a)) or more (Fig. 4.5(b) and Fig. 4.5(c)), it will steer its heading towards a safe direction to avoid the obstacles. Furthermore, in the ambiguous cases where two obstacles are considered as "dangerous" by the robot, the robot is able to decide whether to go through the middle of gap between the obstacles (when the space is sufficient in Fig. 4.5(b)) or go around the obstacles (when the space is too small in Fig. 4.5(c)). The overall path is shown in Fig. 4.5(d). This simulation demonstrate the capability of the proposed navigating algorithm to distinguish ambiguous situation when multiple obstacles are considered "dangerous" and make the correct decisions on-the-fly, which is found difficult by many of the existing approaches.

The performance of the proposed navigation algorithm is compared with that

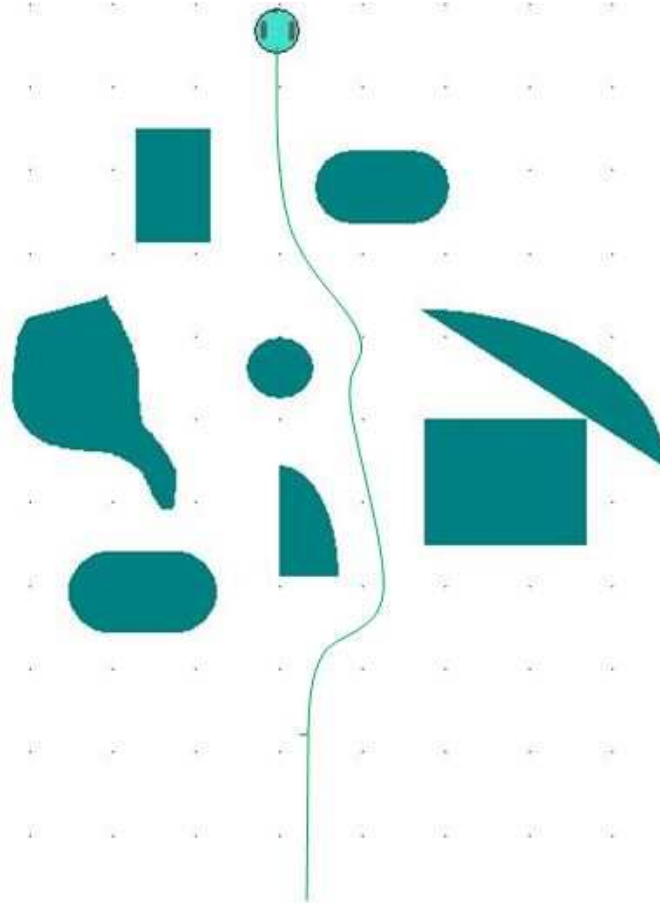


Figure 4.4: Robot navigating in unknown static environment with irregular obstacles

of the Velocity Obstacle Approach (VOA) [27, 28], which is one of the most well-known navigation algorithms. It should be mentioned that in order to compare the performance of these two algorithms, we slightly change the objective of our proposed navigation algorithm from "desired direction reaching" to "target position reaching" by making the desired direction time-varying, which equals to the direction from the robot current location to the target position.

In the following simulation, the velocity obstacles estimated by VOA are depicted by gray circles. Some of the potentially safe area are occupied by the these velocity obstacles because of the estimation, whereas the proposed navigation algorithm efficiently utilises these paths and bypass the obstacles with a shorter path. In other words, with the proposed navigation algorithm, the robot efficiently seeks a free path

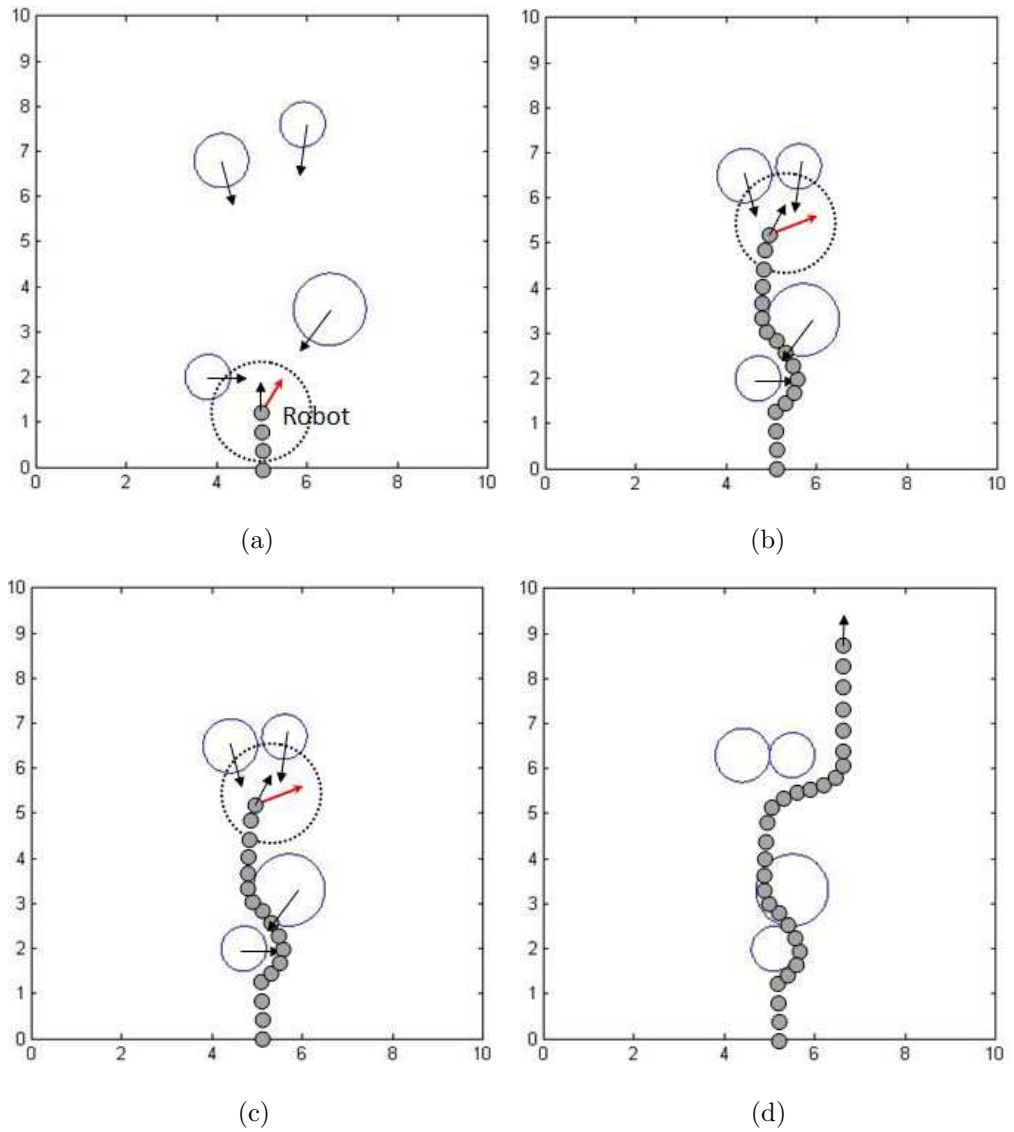


Figure 4.5: Robot navigating in a unknown dynamic environments with multiple moving obstacles

through the group of obstacles, whereas with the VOA, the robot is avoiding the crowd of obstacles which results in a much longer path. The performance of the proposed navigation algorithm is shown in figures in upper row and that of VOA is shown in lower row

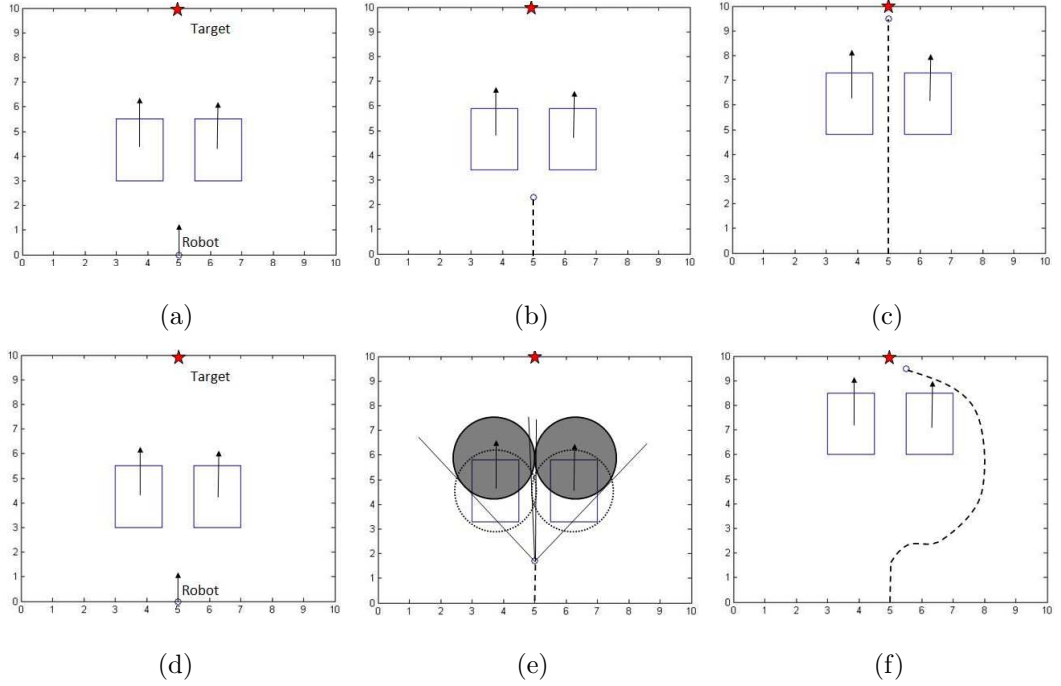


Figure 4.6: Performance comparison: two square obstacles moving side by side

## 4.4 Experiments with Real Mobile Robot

The experiments with the proposed navigation algorithm are carried out with an ActiMedia Pioneer 3-DX wheeled mobile robot to demonstrate its applicability in real life scenarios.

The only information available to the proposed navigation algorithm is measured by SICK range finder and the ultrasonic sensors: the "dangerous" angle ranges at which the enlarged environments  $\hat{\mathcal{E}}(t)$  cross the distance expressed at (4.5), see Fig. 4.9. Therefore, the safe open intervals  $(A_i^-, A_i^+)$  are found by excluding the "dangerous" directions. The safe interval which is closest to the robot's current heading  $\theta(t)$  is found by (4.8) and the desired avoiding direction (middle of vacancy) is calculated by (4.9). The movements of the robot is controlled by a notebook connected via WIFI connection.

In the following figures, the planned path of the robot is depicted as a red dashed line and that of the obstacles are shown as black dashed lines

We start with a relatively simple scenario, where the robot is navigating in a

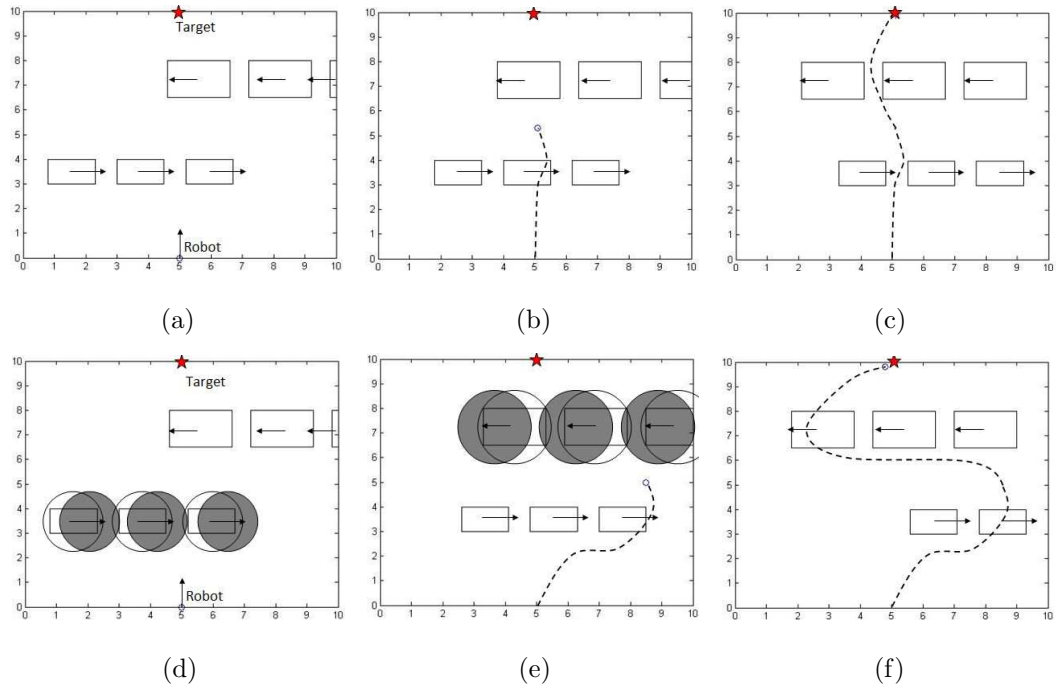


Figure 4.7: Performance comparison 2: chains of obstacles

static environments with a number of obstacles. The the obstacles are placed so that they block most of the passage, leaving limited safe interval for the robot, also the shapes of the obstacles are different from each other. The robot does not have access to any of this information in prior to the experiment. Fig. 4.10(a), Fig. 4.10(b) and Fig. 4.10(c) show the moments when the robot bypasses the obstacles through the safe intervals (middle of vacancy). and the overall path is depicted in Fig. 4.10(d).

The ambiguous situation which is frequently encountered in real life where two or more obstacles are considered as "dangerous" is again investigated in Fig. 4.11. In this experiment, two obstacle are moving towards the robot so that the robot finds itself trapped between the obstacles. Unlike many of the existing navigation approaches only consider the "closest" or "most dangerous" obstacle, which likely to result in a longer avoiding path (go around the obstacles). The proposed navigation algorithm guides the robot through the vacancy between the obstacles when the robot senses that the space between the obstacle is large enough for it to bypass. The overall path taken by the robot is shown in Fig. 4.11(d) which is very efficient.

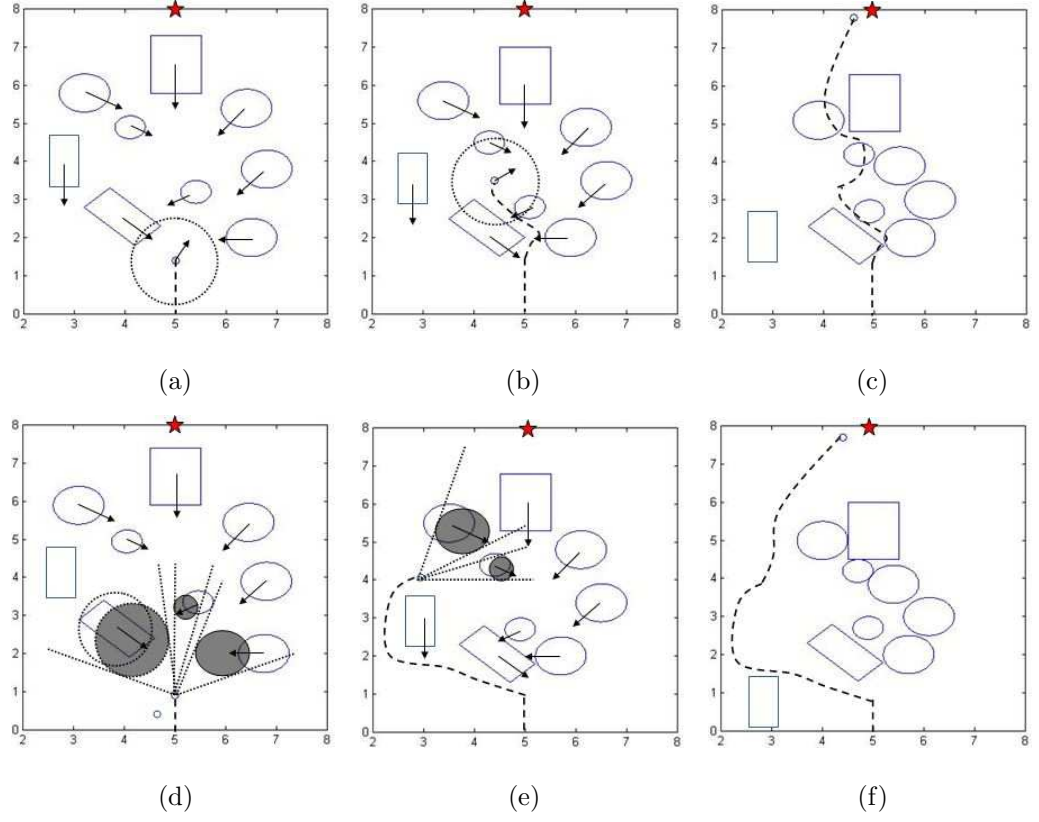


Figure 4.8: Performance comparison 3: robot navigating in a crowded environment

The performance of the proposed navigation algorithm in a complicated unknown dynamic environment with both stationary and dynamic obstacles is examined in Fig. 4.12. The avoidance of dynamic obstacles is more difficult than that of stationary obstacles, especially when the information available to the robot is very limited. In this experiment, the robot use only available information which is the binary function  $M(\alpha, t)$  to avoid the obstacles, see Fig. 4.12(a), Fig. 4.12(b) and Fig. 4.12(c) and achieve the desired heading  $\theta_0$  as seen in Fig. 4.12(d). More complicated scenarios of navigating a robot in unknown environments are shown in Fig. 4.13 and Fig. 4.14



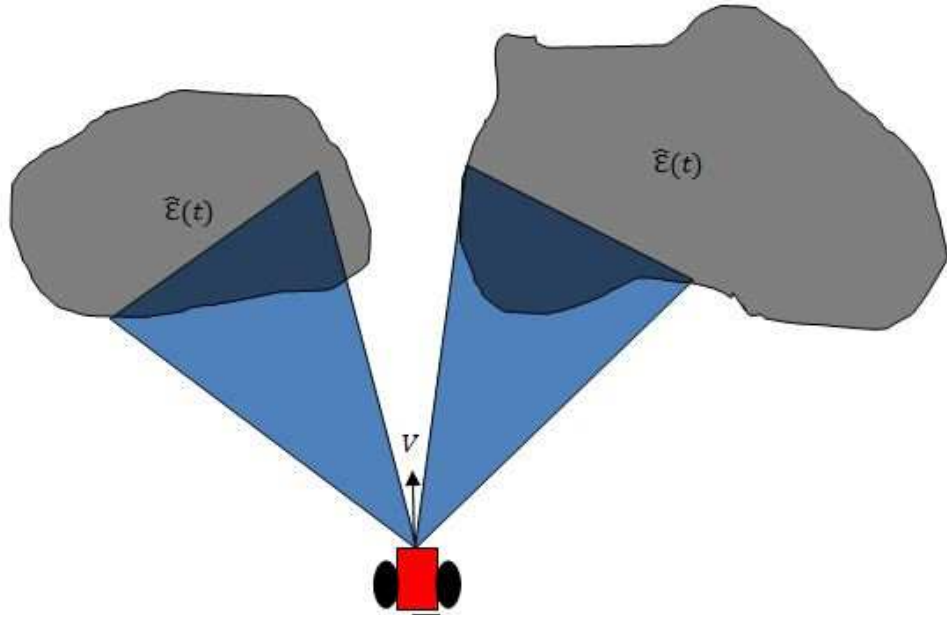
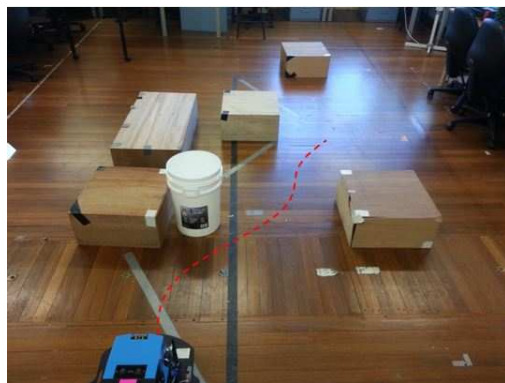


Figure 4.9: Illustration of obstacle detection

## 4.5 Summary

In this chapter, we propose a navigation algorithm for non-holonomic mobile robot in unknown dynamic environment using integrate environment representation. The proposed navigation is efficient in many scenarios which other algorithms are found difficult or impossible to solve. In particular Unlike many of the existing navigation algorithm which focus on avoiding the "closest" or "most dangerous" obstacle, the proposed navigation seek a safe path through the crowd of obstacles, which is proven to be efficient in many scenarios. The extensive computer simulations show the efficiency of the proposed navigation algorithm and the applicability in real life scenario are demonstrated by experiments with P3 mobile robot.



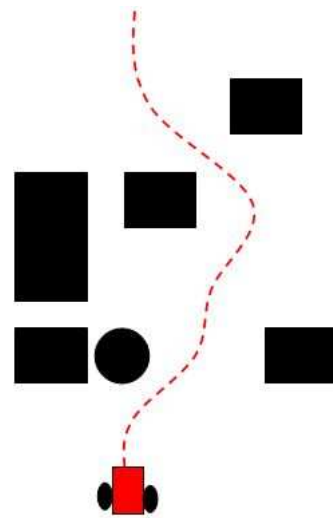
(a)



(b)

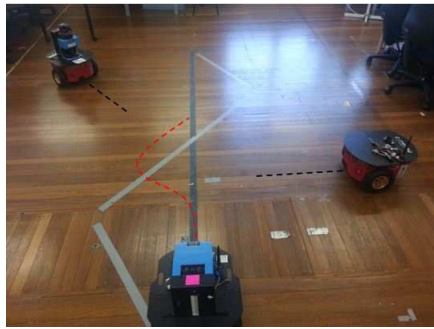


(c)



(d)

Figure 4.10: Robot avoids static obstacles



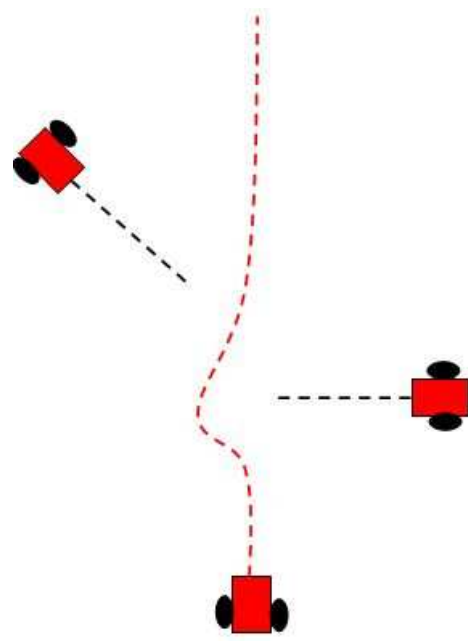
(a)



(b)

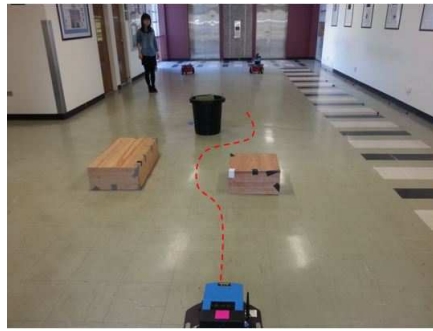


(c)



(d)

Figure 4.11: Robot avoids obstacles in ambiguous scenario



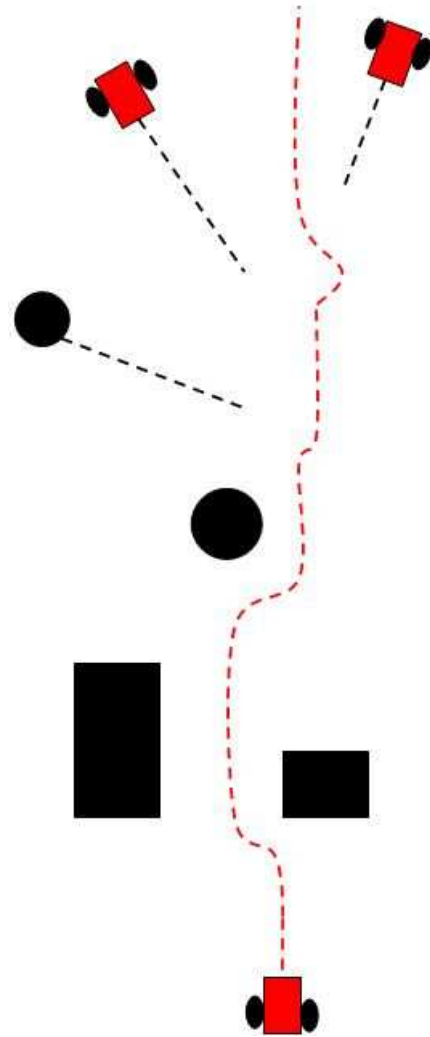
(a)



(b)

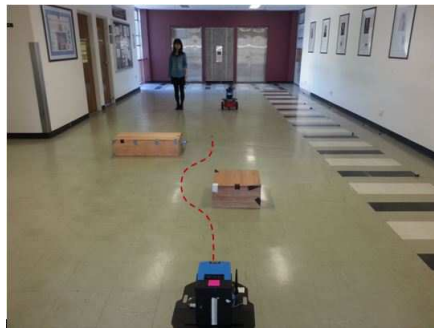


(c)



(d)

Figure 4.12: Robot navigating in complicated unknown environment with stationary and dynamic obstacles case 1



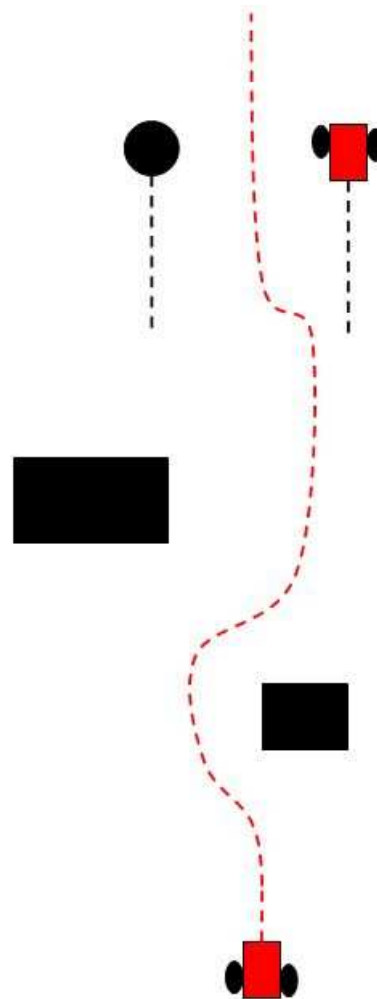
(a)



(b)

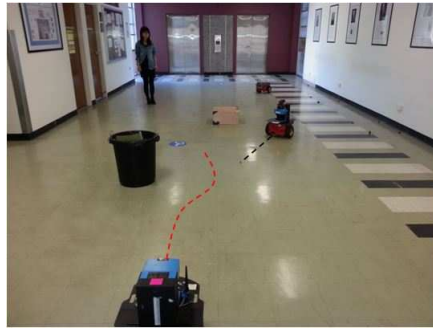


(c)



(d)

Figure 4.13: Robot navigating in complicated unknown environment with stationary and dynamic obstacles case 2



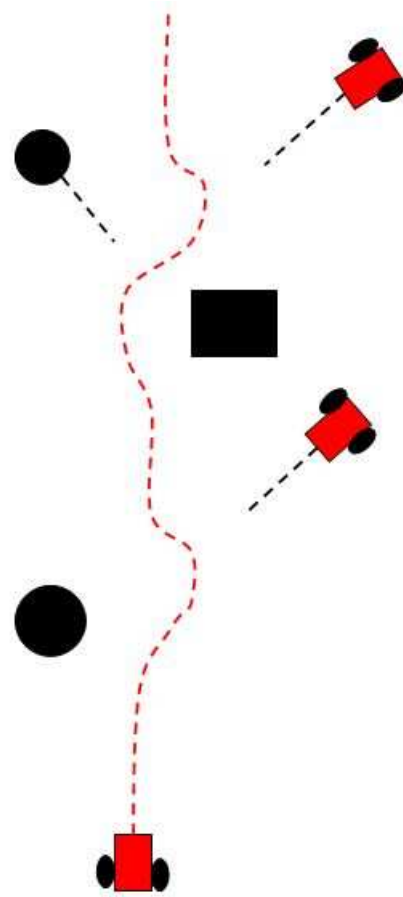
(a)



(b)



(c)



(d)

Figure 4.14: Robot navigating in complicated unknown environment with stationary and dynamic obstacles case 3

# Chapter 5

## Comparison Between the Navigation Algorithms

In this chapter, we compare the navigation algorithms, proposed in Chapter 2, 3, 4 respectively, in various aspects. The purpose of this comparison is to identify the merits of each of the proposed navigation algorithm. It also provides more insights to the proposed navigation algorithms, for example, one algorithm may be more implementation cost efficient than the others for a certain project or one may be more efficient when avoiding obstacles in particular scenarios.

### 5.1 Essential Measurements

The proper execution of the proposed navigation algorithm relies on the acquisition of several measurements from the environments. Some of these measurements are common for all three algorithms, i.e., the position  $(x, y)$  and the orientation  $\theta$  of the robot, the angular difference  $H(t)$  between the current heading of the robot and the direction of the target. The required measurements by the algorithms to avoid obstacles are different from one to another, which has been described in section 2.1, 3.1 and 4.1, respectively. Fig. 5.1 shows the measurements required by the algorithm to avoid obstacles.

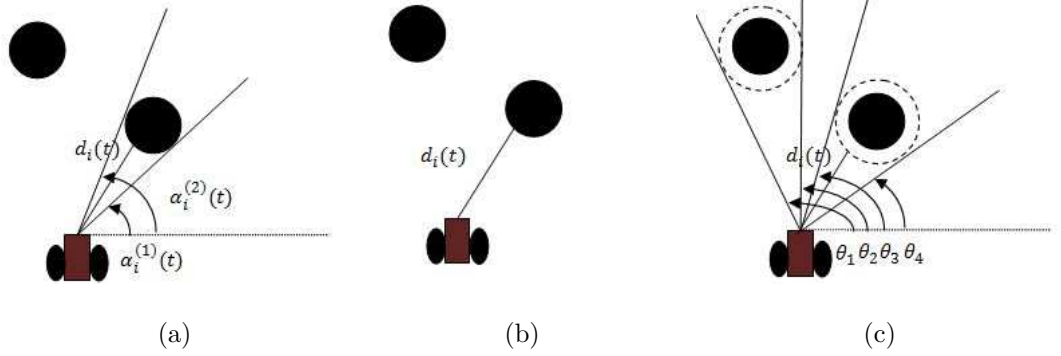


Figure 5.1: (a) Essential measurements for BINA (b) Essential measurements for ENA (c) Essential measurements for NAIER

It can be seen from Fig. 5.1 that, to successfully avoid the obstacles, ENA only requires the minimum distance  $d_i(t)$  between the robot and the obstacle, whereas BINA and NAIER require extra angular measurements regarding to the obstacles, i.e. the vision cone  $(\alpha_i^{(1)}, \alpha_i^{(2)})$  for BINA and the angular sectors covered by the enlarged environments for NAIER.

This implies that when designing hardwares for the algorithms in a control system, we can select a simple sensory device for ENA which only requires the distance measurement. More expensive and accurate sensory devices are required for BINA and NAIER. Therefore, ENA is potentially implementation cost efficient than BINA and NAIER.

## 5.2 Computation Complexity

Computation complexity directly affects the performance of the navigation algorithms in real life scenarios. The amount of computation should be reasonable to obtain the proper control signals within a certain time interval, this is crucial for many time critical navigation tasks such as navigation in a highly populated dynamic environment where the algorithm needs to react to the changes in the environment quickly. The following Fig. 5.2 shows the flowcharts for the proposed navigation algorithms to compute the control signals. We only present the flowcharts for obstacle



avoidance strategy for the proposed algorithms since the target reaching strategy is quite similar for all the algorithms. The flowchart starts with the measurements acquired from the environments and ends with the proper control signals which are computed using acquired measurements. Note that we do not include the descriptions of the defined variables and functions. The detailed description of the variables and functions are explained in Section 2.2, 3.2 and 4.2, respectively.

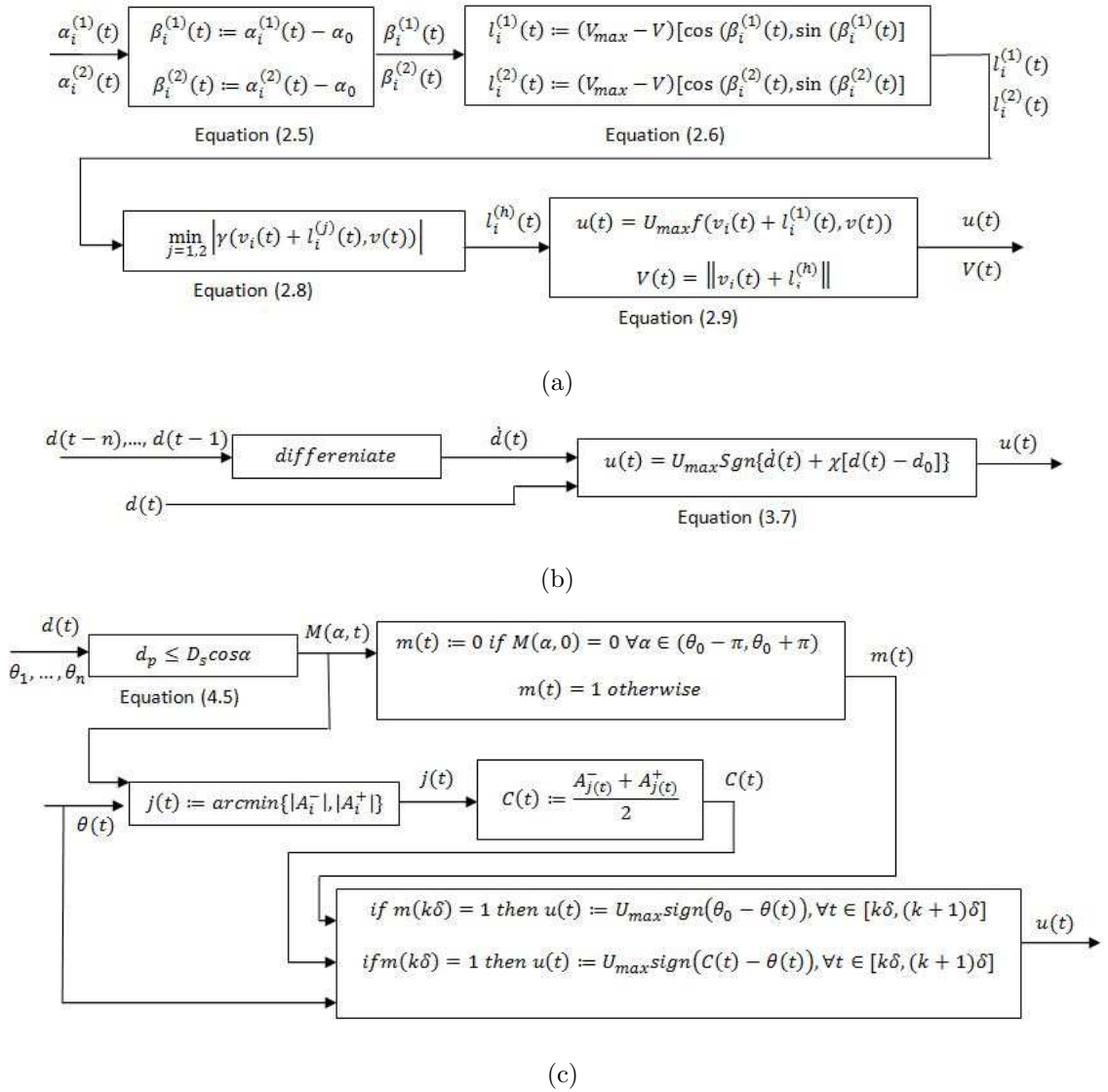


Figure 5.2: (a)Flowchart for BINA (b)Flowchart for ENA (c)Flowchart for NAIER

It can be seen from Fig. 5.2, Among all three algorithm, ENA has the minimum amount of computation steps. The overall performances of the proposed algorithms

are quite similar because they do not rely on extensive computations within a short period of time. The computation of all three navigation algorithms require only the arithmetic calculations which is quite easy to compute based on current average computation power. Therefore, all of these proposed navigation algorithms are considered as computationally efficient in certain scenarios.

### 5.3 Performance Comparison

In this section, we compare the performances of the three proposed navigation algorithms in different scenarios. Although all the proposed navigation algorithm are able to accomplish navigation tasks under various challenging scenario as shown in corresponding computer simulation sections and real experiment sections, each of the proposed navigation algorithms has its own unique characteristics which make them more efficient in some particular scenarios.

In order to compare these navigation algorithms with the same objective, we slightly change the objective of NAIER from "desired direction reaching" to "target position reaching" by making the desired direction time-varying, which equals to the direction from the robot current location to the target position.

#### 5.3.1 Stationary Obstacles

The examples of navigation in the environments with stationary obstacles are very easily found in our everyday life, e.g. the autonomous vacuum cleaner robots clear the dust while avoid colliding with the furnitures and walls inside houses, the transportation robots deliver items from a certain place to another in a warehouse in pre-defined routes which avoid the en-route obstacles. The obstacles in these scenarios can be estimated by circles or regular polygons for simplicity and are easy to avoid. The global navigation algorithms are commonly used to avoid stationary obstacles which require a complete map of the environments and these algorithms are computationally expensive. Our proposed navigation algorithms does not require

the complete knowledge of the environments and are able to make proper decision on-the-fly during a navigation task. Furthermore, we do not restrict the shapes of the obstacles to be only circles or regular polygons. The shapes of the obstacles can be irregular (convex) which can be seen in many real life scenarios. For example, obstacles encountered by exploration or rescue robots in hazardous environments are usually rocks and swamp of irregular shapes.

Fig. 5.3 shows the performance of the proposed algorithms with one single stationary obstacle of circular shape. Many of the real world obstacles can be estimated as circles which are considered as one of the simplest test subjects for obstacle avoidance algorithms. The performance of BINA and ENA is slightly better than that of NAIER since the NAIER has to switch between obstacle avoidance maneuver and target reaching maneuver when the obstacle is nearby (partially due to the change of objective). The performance of BINA and ENA is almost identical which can be explained by the features of both algorithms: BINA guides the robot so that the robot's trajectory converging to the circle of radius  $\frac{R_i}{\cos \alpha_0}$  (the deviation is given in [155]), whereas ENA drives the robot to a  $d_0$ -equidistant curve around the obstacle. Therefore, both algorithms drive the robot to a circle around the obstacle in this particular scenario and it is a quite efficient path to avoid a circular obstacle while retaining a safety margin.

In the next figure, we replace the circular obstacle with a rectangular obstacle. Obstacles with rectangular shapes are very common in real life scenarios. The shapes of many obstacles, such as tables, benches, can be estimated by a rectangle. In Fig. 5.4, we depict the crucial parameters during obstacle avoidance maneuvers for each of the algorithms, i.e., vision cone for BINA,  $d_0$ -equidistant curve for ENA and the detection range for NAIER. In this simulation, BINA guides the robot to the target location while avoiding the obstacle with minimum time ( $23.5sec$ ). ENA and NAIER achieve the same navigation task with  $27.6sec$  and  $29.8sec$ , respectively.

Fig. 5.5 presents a more challenging scenario with obstacle of irregular shape. Although shapes of most of obstacles in real life can be estimated by circle or rect-

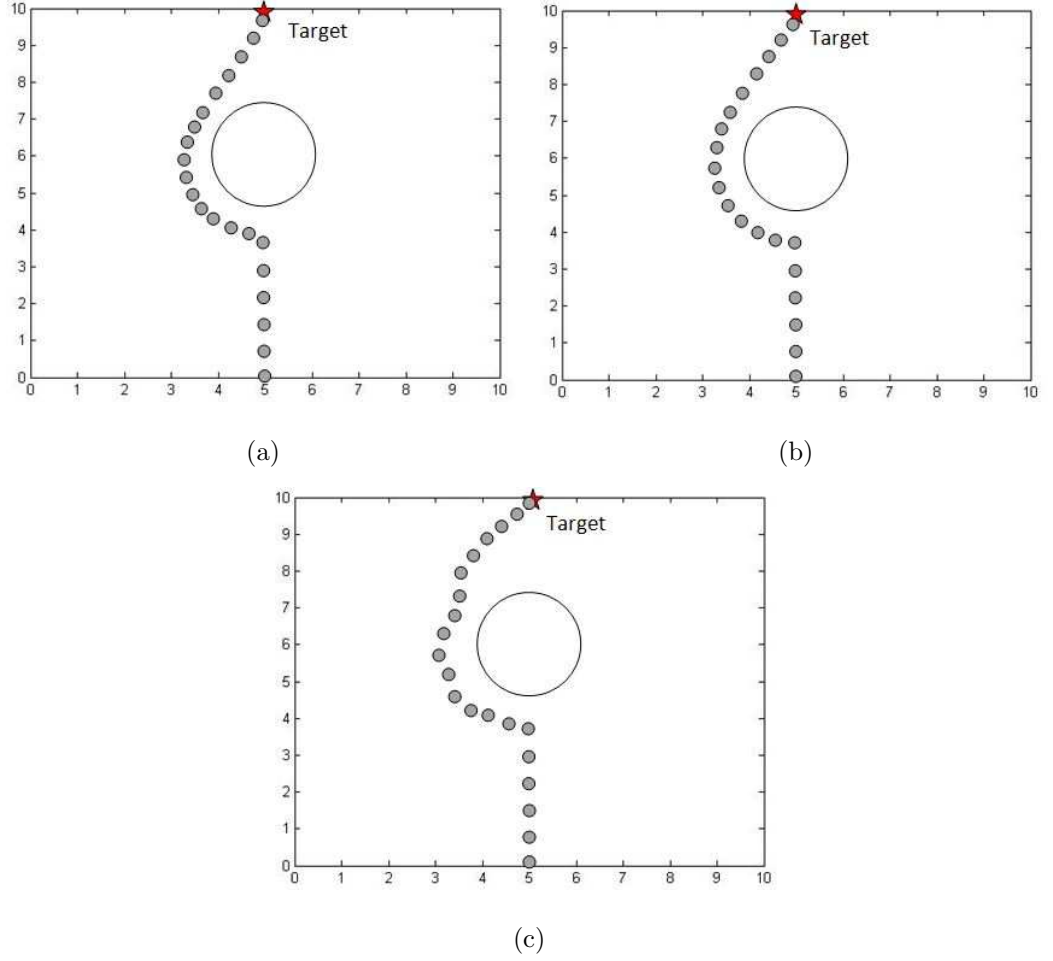


Figure 5.3: Performance comparison: single stationary obstacle for (a) BINA (b)ENA (C)NAIER

angle, some of the potentially safe path may be occupied when the estimation is applied. Therefore, it is advantageous for an algorithm to avoid obstacles with irregular shapes. In this case, ENA is most efficient in term of navigation time (18.1sec) since it is able to guide the robot so that it tracks the border of the obstacle ( $d_0$ -equidistant curve) at close distance. The navigation time for BINA and NAIER are 24.6sec and 23.5sec, which are quite close to that of ENA.

In the last simulation, we show an extension scenario of Fig. 5.5. The proposed navigation algorithms need to guide the robot though environments crowded with obstacles of irregular shapes. In this case, NAIER has the best performance with

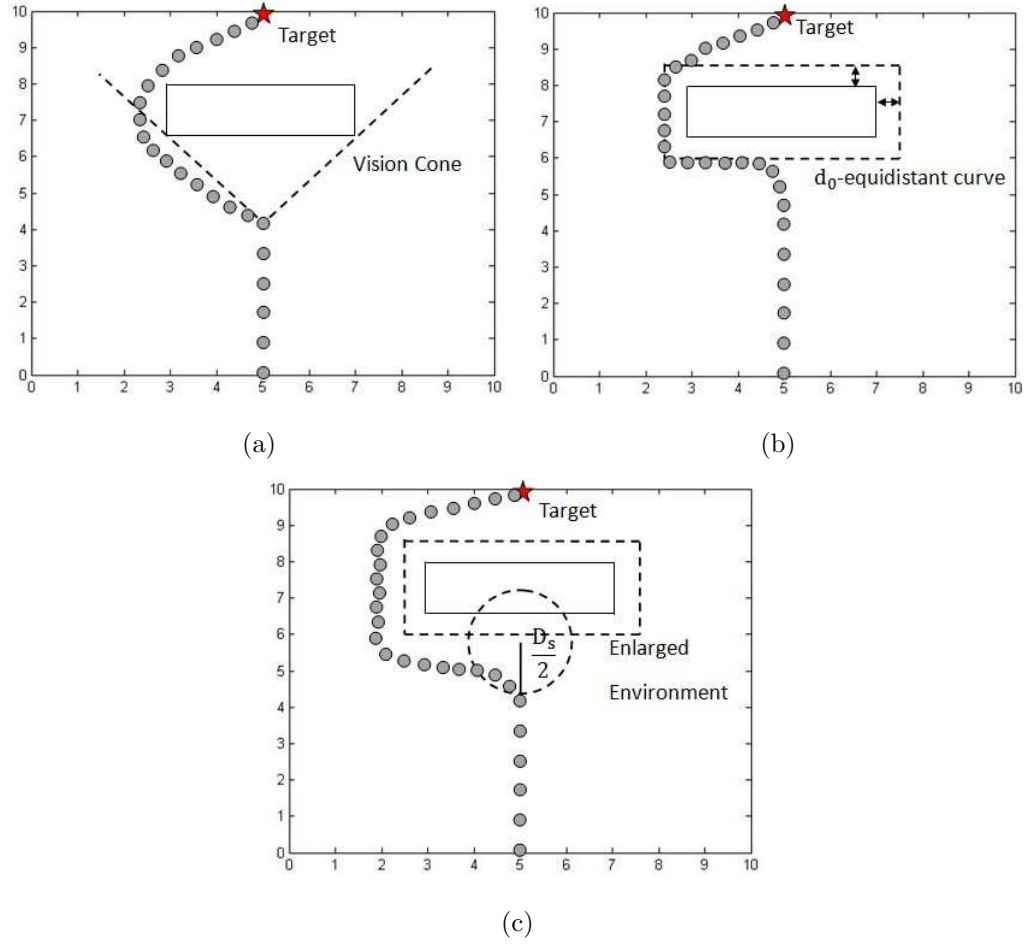


Figure 5.4: Performance comparison: single rectangular obstacle for (a) BINA (b) ENA (c) NAIER

overall navigation time of 21.5sec. The advantage of NAIER is that it is able to seek a free path through obstacles. This is very efficient when the environment is populated with multiple closely positioned obstacles. ENA achieves navigation task with 25.3sec. The robot follows the  $d_0$ -equidistant curve of every en-route obstacles under the guidance of ENA. It takes 35.5sec for BINA to complete the navigation task because the use of vision cone forces the robot to take a longer detour to avoid the crowd of obstacles.

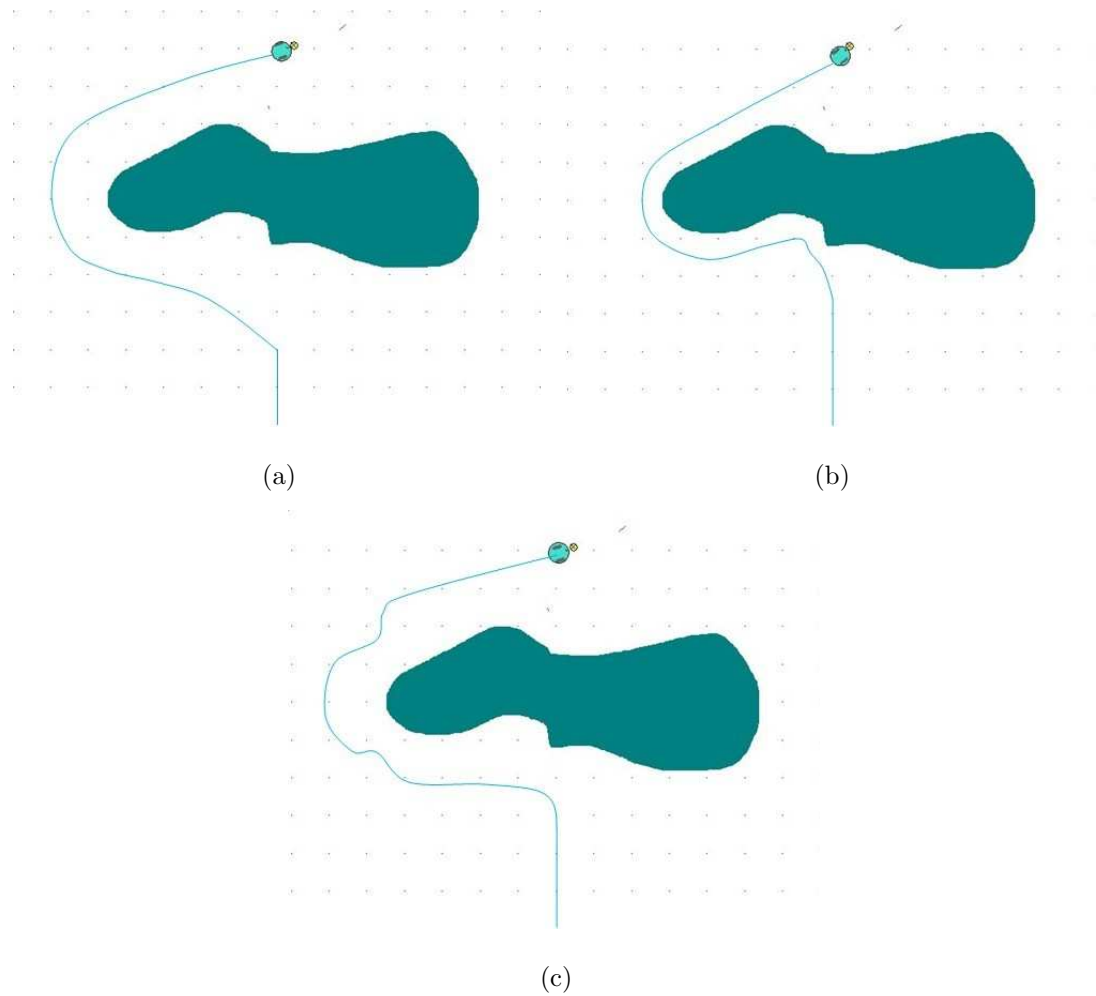


Figure 5.5: Performance comparison: single obstacle with irregular shape for (a) BINA (b)ENA (C)NAIER

### 5.3.2 Dynamic Obstacles

In many of real life scenarios, the obstacles are often moving with various speed rather than staying stationary. For example, the museum tour robots and the service robots in nursing houses are usually operating in the environments with multiple moving objects. It is much more difficult for an algorithm to navigate a vehicle in a dynamic environment with moving obstacles. There are several reasons for this: firstly, the navigation algorithms need to consider more real time parameters when dealing with moving obstacles, such as obstacles' velocities and accelerations, obstacles' future trajectories. Secondly, the obstacles are not always moving with

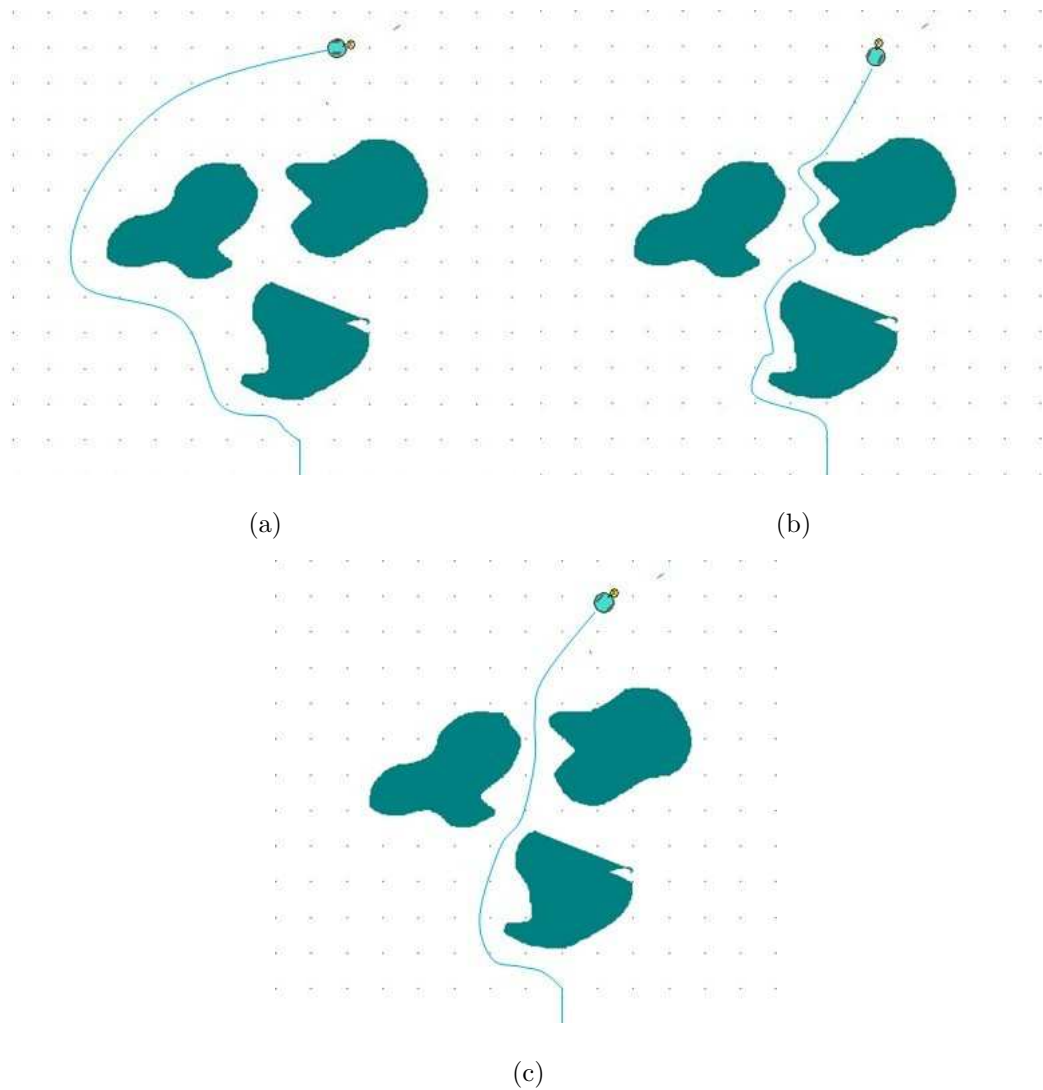


Figure 5.6: Performance comparison: a crowd of obstacles with irregular shapes for (a) BINA (b)ENA (C)NAIER

constant speeds, some obstacles may move with some complicated and unpredictable non-linear velocities. Finally, the shapes of the obstacles may be time-varying in the dynamic environments.

We first examine the performance of the proposed navigation algorithms in the dynamic environments with obstacles moving at constant speeds. In Fig. 5.7, Fig. 5.8 and Fig. 5.9, we gradually increase the number of obstacles within the environments. The obstacles are moving with constant speeds at random directions. These simula-

tions show that the proposed navigation algorithms are capable of avoiding moving obstacles and their performance is consistent regardless the number of obstacles.

Statistically, BINA has the best performance over ENA and NAIER in terms of overall navigation time. Table 5.1 shows the record of navigation time for all three algorithms over 25 simulation runs. The number of the obstacles is different and also the positions, speeds and moving direction of the obstacles are randomly assigned for all the simulation runs. The results in Table 5.1 shows that BINA has the shortest navigation time for most of the experiments (23 out 25, 92% rates).

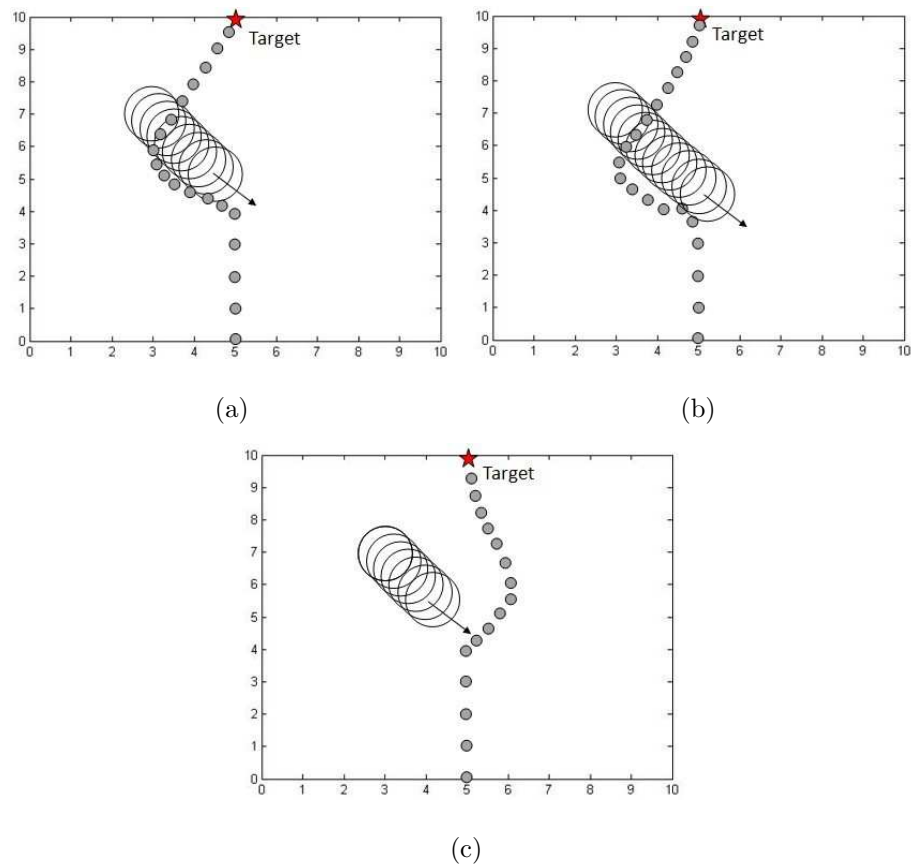


Figure 5.7: Performance comparison: dynamic environment with single moving obstacle for (a) BINA (b) ENA (c) NAIER

We can not always expect the velocities of the obstacles in environments to be constant in every of the real life scenarios. Obstacles such as many animals (birds, fish, cats etc) are likely to be moving in a more complicated non-linear velocities.



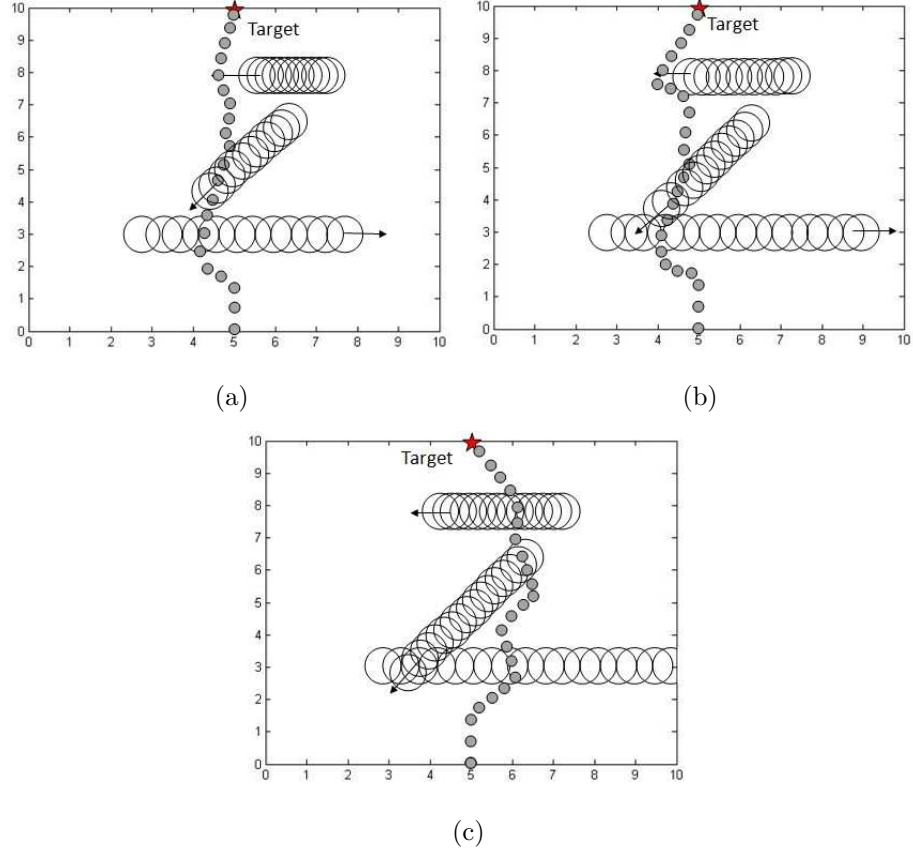


Figure 5.8: Performance comparison: dynamic environment with three moving obstacles for (a) BINA (b)ENA (C)NAIER

The movements of these obstacles are even more difficult to predict or estimate.

In the next simulation, the performances of the proposed navigation algorithms against obstacles with non-linear velocities are shown. We assume that the maximum speed and the maximum angular velocities of the obstacles are strictly less than those of the robot, i.e.,  $\|V_{ob}\| < \|V_{robot}\|$ ,  $\|\omega_{ob}\| < \|\omega_{robot}\|$ . All three proposed navigation algorithms are able to avoid obstacles with non-linear velocities with their own strategies: BINA guides the robot so that it keeps a constant avoiding angle between the instantaneous moving direction of the obstacle. In this case the moving direction of the obstacle is time-varying. ENA drives the robot to the  $d_0$ -equidistant curve around the obstacle. NAIER always direct the robots to a collision free path by assessing the angular segments within the sensing range. In this particular case,

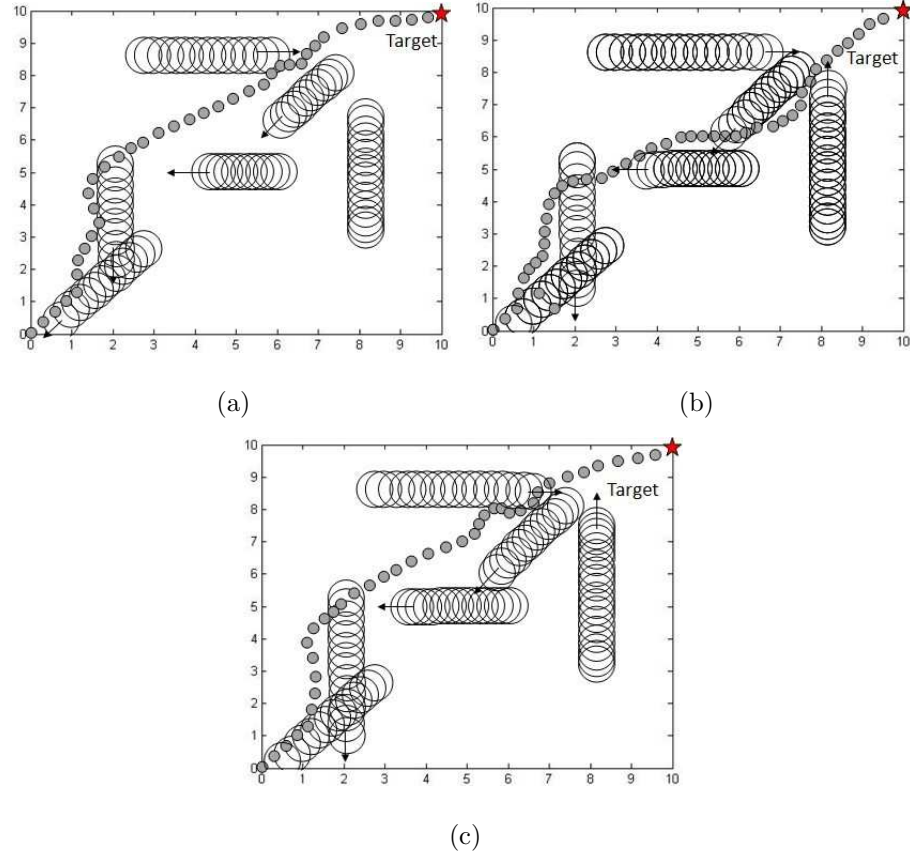


Figure 5.9: Performance comparison: dynamic environment with six moving obstacles for (a) BINA (b)ENA (C)NAIER

BINA has the shortest navigation time of all three navigation algorithms. However, Table 5.2 shows the record of navigation time for all three algorithms over 20 simulation runs. The obstacle is assigned with different non-linear velocity and initial position in each simulation run. There is no solid conclusion to which algorithm is more efficient for avoiding obstacle with non-linear velocity.

Finally, we compare the performance of three proposed navigation algorithm in an extremely cluttered environments. Although it is demonstrated that the proposed algorithms are capable of avoiding dynamic obstacles, the performance of the algorithms may varies when the obstacles are extremely cluttered within the same environments, such as passengers in train stations at busy hours. We slightly change the presentation of the result in order to make it clear and easy to understand. In

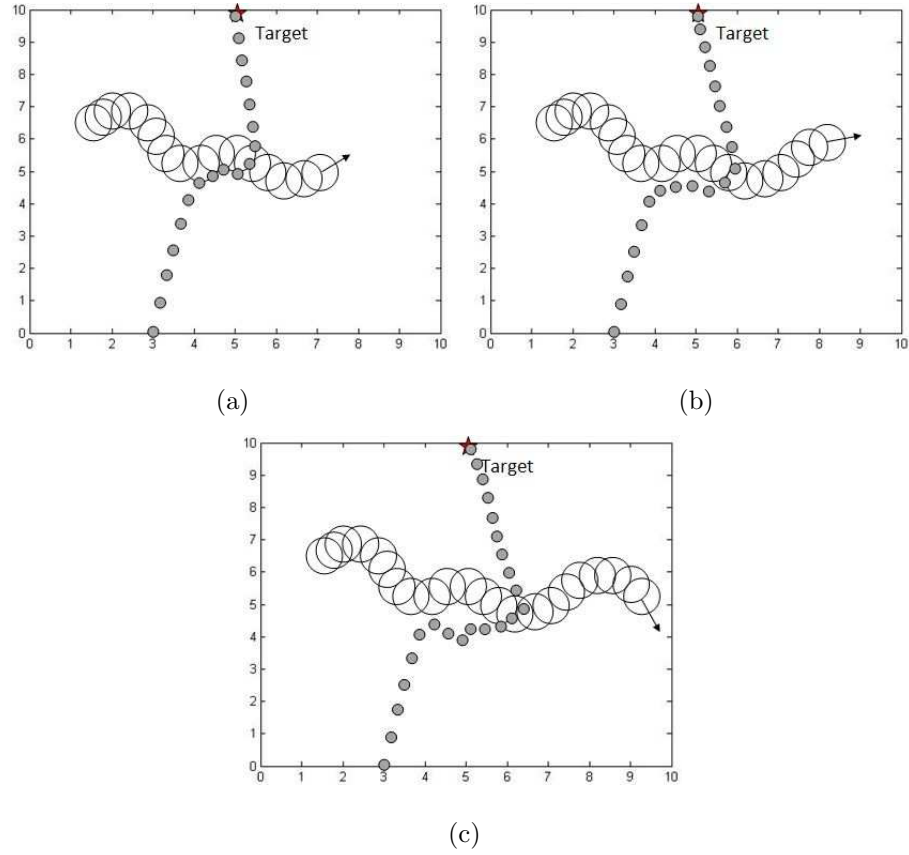


Figure 5.10: Performance comparison: obstacle with non-linear velocity for (a) BINA (b)ENA (C)NAIER

Fig. 5.11, the initial position of the obstacle is shown by a dashed circle and moving direction of the obstacle is depicted by an arrow connecting its initial position and final position.

As we can see from the results in Fig. 5.11, NAIER has the best performance over the other two algorithms. The advantage of NAIER is that it is able to find the collision-free angular sectors in the sensing range and steer the moving direction of the robot to the middle of the vacant angular sector. It allows the robot to find a safe path through the cluttered environments. BINA and ENA are also able to guide the robot to the target location while ensuring the safety of the robot in this cluttered environment. However, the employment of enlarged vision cone for BINA often force the robot to a detour when the obstacles are closely positioned,

see e.g. the first three obstacles the robot avoids in Fig. 5.11(a). The interpolation technique is put in use for ENA when the obstacles are cluttered, which enlarges the  $d_0$ -equidistant curve of this group of obstacles for the robot to follow.

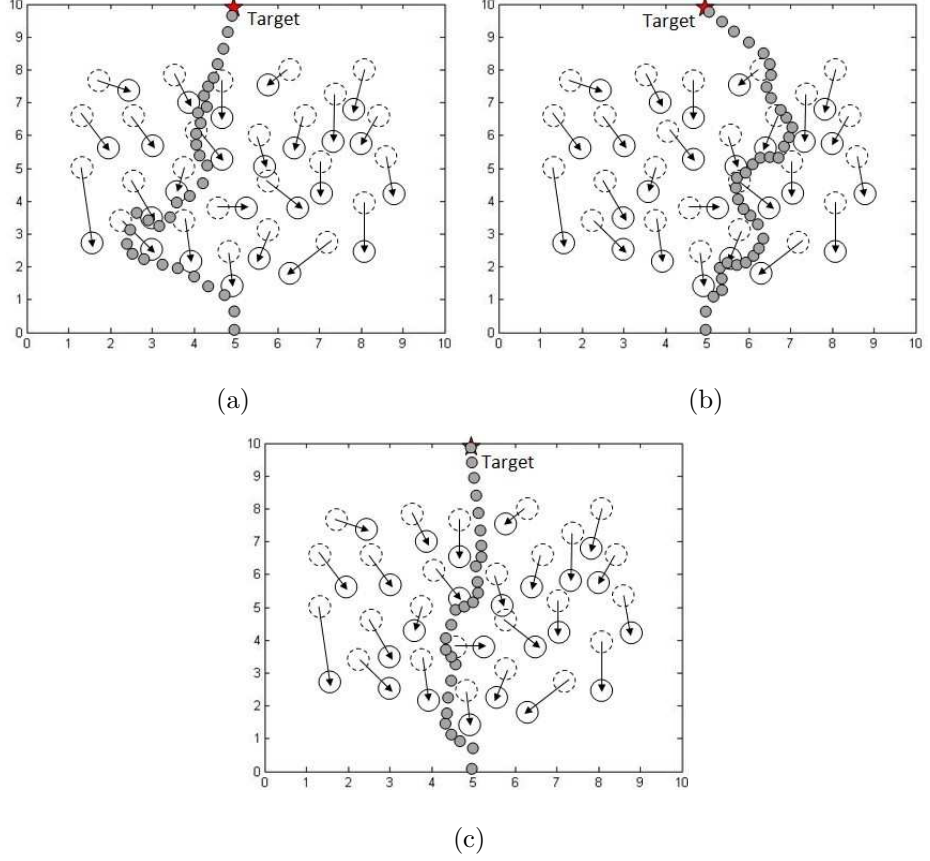


Figure 5.11: Performance comparison: navigation in a extremely cluttered dynamic environments for (a) BINA (b) ENA (c) NAIER

### 5.3.3 Section Summary

In this section, we demonstrate that the proposed navigation algorithms are capable of navigating a robot in various scenarios. The simulation results are presented to show the characteristics of the algorithms. BINA has the most efficient navigation time when facing obstacles of regular shapes (circle or regular polygons) in both stationary and dynamic environments. ENA is applicable in a large variety of scenarios and is efficient when avoiding obstacles of irregular shapes. ENA has

the average and most stable navigation time in all three algorithms. Finally, the advantage of NAIER is its superior efficiency in extremely cluttered stationary and dynamic environments, which the other two algorithms take relative longer to deal with.

## 5.4 Summary

In this chapter, we present the comparison between BINA, ENA and NAIER in various aspects including the measurements required by the algorithms which directly influence the implementation cost and the design of the control system, the computation complexity which affects the real time performance of the algorithm and finally the performance comparison between the algorithm in various static and dynamic environments.

Table 5.1: Navigation time (in *sec*) for BINA, ENA and NAIER over 25 experiment runs (obstacles moving with constant speeds)

	Result for BINA	Result for ENA	Result for NAIER	Best result
Experiment 1	26.1	28.3	29.5	BINA
Experiment 2	23.3	24.4	27.3	BINA
Experiment 3	30.2	32.6	31.1	BINA
Experiment 4	35.8	38.9	40.1	BINA
Experiment 5	22.5	26.3	26.0	BINA
Experiment 6	27.9	29.9	28.3	BINA
Experiment 7	38.8	40.1	39.9	BINA
Experiment 8	24.2	28.7	26.2	BINA
Experiment 9	28.2	27.1	28.9	ENA
Experiment 10	30.1	35.0	36.2	BINA
Experiment 11	40.1	46.3	43.5	BINA
Experiment 12	27.5	28.7	32.6	BINA
Experiment 13	34.1	40.2	38.5	BINA
Experiment 14	33.9	38.1	32.1	BINA
Experiment 15	39.1	45.8	47.2	BINA
Experiment 16	28.8	30.2	32.1	BINA
Experiment 17	26.9	30.2	27.8	BINA
Experiment 18	28.4	30.5	32.9	BINA
Experiment 19	29.9	28.1	28.3	BINA
Experiment 20	38.2	42.1	35.1	NAIER
Experiment 21	32.6	35.3	34.1	BINA
Experiment 22	34.1	36.3	38.8	BINA
Experiment 23	28.5	32.4	29.1	BINA
Experiment 24	29.7	31.3	32.2	BINA
Experiment 25	23.9	27.3	29.3	BINA

Table 5.2: Navigation time (in *sec*) for BINA, ENA and NAIER over 20 experiment runs (obstacles moving with non-linear velocities)

	Result for BINA	Result for ENA	Result for NAIER	Best result
Experiment 1	18.4	15.3	17.5	ENA
Experiment 2	20.1	26.4	17.3	NAIER
Experiment 3	19.2	22.9	20.1	BINA
Experiment 4	18.8	22.6	16.5	NAIER
Experiment 5	25.5	27.2	29.4	BINA
Experiment 6	21.8	27.3	22.3	BINA
Experiment 7	26.8	22.5	29.2	ENA
Experiment 8	25.2	29.3	21.7	NAIER
Experiment 9	25.8	24.3	20.5	NAIER
Experiment 10	20.9	27.3	29.3	BINA
Experiment 11	30.1	24.5	28.5	ENA
Experiment 12	18.5	25.9	29.6	BINA
Experiment 13	23.4	24.7	18.5	NAIER
Experiment 14	27.7	29.6	21.1	NAIER
Experiment 15	29.9	25.3	28.9	ENA
Experiment 16	21.8	32.8	28.3	BINA
Experiment 17	28.0	21.8	29.9	ENA
Experiment 18	20.4	28.0	26.7	BINA
Experiment 19	19.2	23.9	29.2	BINA
Experiment 20	28.4	23.9	25.7	ENA





## Chapter 6

# The Implementations on an Intelligent Wheelchair Control System

The fundamental concern for operating a wheelchair is the safety of the user. Conventional wheelchairs can be operated manually, or with the aid of joysticks, levers and other accessories, to transport an impaired person from current location to target location. More advanced intelligent wheelchairs allow the users to control the movements of the wheelchairs by their own efforts, i.e., user-wheelchair interactions. These wheelchair control approaches require a fair amount of training and practice and their performance can be easily plagued by many external factors.

The implementations of the navigation algorithms on electric-power wheelchairs solve these problems and guarantee the safety of the users. In this chapter, the navigation algorithms, Biologically-Inspired Navigation Approach (BINA) and Equidistant Navigation Approach (ENA) which are proposed in Chapter 2 and Chapter 3 respectively, are implemented on a real intelligent autonomous wheelchair SAM (Semi-Autonomous Machine). The applicability and performance of the intelligent autonomous wheelchair under the guidance of these navigation algorithms are shown by experiments in real life scenarios.

## 6.1 Background and Motivation

The population of the impaired persons was growing over the past decades [51, 159]. Numerous people with mobility impairments are experiencing problems such as losing social connections (which leads to social isolation, depression and anxiety), emotional damage (which leads to fear, loss of self-esteem) [25, 75] etc. Studies also show that the utilization of independent mobility aids help the user to ease the problem and significantly improve his/her lifestyle [58, 169]. Wheelchairs are one of the most commonly used mobility aids to assist the movement of user [25, 139] and a large number of users are benefited from it [170].

The existing approaches to the safe navigation of wheelchairs can be generally classified into two categories: the user-wheelchair interaction approach and the autonomous navigation approach.

The user-wheelchair interaction approaches control the movements of the wheelchair by giving "commands" to the wheelchair by different parts of body. e.g. hand gesture [80, 196], head position and movement [45, 130, 190], oral motion [140] etc. voice command [60, 128, 168], brain signal [131, 143, 166], etc. These approaches give the maximum control freedom to the users, allowing them to control the wheelchairs according to their judgments and efforts. However, this also raises several problem because the information about the environments is acquired by the users' reaction. These perception and reaction can be easily plagued by many factors such as bad perceptual condition (tiredness, stress) or poor operating environment (darkness, noise). Inaccurate information about the environment can dramatically increase the chances of misjudgments, which lead to inappropriate decisions, and so the safety of the users is not guaranteed. These approaches also require the users to stay active and concentrates for any potential dangers during the whole navigation process which is fatiguesome. Furthermore, a clinical survey shows that forty percent of the users found it difficult to perform steer tasks using these intelligent wheelchairs, and a number of users cannot operate the intelligent wheelchairs due to various reasons [23]. This is an indication that most of user-wheelchair interaction methods

cannot be learned easily and require a fair amount of practice and training in order to properly operate the wheelchair.

The autonomous navigation approaches, on the other hand, take over the control of the wheelchair from the users. The advantages of these approaches are that the wheelchairs can be operated in poor perceptual environments and responses to the changes in the environments are generally faster. Moreover, it does not require any practice and training to operate the wheelchairs. A number of navigation algorithms have been implemented in various intelligent wheelchairs. The Vector Field Histogram (VFH) [6] and Vector Force Field [7] are implemented in the NavChair Assistive Wheelchair navigation system, the obstacle avoidance strategy based on optimized Bayesian Neural Networks [180] and shared control strategy [181] are implemented in SAM (semi-Autonomous Machine). A biologically inspired approach [178], which was implemented with a mobile robot and which performance was confirmed by extensive real world experiments, can also be applied to intelligent wheelchairs. These navigation algorithms have demonstrated great successes in static environments. Furthermore, the velocity obstacle approach (VO) is implemented in a commercial wheelchair model SPRINT in [121, 127], the VO approach allows the SPRINT wheelchair to cope with environments with moving obstacles.

These autonomous navigation approaches only deal with static environments which is not relevant to many real world scenarios, where the users of the wheelchairs often find themselves involved in dynamic crowded environments with multiple moving obstacles. The proposed navigation algorithms ensures the safety of the users of the wheelchairs in both static and dynamic environments, the performance of the proposed navigation algorithms BINA and ENA has been confirmed by the simulation results and the experiments with a real non-holonomic mobile robot in Chapter 2 and Chapter 3. The intelligent wheelchair SPRINT [121, 127] is a rare example of a wheelchair that can operate in dynamic environments, Both BINA and ENA have their own advantages over SPRINT when they are implemented on SAM. The experiment results of the implementation of BINA and ENA on SAM are presented

in this chapter.

## 6.2 System Model

We consider a wheelchair that travels in a plane and has two independently actuated driving wheels mounted on the same axle and castor wheels. The position of the wheelchair is represented by the absolute Cartesian coordinates  $x, y$  of the reference point located at the center of the axle, whereas its orientation is given by the angle  $\theta$  between the wheelchair centerline and the abscissa axis. The driving wheels roll without sliding. The wheelchair is controlled by the angular velocities  $\omega_l$  and  $\omega_r$  of the left and right driving wheels, respectively, which are limited by a common and given constant  $\Omega$ . The relevant mathematical model of kinematics of the wheelchair is as follows:

$$\begin{aligned} \dot{x} &= v \cos \theta, & v &= \frac{v_l + v_r}{2}, & x(0) &= x_0 \\ \dot{y} &= v \sin \theta, & u &= \frac{v_r - v_l}{2L}, & y(0) &= y_0 \\ \dot{\theta} &= u, & v_i &= R_w \omega_i, & \theta(0) &= \theta_0 \end{aligned} \quad (6.1)$$

where  $R_w$  is the radius of the driving wheels,  $2L$  is the length of the axle, and  $\omega_i = \omega_i(t) \in [-\Omega, \Omega], i = l, r$ . To simplify the matters, we treat  $v$  and  $u$  as control variables. They uniquely determine the rotational velocities  $\omega_r = (v + Lu)/R_w, \omega_l = (v - Lu)/R_w$  and obey the bound:

$$|v| + L|u| \leq V := R_w \Omega. \quad (6.2)$$

This bound implies restrictions on the forward and rotational movements of the wheelchair. In particular, its speed cannot exceed  $V$ , and for given  $v \in (-V, V)$ , the turning radius of the wheelchair is bounded from below

$$R = \frac{L|v|}{V - |v|}. \quad (6.3)$$

## 6.3 Wheelchair System Description

The algorithms BINA and ENA are implemented on the wheelchair SAM. Motions of this wheelchair can be controlled by many ways such as joystick, EEG signals [19], head movement [180] etc. A number of control methods have been proposed and implemented on the SAM wheelchair, see e.g. [108–110, 181].

The SAM wheelchair features two rear driving wheels (see Fig. 6.1(a)) and two front caster wheels (see Fig. 6.1(b)). The motor for driving the wheels is powered by a 24V battery. The joystick mounted on the right rack of the wheelchair at the front of the wheelchair which can be used to control the motion of the wheelchair. The LDC monitor is mounted on the left rack, this monitor is used to display information such as the map of the environment, the GPS information or the laser data. There is also a laser range finder on the left rack which is the main interface between the wheelchair to the environment. An on-board computer is available at the back of the wheelchair for those programs running in Linux environment. The DC/AC are responsible to convert the control signals and the data into the correct format.

The following devices are particularly important for our experiments, therefore their functionalities and specifications should be emphasised:

- A notebook (Windows XP operating system with dual-core CPU running at 1.66GHz and 2GB RAM). For these experiments, LabWindows are used to program the algorithms. The notebook acts as the core of the entire intelligent wheelchair control system, it receives information from various devices and computes the control signals, which is then sent to the driving system.
- The URG-04LX laser is mounted on the left rack at the front of the wheelchair. The laser scans the environment and provides necessary information to the wheelchair such as distance to the obstacles (required by both BINA and ENA), the vision cone (required by BINA) etc. The maximum scan angle for this laser range finder is  $240^{\circ}$  and the maximum scan range is  $4m$  with accuracy of  $\pm 1\%$  of the measurement, the scan frequency is  $10Hz$ . Fur-

thermore, the laser is able to scan and provide two-dimensional map of the environment if necessary.

- The USB1 adapter (By USDigital). It is an interface between the computer and the encoders which are attached to the driving wheels. The adapter interprets the information from the encoders, convert them into the revolution of both wheels. This information is used to estimate the position and orientation of the wheelchair.
- The National Instrument NI USB-6008 DAQ device. This DAQ devices converts control signals into appropriate voltages and sent them to the motor of the wheelchair.

The interconnections between these hardwares of SAM wheelchair is depicted in Fig. 6.2. Note that the variables  $T_x$  and  $T_y$  are the coordinates of the target location.

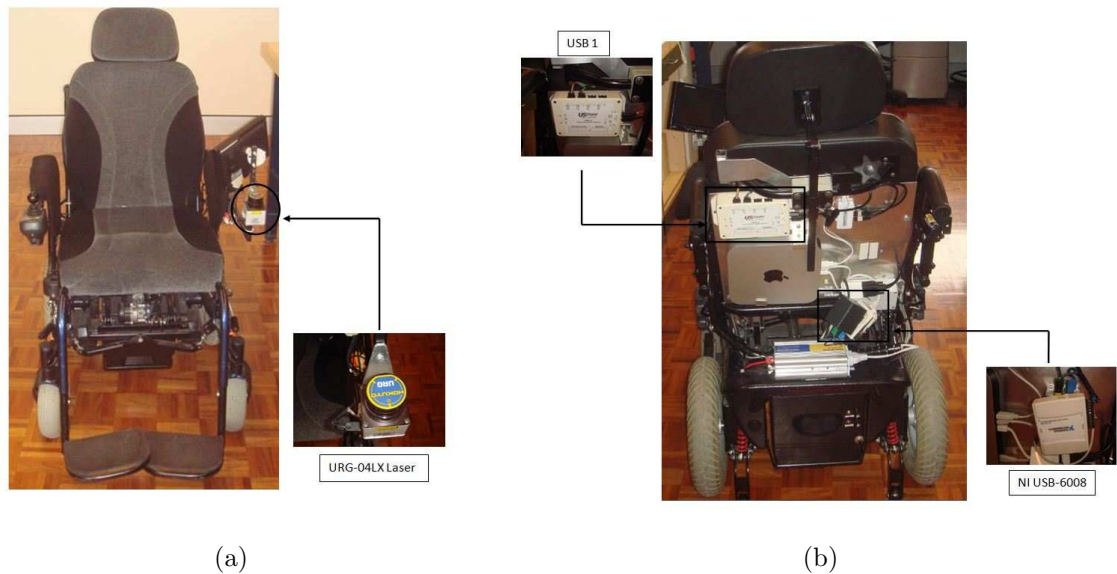


Figure 6.1: (a)Front view of the wheelchair; (b)Rear view of the wheelchair

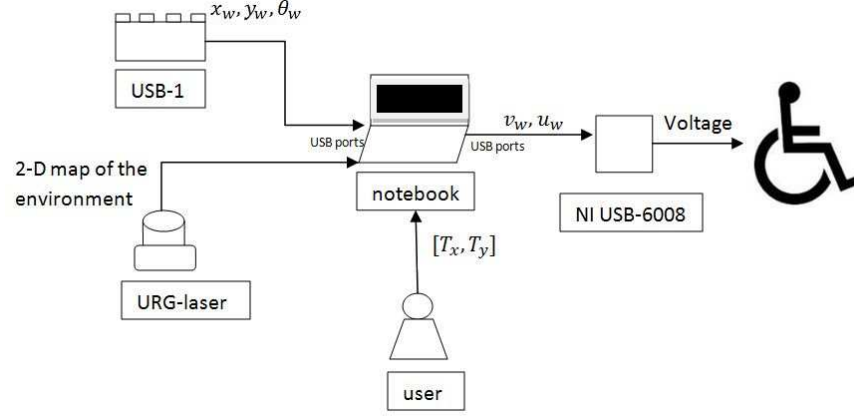


Figure 6.2: Interconnections between hardware components of wheelchair control system

## 6.4 Implementation and Experiments of Biologically-Inspired Navigation Algorithm (BINA)

### 6.4.1 Parameter Measurements

In this section, we describe the methodology to acquire the essential parameters required by BINA, which is presented in Section 2.1.

- The measurements to the environments are carried out by the URG-04LX laser range finder. The laser returns the measurements as an array of data. Each of the indices shows the distance to the closest obstacle at a certain angle. If there is no obstacle within the sensing range of the laser, it will return the maximum scan range of the laser (4m). Table 6.1 shows a fragment of data returned by the laser and the graphic illustration of the data is depicted in Fig. 6.3. This data can be displayed on the LCD monitor of the wheelchair.

Table 6.1: Fragment of data from URG-04LX laser range finder

index	...	80	81	82	83	84	85	86	87	88	89	90	91	...
<i>dis</i> (m)	...	4.0	4.0	2.8	2.6	2.4	2.2	2.2	2.2	2.6	2.8	4.0	4.0	...

The minimum distance  $d_i(t)$  and the vision cone ( $\alpha_i^{(1)}$  and ( $\alpha_i^{(2)}$ )) of the obstacle

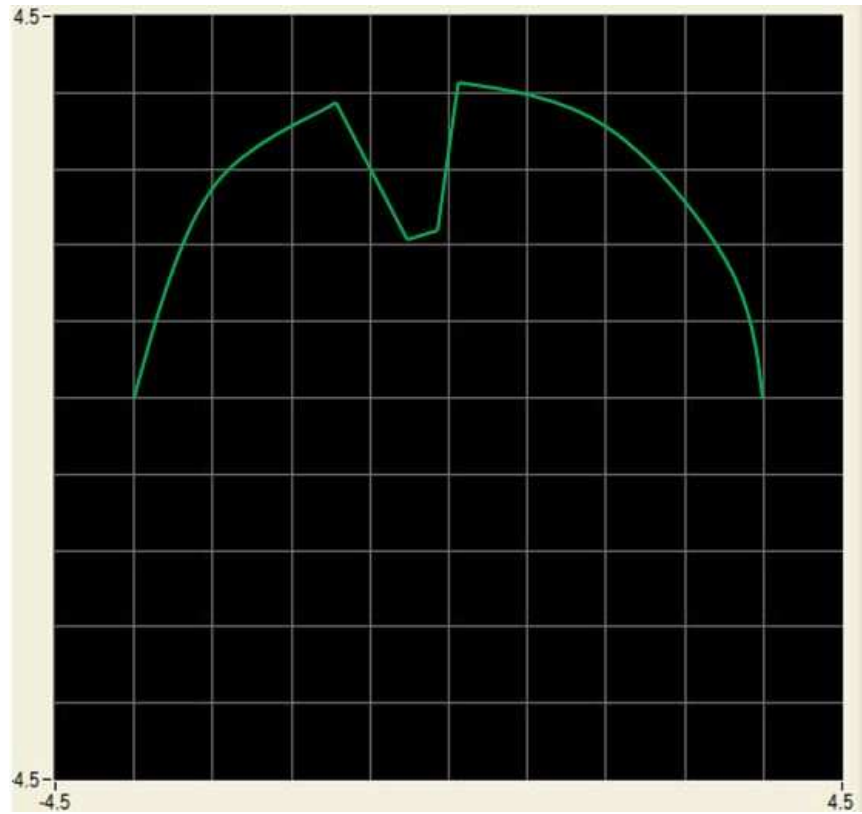


Figure 6.3: Graphic Illustration of the received data

can be found from the array of data returned from laser range finder. The minimum distance to the obstacle  $i$  is simply the minimum values in the array. The vision cone of the obstacle  $i$  can be found by searching for the "start" index and the "end" index for the distance less than the maximum sensing range of the laser, for example, in Table 6.1, the start index is 82 and the end index is 90. The appropriate angle of the boundaries of the vision cone are found by converting these two indices into proper angle.

- The velocity of the obstacle  $i$  can be estimated using the laser data by some existing approaches, see e.g. [49, 77]. In this case, since we have assumption (2.4) that the velocity of the obstacle  $v_i(t)$  is less than the maximum speed of the wheelchair, the numerical differentiate method is also applicable if the data are sampled at a reasonably fast rate.



- The bearing to the target  $H(t)$  can be easily computed when the orientation of the robot is known (by estimation from encoders) and the relative angular position of the target with respect to the wheelchair is known (by simple geometry), see Fig. 2.2(a).

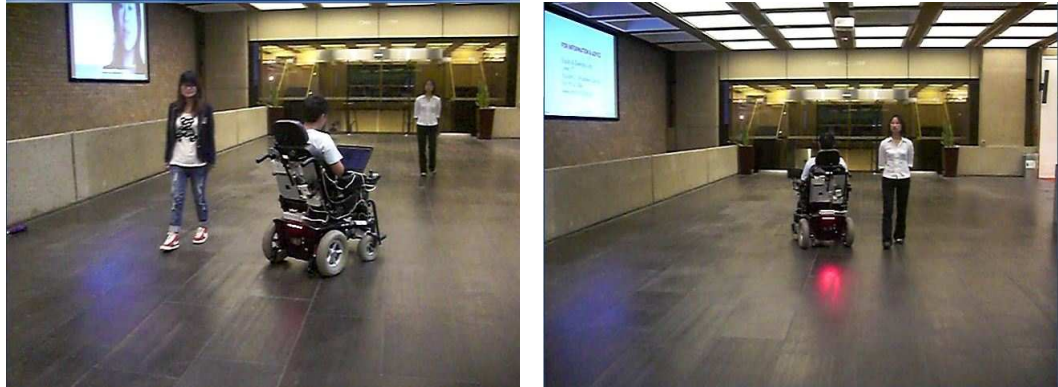
### 6.4.2 Experiments Results with a SAM Wheelchair

The experiments are conducted in real life scenarios to demonstrate the applicability of BINA on SAM wheelchair. Table 6.2 shows the wheelchair and controller parameters.

Table 6.2: Wheelchair and controller parameters

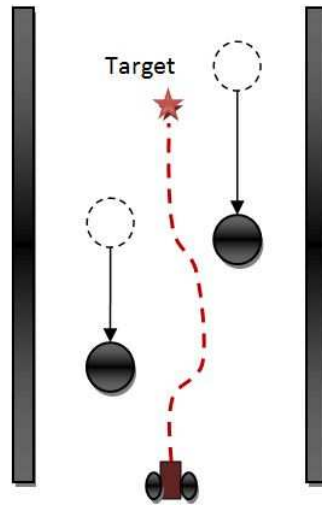
Parameter	Value	Comments
$T_s$	$0.1s$	Sampling interval
$2L$	$0.55m$	Distance between two driving wheels (the axle)
$D_w$	$0.35m$	Diameter of the driving wheels
$V_{max}$	$0.9m/s$	Maximum speed of the wheelchair
$U_{max}$	$\pi/4rad/s$	Maximum angular velocity
$\alpha_0$	$\pi/3.5rad$	Avoiding angle

In the first experiment, we present the simple experimental result of the wheelchair navigating in a dynamic environment with two moving obstacles. Fig. 6.4(a) and Fig. 6.4(b) show the moments when the wheelchair bypasses each of the obstacles. It can be observed that the space between the wheelchair and the obstacles are reasonable, meaning that the distance is large enough so that potential collision is impossible to happen and small to keep the efficiency of the avoidance maneuver. The complete path is depicted in Fig. 6.4(c). It can be seen that the wheelchair avoids the obstacle very efficiently. This experiments can be easily extended to a complicated scenario with many more obstacles, which represents many real life situation with cluttered obstacles such as train station, busy streets. The wheelchair is able to avoid each of the obstacles with the same fashion as shown in Fig. 6.4.



(a)

(b)



(c)

Figure 6.4: Wheelchair navigating in a dynamic environment with two moving obstacles

In many of the real life scenarios, it is likely that there is a mix of stationary and dynamic obstacles in the same environments. Museums and art galleries are examples of such environment with exhibitions (stationary) and many visitors (moving). Fig. 6.5 shows a similar environment with stationary (two chairs) and dynamic obstacles (the experimenter). The process of avoiding these obstacles are shown in Fig. 6.5(b), Fig. 6.5(c) and Fig. 6.5(d). The wheelchair reaches target at Fig. 6.5(e).

The last experiment in Fig. 6.6 shows a complex scenario of navigating a wheelchair in a narrow corridor with stationary and dynamic obstacles. Another challenge

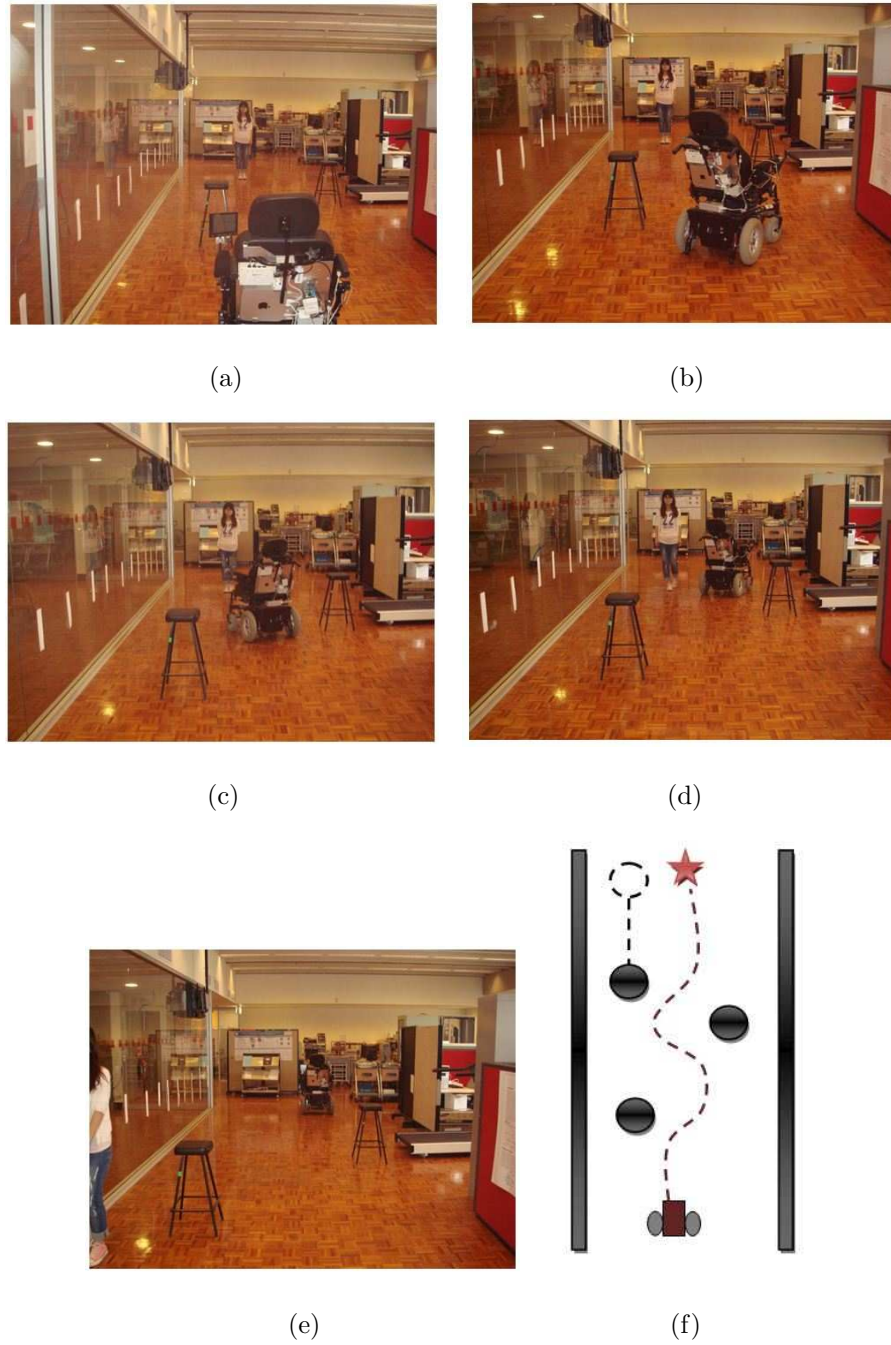


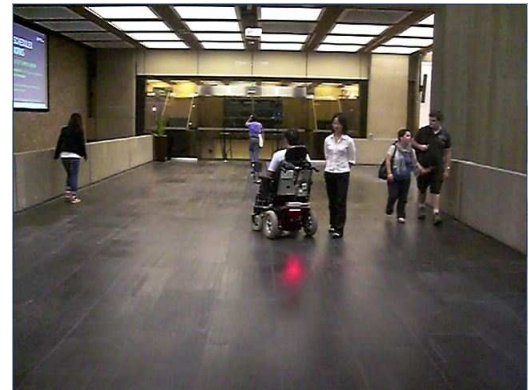
Figure 6.5: Wheelchair avoiding static and moving obstacles

of this experiment is that the final target can not be seen directly at the starting point. The wheelchair has to reach the target via a sub-target point. The wheelchair avoids a number of en-route obstacles (pedestrians, wall, trash bin and couches) in Fig. 6.6(a), Fig. 6.6(b), Fig. 6.6(c), Fig. 6.6(d), Fig. 6.6(e), Fig. 6.6(f). This experi-

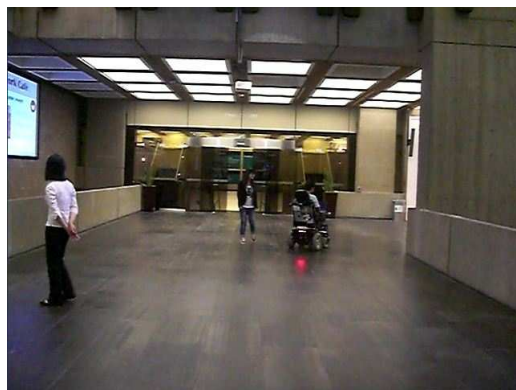
ment environment presents numerous public environments with pedestrians such as parks, streets.



(a)



(b)



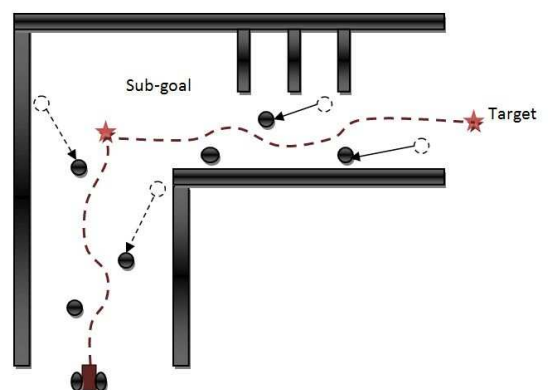
(c)



(d)



(e)



(f)

Figure 6.6: Wheelchair navigating in a cluttered corridor with moving pedestrians

## 6.5 Implementation and Experiments of Equidistant Navigation Algorithm (ENA)

### 6.5.1 Parameter Measurement

The only measurement required by ENA is the minimum distance  $d_i(t)$  from the wheelchair to the obstacle  $i$ . This information is measured by URG-04LX laser range finder in a similar but simpler fashion as introduced in Section 6.4.1. Since ENA does not require the direction for which the minimum distance is achieved, the data received by the notebook is an array of data without index, see e.g. Table 6.3. Therefore, it is more cost-efficient to implement the ENA on the wheelchair because the algorithm can work with other simpler or cheaper detection devices which provide distance information.

Table 6.3: Fragment of data from URG-04LX laser range finder

$dis(m)$	...	4.0	4.0	2.8	2.6	2.4	2.2	2.2	2.2	2.6	2.8	4.0	4.0	...
----------	-----	-----	-----	-----	-----	-----	-----	-----	-----	-----	-----	-----	-----	-----

The bearing to target  $H(t)$  can be easily obtained and is described in Section 6.4.1.

### 6.5.2 Experiment Results with SAM Wheelchair

We first show that the wheelchair with ENA is able to perform basic navigation tasks in a static environment. The wheelchair has to arrive at various target positions without any collision. The most challenging part of the experiment was to maintain a given margin between the wheelchair and the obstacles (mainly the walls). This experiment also presents solutions to the challenging scenarios that can not be solved by many existing approaches, i.e. narrow passage (see location c in Fig. 6.7(e)), hidden target location (see all the target locations in Fig. 6.7(e)). The figures capture crucial moment of the experiment and demonstrate maintaining a given margin to the wall (see Fig. 6.7(a)), straight motion to the target (Fig. 6.7(b)),

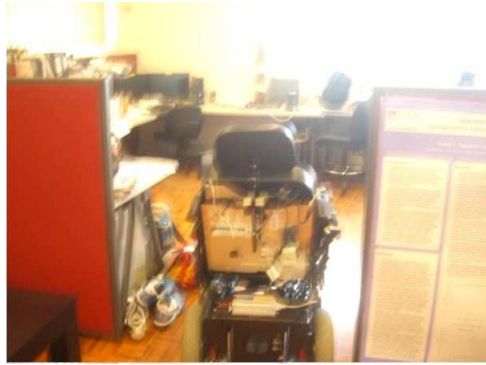




(a)



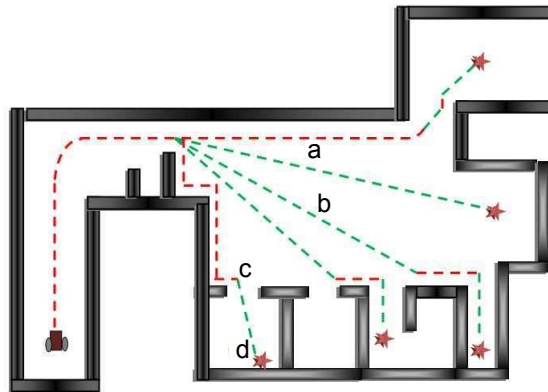
(b)



(c)



(d)



(e)

Figure 6.7: Wheelchair performs basic navigation tasks

crossing a narrow passage (similar to a door passage, Fig. 6.7(c)), and arrival at target position (Fig. 6.7(d)). The corresponding points are indicated by marks in Fig. 6.7(e). Fig. 6.7(e) also depicts the complete paths for all experiments. The green

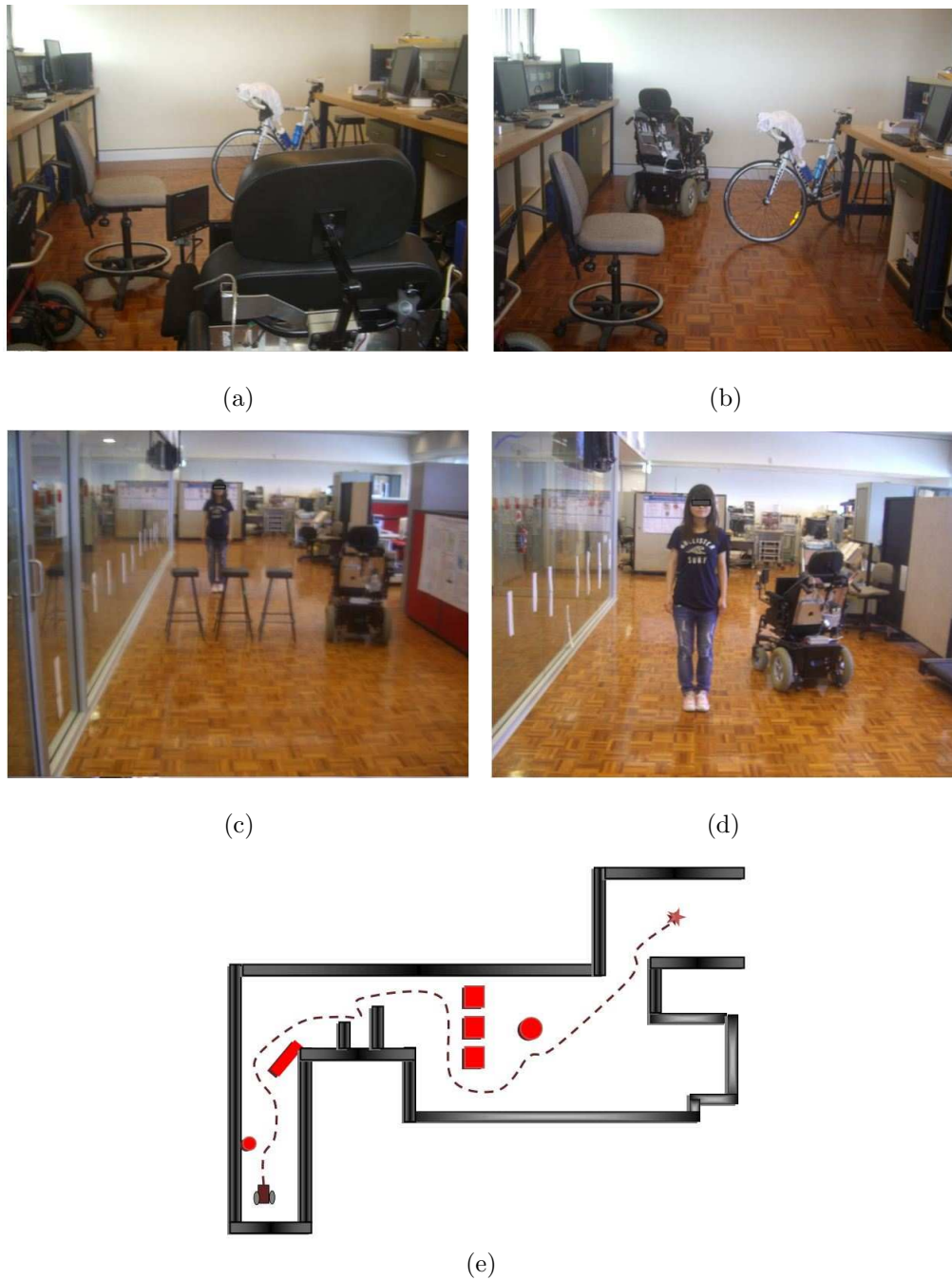


Figure 6.8: Wheelchair avoids random obstacles

dashed lines indicate the path for which the straight motion to the target is activated and the red dashed lines indicates the path for which the obstacle avoidance law is put in use.

We also added some occasional obstacles (bike, a chain of chairs, personal) in the

scene and examined the resultant performance of the proposed navigation algorithm. It can be seen from Fig. 6.8(e) that the shapes of the obstacles are arbitrary. The initial position of the wheelchair is shown in Fig. 6.8(a). Fig. 6.8(b) and Fig. 6.8(c) correspond to the moments when the wheelchair avoids a specific obstacle. The overall path is shown in Fig. 6.8(d). As can be seen, the wheelchair is still able to reach the target while respecting the required safety margin.

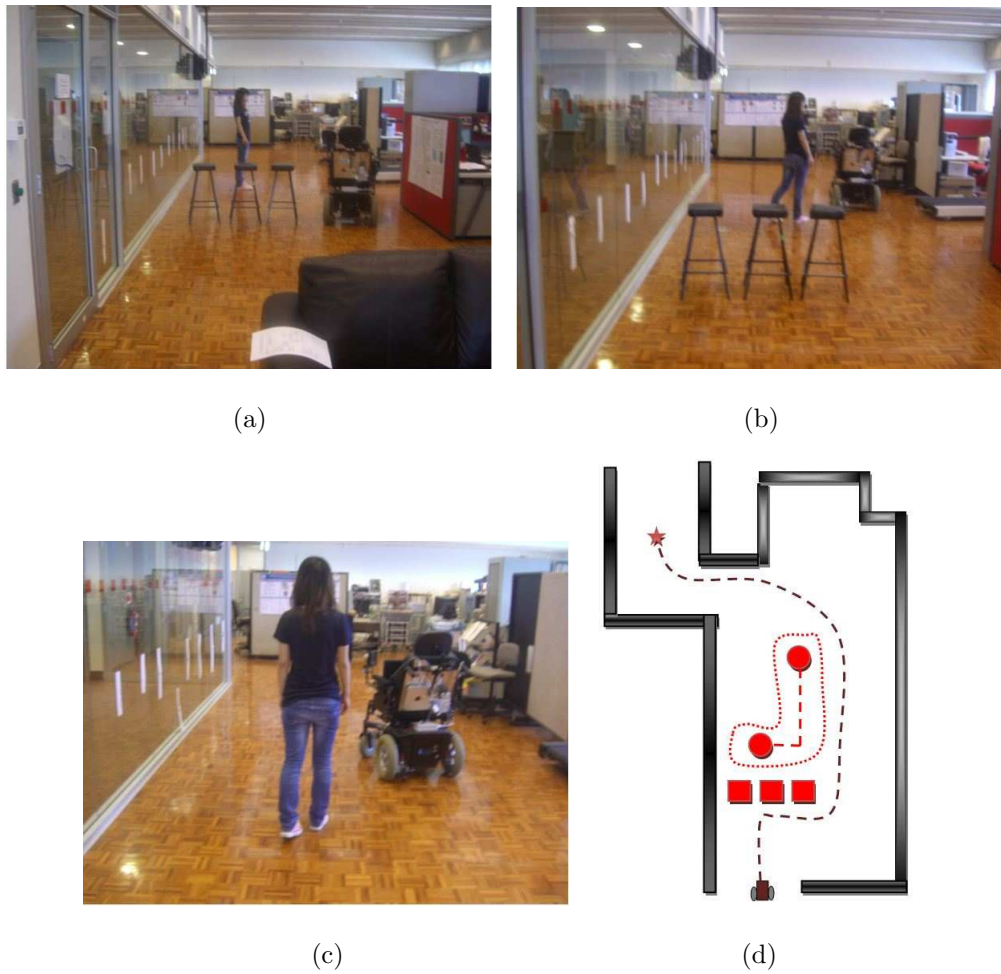


Figure 6.9: Wheelchair navigating among stationary and dynamic obstacles

In the next experiment, the wheelchair encounters a moving obstacle (the personal) just after bypassing the chain of chairs. This moving obstacle traverses the path from the wheelchair to the target and moves towards the target. In this scenario, the wheelchair is still able to track the  $d_0$ -equidistant curve of the moving



obstacle, which is shown by red dashed line around the obstacle, see Fig. 6.9(b) and Fig. 6.9(c). The complete path of this experiment is shown in Fig. 6.9(d).

The capability of the proposed navigation algorithm to avoid multiple moving obstacles is examined in Fig. 6.10. In these experiments, the obstacle moves in random directions as shown in Fig. 6.10(c) and Fig. 6.10(f). The wheelchair is still able to arrive at the target while avoiding all the obstacles. These experiments are repeated many time with the obstacles moving in various directions, the safety of the wheelchair is always guaranteed under the guidance of the ENA.

## 6.6 Summary

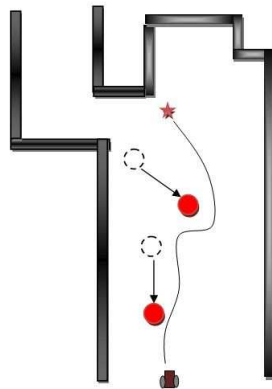
The implementation of BINA and ENA on the SAM wheelchair are presented in this chapter. Both of the algorithm ensures the safety of the wheelchair in static and dynamic environments with multiple obstacles. The performance of the algorithms has been confirmed by experiments with SAM wheelchair in real life scenarios.



(a)



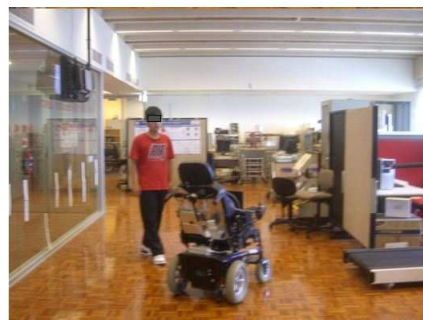
(b)



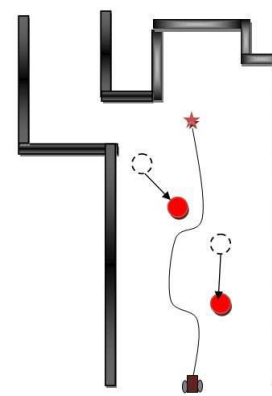
(c)



(d)



(e)



(f)

Figure 6.10: Wheelchair avoids multiple moving obstacles

## Chapter 7

# The Implementations on an Autonomous Intelligent Hospital Bed

The hospital beds had evolved from some crude stretchers to sets of convenient multi-functional medical devices over the centuries. Although we have seen these great improvements on the parts of hospital beds, most of the navigation tasks are still achieved manually. The manual steering of the hospital beds is the earliest and simplest way to control the motion of the hospital beds, but it may not be the most efficient one.

The existing hospital bed systems which are only motorised to adjust their own positions to a certain extend such as Trendlenburg, up, down positions, none of them is motorised for transportation. Designing an intelligent hospital bed system with obstacle avoidance ability is a good solution to the substantial labor required to transport the hospital bed. In this chapter, we present the implementations of Biologically-Inspired Navigation Approach (BINA) and Equidistant Navigation Approach (ENA), which are proposed in Chapter 2 and Chapter 3, respectively, on an automated hospital bed FlexBed. The implementations allow Flexbed to avoid en-route obstacles and arrive at target location safely. The performance of the Flexbed

with the proposed navigation algorithms is confirmed by real life experiments.

## **7.1 Background and Motivation**

The hospital beds had been widely used in hospitals to aid the transpiration the patients who need different types of medical attentions. Over the centuries, the hospital beds had evolved from some crude stretchers to sets of convenient multi-functional medical devices: various features and functions such as side rails, wheels, adjustable sections for different parts of body, etc, see e.g. [29,46,138,177,192]. These improvements provides better services to patients and conveniences to medical care personnels.

The most important purpose for utilising hospital beds is to safely transport the patients from current location to the target location. However, despite these great improvements on various parts of hospital beds, the navigation system of the hospital beds has never been improved. The motion of the hospital beds are controlled by manual steering of the hospital personnels. Manual steering is the earliest and simplest method to drive the hospital beds, but it may not be the most efficient and reliable method nowadays. The most convincing reason is that the performance of the transportation tasks by manual steering heavily rely on the personnels' reaction and decision which is subject to various factors such as the personnels' concentration on the navigation task, proficiency on operating hospital beds during transportation, etc. Reports and studies has shown that human-based mistake is a major contributing factor for the potential and unexpected risks of hospital beds transportation within hospitals, especially for critically ill patients [4, 119]. Furthermore, the force or torque provided by the hospital personnels may not be sufficient to steer the hospital bed due to its heavy load, especially in the emergency case. The implementation of navigation strategies on different transportation facilities is proven to be successful for improving the safety and efficiency of the facilities, e.g. wheelchairs, transport robots. Therefore, there is no doubt that the performance of the hospital

beds can be greatly boosted by helps of a safe and reliable autonomous navigation strategy.

None of the existing hospital bed system is considered as autonomous intelligent system with obstacle avoidance ability up to date, although some of them are motorised so that they are able to adjust their own position to a certain extend. The implementation of the algorithm BINA and ENA allows the hospital beds to safely navigate in a hospital environments with stationary and dynamic obstacles. The BINA allows the hospital beds to efficiently avoid obstacle and it is easy to compute. The ENA allows the hospital bed to navigate in a variety of unknown environments due to its flexibility and it is cost-efficient. These two algorithm are able to work independently to drive the hospital beds to the target location without collisions. They can also be integrated into other control schemes, for example, when there is no thread of collision, the motion of the hospital beds are controlled by some global navigation algorithms or Ipad controllers. The algorithms take over the control of hospital beds when the sensory system detects some obstacles within certain range.

## 7.2 System Model

We consider a hospital bed modeled as unicycle. The mathematical model of the hospital bed is as follows:

$$\begin{aligned} \dot{x} &= v(t) \cos \theta, & x(0) &= x_0, \\ \dot{y} &= v(t) \sin \theta, & y(0) &= y_0, \\ \dot{\theta} &= u & \theta(0) &= \theta_0 \end{aligned} \tag{7.1}$$

where

$$u \in [-U_{max}, U_{max}], \quad v(t) \in [0, V_{max}]. \tag{7.2}$$

Here the position of the wheeled mobile robot is represented by the absolute Cartesian coordinates as  $(x, y)$  of the reference point, which is the center of mass of the hospital bed. The orientation of hospital bed, measured in counterclockwise

direction from the reference axis, is given by  $\theta$ .  $v(t)$  and  $u(t)$  are the speed and angular velocity of the hospital bed.  $V_{max}$  and  $U_{max}$  are the non-holonomic constraints on the speed and angular velocities, which limits the minimum turning radius of the hospital bed by:

$$R = v/U_{max}. \quad (7.3)$$

### 7.3 Hospital Bed System Description

The BINA and ENA are implemented on a hospital bed, named Flexbed. Flexbed features two driving wheels located at the sides of the base section, two supportive wheels in the front and the rear sides of the base section. The encoders (model 775) has been attached to the driving wheels to measure the distance traveled by both wheels. There are totally three support lifts upon the base section, these lifts are able to support up to  $150kg$  of weight. They contain DC actuators for extension and contraction movements which allow the personnel to adjust the bed position to Trendelenburg, Anti-Trendelenburg, tilt to right or to left mode from motor controller implemented in iPad. iPad can also be used to control the motion of Flexbed. The available connection between iPad and the Flexbed is RS232 serial cable or WIFI. The motors for driving Flexbed and the actuators are powered from two  $12volts$  batteries in series, all other electronics are supplied from a separate  $12volts$  battery. The power switch is located at one side of Flexbed together with the emergency stop button. Flexbed uses various sensor devices, such as laser range finder and Microsoft Kinect, to interact with the real world. The appearance of Flexbed and the position of these key components are shown in Fig.7.1 and the schematic for the motor control system of Flexbed is presented in Fig.7.2.

Some of these components of Flexbed are particularly critical in the experiments, therefore they are described in more details as follows:

- A notebook (Windows 7 operating system with dual-core CPU running at  $2.66GHz$  and  $4GB$  RAM) with the proposed navigation algorithm BINA and

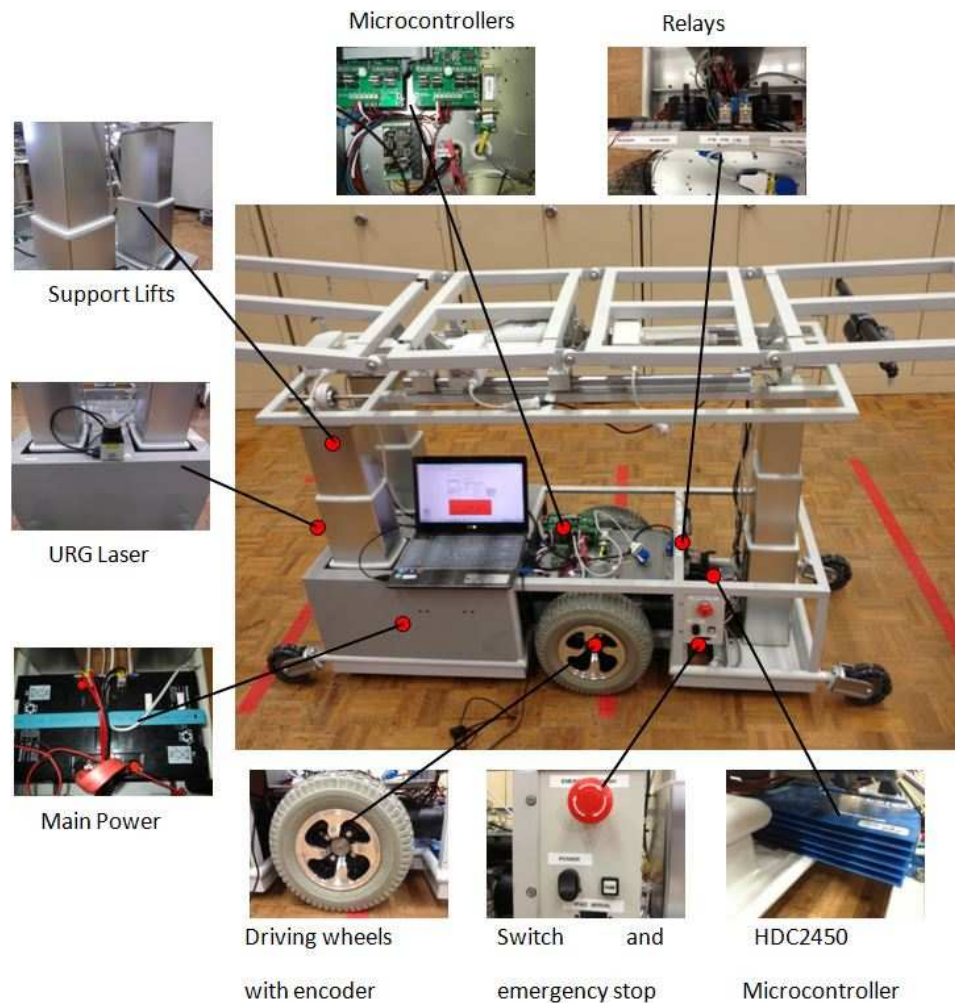


Figure 7.1: Key components in Flexbed

ENA implemented in LabView is the core to control the Flexbed system. It acquires all the necessary data from various devices to compute the control signals which is sent to the motor system to control the movement of the Flexbed.

- The URG-04LX laser is mounted on the middle at the front of the Flexbed. The laser scans the environment and provides necessary information to the wheelchair such as distance to the obstacles (required by both BINA and ENA), the vision cone (required by BINA) etc. The maximum scan angle for this laser range finder is  $240^{\circ}$  and the maximum scan range is  $4m$ .

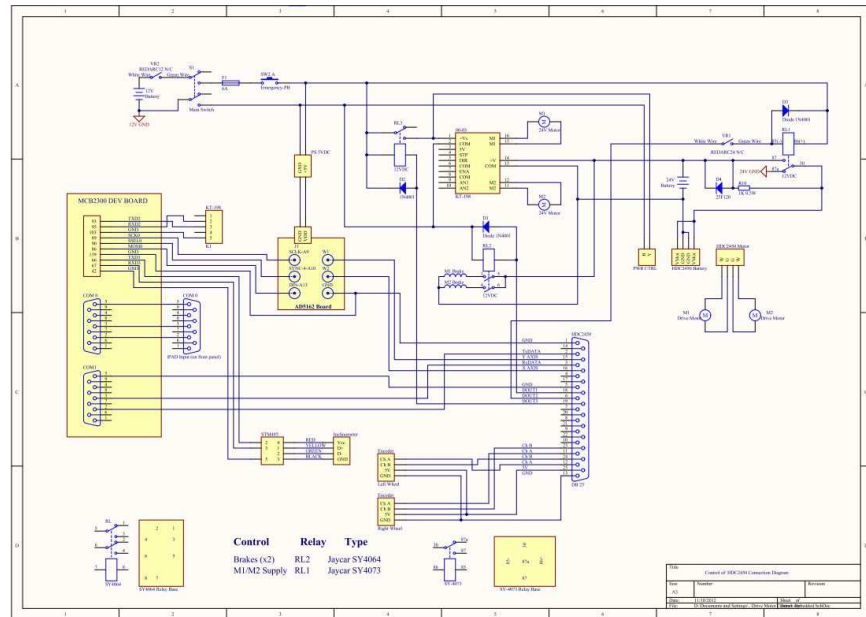


Figure 7.2: Schematic for the motor control system of Flexbed

with accuracy of  $\pm 1\%$  of the measurement, the scan frequency is  $10Hz$ . Furthermore, the laser is able to scan and provide two-dimensional map of the environment if necessary.

- The encoders that are attached to the driving wheels of the Flexbed are Model 775 Slim Thru-Bore encoders. Each encoder generate two square waves in incremental quadrature mode which provides the distance traveled by each wheel (Channel A leading B for clockwise rotation viewed from mounting face and vice versa). The rising time for these waves are less than  $1ms$ . The position  $(x, y)$  and the orientation  $\theta$  of the Flexbed can be estimated from the distance traveled by both wheels.
- The micro-controller RobotQ HDC2450 is responsible for receives information (distances, velocities, accelerations, power etc) from the encoders and send to control signals to the motor. It has four inputs for two incremental encoders to be connects. The control signals are sent to the motor system via serial interface or USB interface. This micro-controller comes with a utility software



called Robotrun Plus. This utility allows the user to check the connection on analogue or digital inputs/outputs pins and set the speed of the wheels to perform some simple motions. More importantly, it is able to adjust the power being sent to the wheels which controls the motions of Flexbed. It also allows the users to change the maximum speed and angular velocity of the Flexibed. The build-in PID controller allows the users to optimise the performance of the encoders and the motor.

## **7.4 Experiments of Flexbed with Biologically-Inspired Navigation Algorithm (BINA)**

In this section, we present the experiments of navigating Flexbed in various real life scenarios under the guidance of BINA. The data acquisition method has been introduced in 6.4.1 with the use of same URG-04LX laser range finder.

In the first experiment, we present and discuss two of the important safety measurements when Flexbed is guided by the obstacle avoidance law (2.9). These two measurements are 1) the angular difference between the instantaneous moving direction of the Flexbed and the closest boundary of the enlarged vision cone. 2) the minimum distance between the Flexbed and the obstacle. In this experiment, we deliberately position the experimenter within the sensor range of Flexbed and it is treated as an obstacle by Flexbed at all time. The snapshots of this experiment are shown in Fig. 7.3(a), Fig. 7.3(b) and Fig. 7.3(c), the complete paths taken by the Flexbed and the obstacle are shown in Fig. 7.3(d). The angular difference between the instantaneous moving direction of the Flexbed and the closest boundary is shown in Fig.7.3(e), it can be observed that there is a constant avoiding angle between them (in this case, the mean value of this angle equals  $-0.3287rad$  with standard deviation of 0.0551), which means the Flexbed will never collide into the Flexbed under the guidance of obstacle avoidance law (4.10). The safety of the Flexbed is further confirmed by the minimum distance between the Flexbed and

the obstacle  $d_i$  which is always greater than a certain safety distance  $d_{safe}$  (in this case, the minimum value of  $d_i$  equals  $0.816m$ ) in Fig.7.3(f).



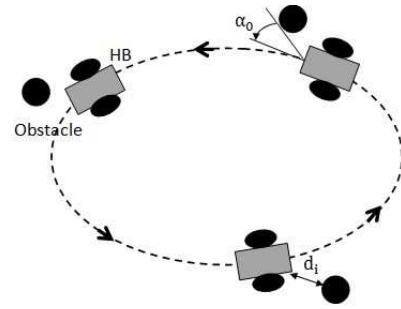
(a)



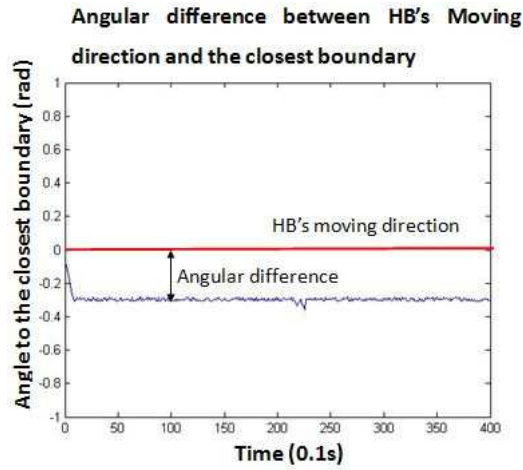
(b)



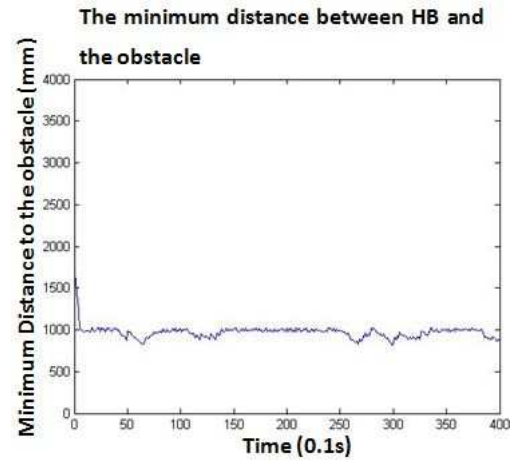
(c)



(d)



(e)



(f)

Figure 7.3: safety measurements during obstacle avoidance maneuver

The ability of BINA to navigate Flexbed in a simple environment with one stationary obstacle and one dynamic obstacle is shown in Fig. 7.4. Fig. 7.4(b) and Fig. 7.4(c) show the moment when Flexbed bypass these two obstacles. Flexbed

arrive safely at target location in Fig. 7.4(d). This experiment proves the capability of BINA to guide Flexbed to target location while avoiding en-route obstacles.

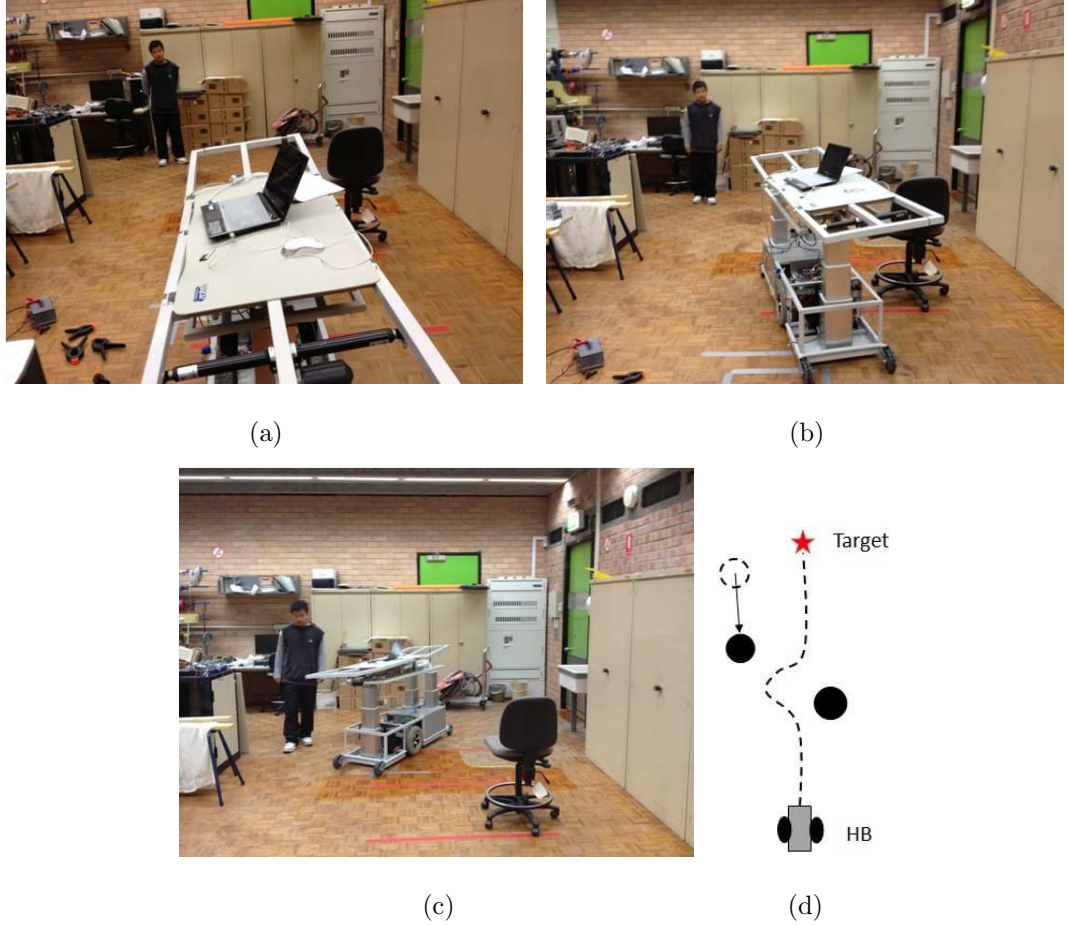


Figure 7.4: Flexbed avoids static and dynamic obstacles

The next experiment shows a more complicated environments with multiple moving obstacles. This is also a more realistic representation of the hospital environments where the obstacles (personals, patients) are moving with various velocities. Fig. 7.5(a), Fig. 7.5(b), Fig. 7.5(c) and Fig. 7.5(d) show the moments when the Flexbed avoids the obstacles. This experiments shows BINA is capable of navigating Flexbed in dynamic environments with moving obstacles, such as hospital environment.

In the last experiment, we examine the scenario which the radii of the obstacles are dynamically-changing. This is a common scenario in real life where a number



(a)



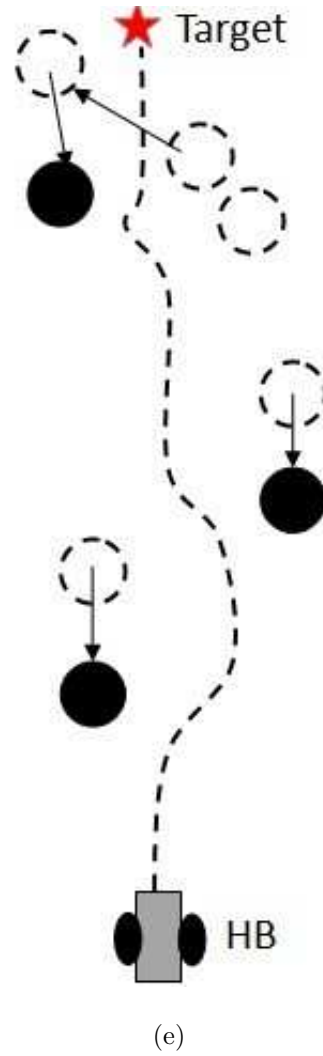
(b)



(c)



(d)



(e)

Figure 7.5: Flexbed avoids multiple dynamic obstacles

of obstacles may join together to form a larger group of obstacles or some obstacles may leave the group. In Fig. 7.6(a), Flexbed senses one obstacle (ob1) with small radius and start to avoid it. At The meantime, the second obstacle (ob2) joins ob1 to form 2 larger obstacle (ob3) in Fig. 7.6(b). It can be seen that BINA is able

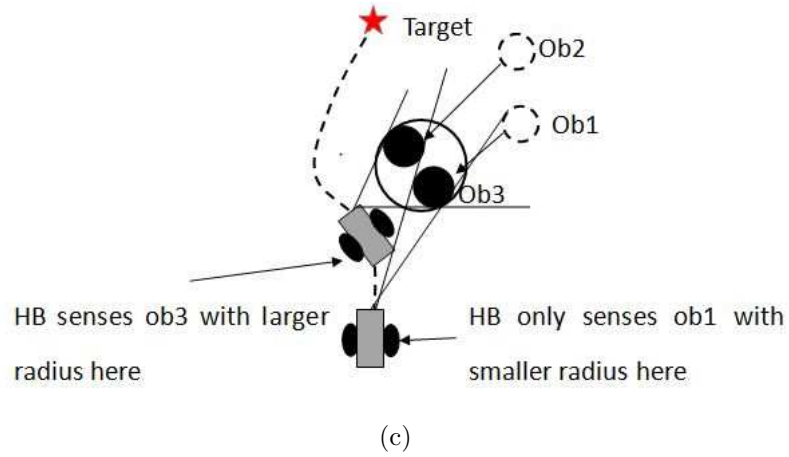
to avoid obstacles with dynamically changing radii by steering Flexbed towards the closest boundary of vision cone of the new obstacle. This experiment can be easily extended to scenario with more obstacles forming even larger group of obstacles or obstacles leaving the group resulting a group of obstacles with smaller radius.



(a)



(b)



(c)

Figure 7.6: Flexbed avoids obstacle with dynamic changing radius

## 7.5 Experiments of Flexbed with Equidistant Navigation Algorithm (ENA)

In this section, we present the experimental results of navigating Flexbed in real life scenarios under the guidance of ENA. Since the only information required by ENA to avoid obstacles is the minimum distance between Flexbed and the obstacle, the URG-04LX laser range finder can be replaced by other detection devices such as



Microsoft Kinect.

In the first experiment, we show that Flexbed is able to keep a constant distance between itself and the obstacle. We deliberately position the experimenter within the switching distance  $C$  so that he is considered as an obstacle at all time. The snapshots of the experiment are shown in Fig. 7.7(a), Fig. 7.7(b) and Fig. 7.7(c). The complete paths taken by the obstacle and Flexbed is depicted in Fig. 7.7(d).



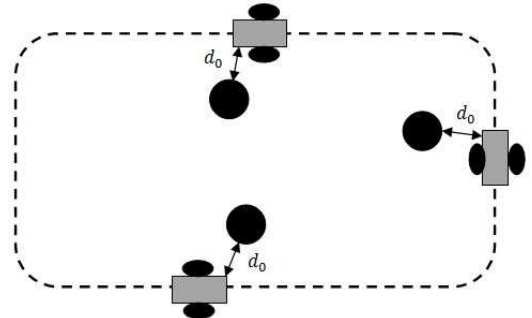
(a)



(b)



(c)



(d)

Figure 7.7: Flexbed keeps a constant distance to the obstacle

Fig. 7.8 shows the experiment of navigating Flexbed in an environment with stationary and dynamic obstacles. More importantly, this experiment shows that the ability of ENA to deal with obstacles with various shapes, which is a more realistic representation of the real life scenarios. Fig. 7.8(b) and Fig. 7.8(c) show the moment when Flexbed bypasses the rectangular obstacle (long bench) and the

moving obstacle (the experimenter). The complete path is depicted in Fig. 7.8(d).

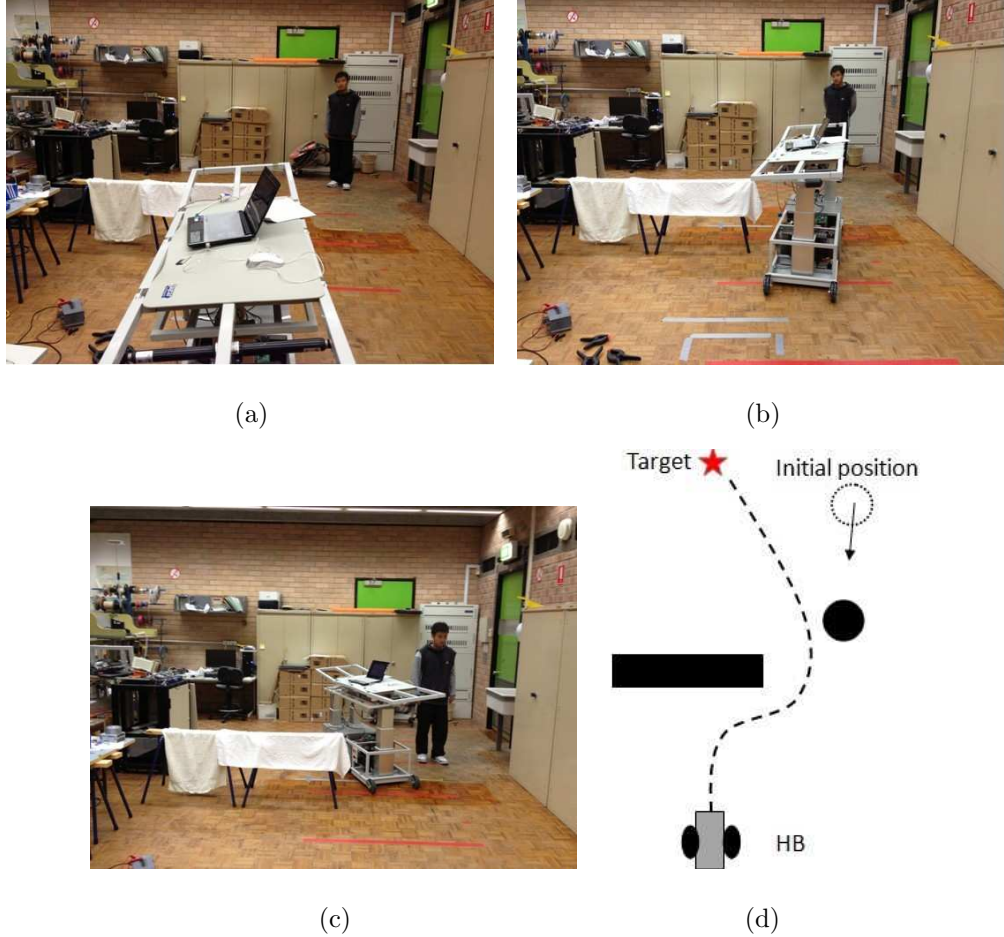


Figure 7.8: Flexbed avoids the stationary obstacle (long bench) and the dynamic obstacle (the experimenter)

The next experiment shows the ability of the Flexbed to navigate in dynamic environments with multiple moving obstacles. In this experiment, the obstacles are moving with various speed at random directions. Fig.7.9(a), Fig.7.9(b) Fig.7.9(c) and Fig. 7.9(d) show the crucial moments when the Flexbed bypasses each of the obstacles, the Flexbed is able to track the  $d_0$ -equidistant curve during its avoidance maneuver. The overall path of the Flexbed is depicted in Fig.7.9(e).

In Fig.7.10, the extension of the experiment shown in Fig.7.10 is presented. In this scenario, The Flexbed faces moving obstacles with different shapes, this is a common scenario in many hospital and other work places: two or more people

are moving side by side which makes the shapes of the group complicated. In the experiment, the group of two obstacles are interpolated as one larger obstacle depicted in Fig.7.10(d), the Flexbed is still able to track the  $d_0$ -equidistant curve and avoid the obstacles.

Finally, the Flexbed is able to deal with a dynamic deforming obstacle. In this experiment, the movement of the group of obstacles are lead by the a pilot (the first obstacle), and the pivot is moving in a sinusoidal fashion, resulting a snake-like deforming obstacle. The Flexbed is able to keep a constant distance with the obstacle as shown in Fig.7.11(a), Fig.7.7(b) and Fig.7.7(c) and Fig.7.7(d).

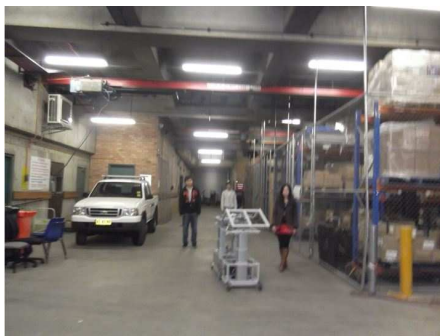
## 7.6 Summary

A novel hospital bed system Flexbed and the experimental results of BINA and ENA on Flexbed are presented in this chapter. Unlike the existing hospital bed systems which are not motorised for transportation, Flexbed offers various options to control its motion. The implementations of BINA and ENA allow Flexbed to safely and automatically navigate in a hospital environment with stationary and dynamic obstacles. The performance and applicability of the algorithms are confirmed by experimental results.





(a)



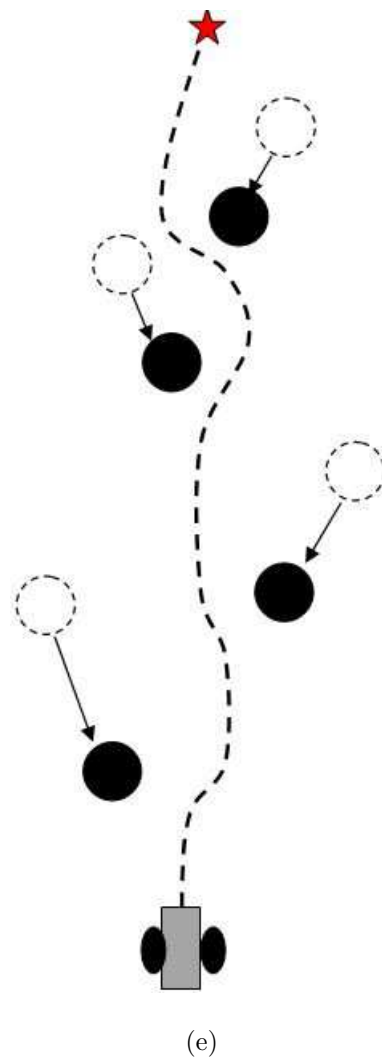
(b)



(c)



(d)



(e)

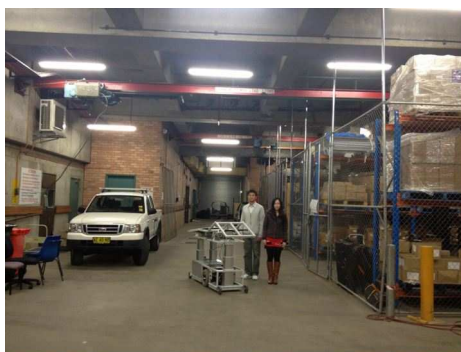
Figure 7.9: Flexbed navigating in dynamic environment with moving obstacles



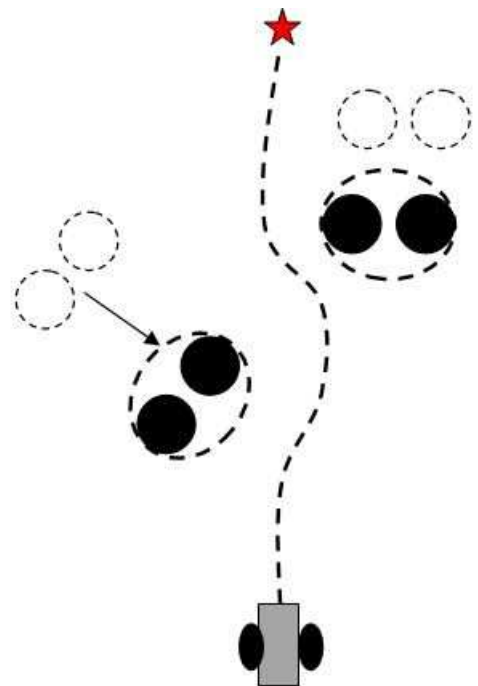
(a)



(b)

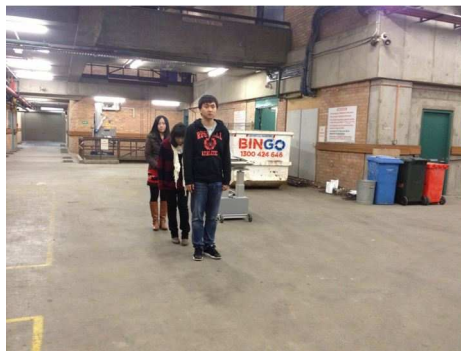


(c)



(d)

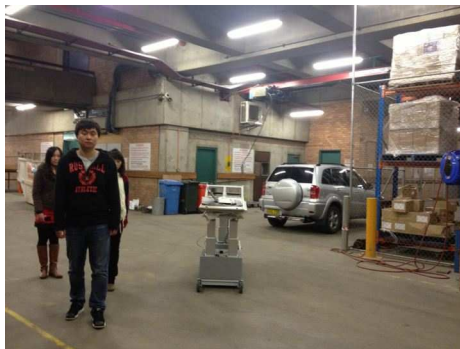
Figure 7.10: Flexbed avoids group of obstacles



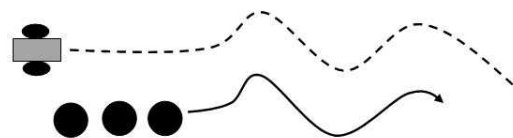
(a)



(b)



(c)



(d)

Figure 7.11: Flexbed avoids obstacle with dynamic deforming shape



## Chapter 8

# Decentralised Formation Building Algorithm for Groups of Mobile Robots

The decentralised control of groups of multiple mobile robots is another interesting and challenging topic in the field of mobile robotics. The decentralised control is a robust control scheme since the groups of mobile robots are dynamically decoupled, meaning that the motion of one robot in the group does not directly affect that of the others. Each robot updates its speed and heading based on its closest neighbors rather relying on receiving updates from centralised agent. This control scheme ensures that failure of single robot (the centralised agent) will not cause the failure of the whole group. A decentralised control law guides the robots so that they will eventually move in the same direction with the same speed

The design of a decentralised control law for formation control of multiple mobile robots is even more difficult in the sense that the robots are only not required to move in the same direction but also in a desired geometric configuration. Many of the existing formation building approaches consider simplest first or second order linear models for the motion of each robot, which causes the results to be heavily based on tools and methods from linear system theory. Such simple linear models

allows the robots to drive with arbitrarily large angular velocity and arbitrarily small turning radius, which is unrealistic in real life application and implementations. Furthermore, many approaches employs the leader-follower scheme which leads to restrictive classes of robot communication graphs. In some other papers the robot communication graph is assumed to be minimally rigid [62, 189] or time-invariant and connected [103] which is also quite restrictive.

In this chapter, we present a constructive and easy-to-implement decentralised formation building algorithm for a group of autonomous wheeled mobile robots. The formation building problem is particularly important for coverage problems for mobile sensor networks [11–14, 16, 38, 64]. The objective is to guide the robots in the group so that they eventually move in the same direction in the desired geometric configuration. This decentralised control law has its advantage of being able to work independently without a leader robot (the centralised agent). The robot uses sine global consensus to achieve and maintain the desired pattern. We consider two problems in this chapter, the first one is formation building with general class of communication graphs which are not assumed to be time-invariant or always connected. The second problem is formation building with anonymous robots which is more challenging because each robot are not aware of his position in the desired configuration, and the robots have to reach a consensus on their positions. The performance of the proposed formation building control laws is confirmed by computer simulations and experiments with real mobile robots.

## 8.1 Multi-Robots System Description

We consider a group of  $n$  autonomous mobile robots traveling in a plane in continuous time, these robots are labeled from 1 to  $n$ . The absolute Cartesian coordinates of the vehicle  $i$  is represented by  $(x_i(t), y_i(t))$ . The orientation of the vehicle  $i$  is represented by  $\theta_i(t)$ , which is measured from the x-axis in the counterclockwise direction. The value of  $\theta_i(t)$  falls into the interval  $\theta_i \in (-\pi, \pi]$  with  $\theta_i(t) = 0$  corresponds to

the direction of positive x-axis. The kinematic equations of the robot motion are given by

$$\begin{aligned}\dot{x}_i(t) &= v_i(t) \cos(\theta_i(t)) \quad ; \\ \dot{y}_i(t) &= v_i(t) \sin(\theta_i(t)) \quad ; \\ \dot{\theta}_i(t) &= \omega_i(t)\end{aligned}\tag{8.1}$$

Here,  $v_i(t)$  and  $\omega_i(t)$  are the speed and angular velocity of the robot  $i$ , respectively. They are also the control inputs of robot  $i$  and their values are limited by the following constraints:

$$-\omega^{max} \leq \omega_i(t) \leq \omega^{max} \quad \forall t \geq 0,\tag{8.2}$$

$$V^m \leq v_i(t) \leq V^M \quad \forall t \geq 0\tag{8.3}$$

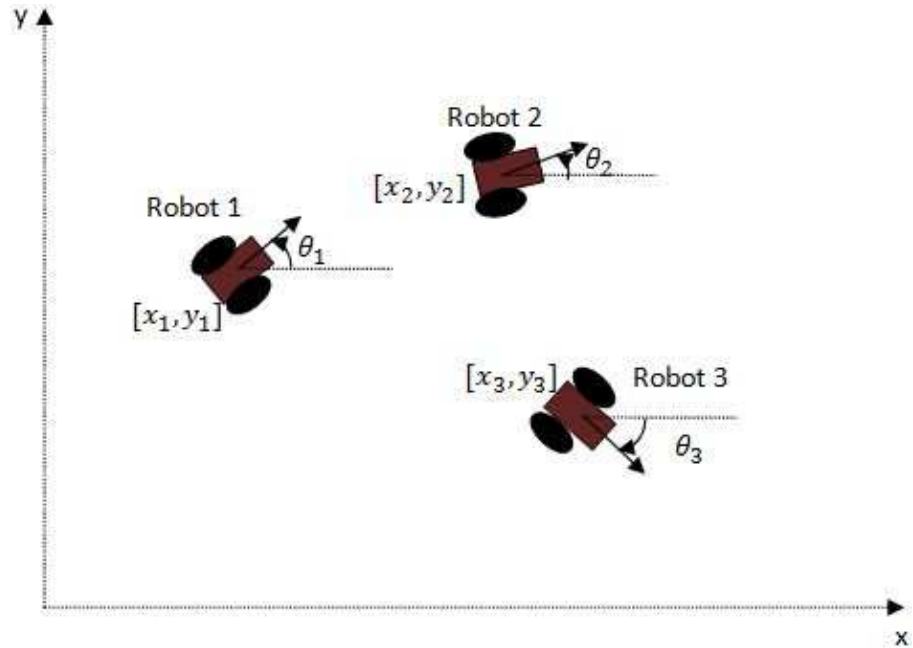


Figure 8.1: Multi-robots system

for all robot serial number  $i = 1, 2, \dots, n$ . Here  $\omega^{max} > 0$  and  $0 < V^m < V^M$  are given constants. Notice that since  $v_i(t) > 0$  for all  $t$ , the vehicles are assumed not to drive backwards. Fig. 8.1 shows the illustration of the multi-robot system.

Introduce two-dimensional vectors  $z_i(t)$  of the vehicles' coordinates and vectors  $V_i(t)$  of the robots' velocities by

$$z_i(t) := \begin{pmatrix} x_i(t) \\ y_i(t) \end{pmatrix}, \quad V_i(t) := \begin{pmatrix} v_i(t) \cos(\theta_i(t)) \\ v_i(t) \sin(\theta_i(t)) \end{pmatrix} \quad (8.4)$$

for all  $i = 1, 2, \dots, n$ .

The vehicles in the groups communicate at discrete time instants  $k = 0, 1, 2, \dots$ . We use a connected undirected graph  $\mathcal{G}(k)$  to determine whether two robots  $i$  and  $j$  ( $i \neq j$ ) are able to communicate at time  $k$ . The  $n$  vertices of the graph  $\mathcal{G}(j)$  corresponds to the  $n$  vehicles in the plane. Two vertices are connected by an edge in the graph  $\mathcal{G}(j)$  if and only if the corresponding robots communicate at time  $k$ . Introduce the following notations.

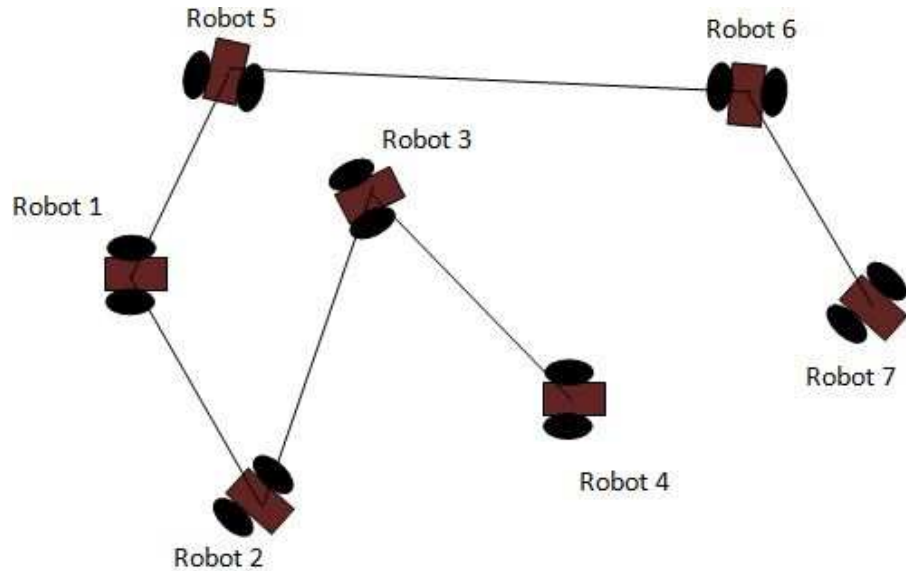


Figure 8.2: Connected undirected graph  $\mathcal{G}(k)$

For any vertex  $i \in \{1, 2, \dots, n\}$ ,  $\mathcal{N}_i(k)$  denotes the set of all vertices  $j \neq i$  of



$\mathcal{G}$  that are connected to  $i$  by an edge. Furthermore,  $n_i(k)$  denotes the number of vertices in the set  $\mathcal{N}_i(k)$ .

We will also need the following assumption.

**Assumption 8.1.1.** There exists an infinite sequence of contiguous, non-empty, bounded time-intervals  $[k_j, k_{j+1})$ ,  $j = 0, 1, 2, \dots$ , starting at  $k_0 = 0$ , such that across each  $[k_j, k_{j+1})$ , the union of the collection  $\{\mathcal{G}(k) : k \in [k_j, k_{j+1})\}$  is a connected graph.

We use the consensus variables  $\tilde{\theta}_i(k)$ ,  $\tilde{x}_i(k)$ ,  $\tilde{y}_i(k)$  and  $\tilde{v}_i(k)$  to achieve common goals of all the robots. The consensus variable  $\tilde{\theta}_i(k)$  is used to achieve the common heading of the formation, the consensus variables  $\tilde{x}_i(k)$  and  $\tilde{y}_i(k)$  are used to achieve the common origin of coordinates of the formation, and the consensus variable  $\tilde{v}_i(k)$  is used to achieve the common speed of the formation.

All the robots starts with different initial values of  $\tilde{\theta}_i(0)$ ,  $\tilde{x}_i(0)$ ,  $\tilde{y}_i(0)$  and  $\tilde{v}_i(0)$ . At time  $k$ , each of the robots in the group estimates  $\tilde{\theta}_i(k)$ ,  $\tilde{x}_i(k)$ ,  $\tilde{y}_i(k)$  and  $\tilde{v}_i(k)$  of the consensus formation parameters. This allows the robots to eventually converge to some consensus values which define a common formation and speed for all the robots.

**Assumption 8.1.2.** The initial values of the consensus variables  $\tilde{\theta}_i$  satisfy  $\tilde{\theta}_i(0) \in [0, \pi)$  for all  $i = 1, 2, \dots, n$ .

We assume that the information on other vehicles that is available to the vehicle  $i$  at time  $k$  is the coordinates  $(x_j(k), y_j(k))$  (in practise, in mobile wireless networks, these coordinates can be estimated using robust Kalman filtering approach [123–125, 152, 158]) and the consensus variables  $\tilde{\theta}_j(k)$ ,  $\tilde{x}_j(k)$ ,  $\tilde{y}_j(k)$  and  $\tilde{v}_j(k)$  for all  $j \in \mathcal{N}_i(k)$ . Also, the vehicle's own coordinates, orientation and speed are measured at any time  $t \geq 0$ .

## 8.2 General Formation Building

We propose the following rules for updating the consensus variables  $\tilde{\theta}_i(k)$ ,  $\tilde{x}_i(k)$ ,  $\tilde{y}_i(k)$  and  $\tilde{v}_i(k)$ :

$$\begin{aligned}
 \tilde{\theta}_i(k+1) &= \frac{\tilde{\theta}_i(k) + \sum_{j \in \mathcal{N}_i(k)} \tilde{\theta}_j(k)}{1 + |\mathcal{N}_i(k)|}; \\
 \tilde{x}_i(k+1) &= \frac{x_i(k) + \tilde{x}_i(k) + \sum_{j \in \mathcal{N}_i(k)} (x_j(k) + \tilde{x}_j(k))}{1 + |\mathcal{N}_i(k)|} - x_i(k+1); \\
 \tilde{y}_i(k+1) &= \frac{y_i(k) + \tilde{y}_i(k) + \sum_{j \in \mathcal{N}_i(k)} (y_j(k) + \tilde{y}_j(k))}{1 + |\mathcal{N}_i(k)|} - y_i(k+1); \\
 \tilde{v}_i(k+1) &= \frac{\tilde{v}_i(k) + \sum_{j \in \mathcal{N}_i(k)} \tilde{v}_j(k)}{1 + |\mathcal{N}_i(k)|}.
 \end{aligned} \tag{8.5}$$

In multi-robots systems, the essential informations have to be shared among the robots for them to achieve common goals. In the case of formation building, the use of rules in (8.5) allow the robots to achieve a consensus on the heading, speed and mass centre of the formation.

**Lemma 8.2.1.** *Suppose that Assumptions 8.1.1 and 8.1.2 hold and the consensus variables are updated according to the decentralized control algorithm (8.5). Then there exist constants  $\tilde{\theta}_0$ ,  $\tilde{X}_0$ ,  $\tilde{Y}_0$  and  $\tilde{v}_0$  such that*

$$\begin{aligned}
 \lim_{k \rightarrow \infty} \tilde{\theta}_i(k) &= \tilde{\theta}_0; \\
 \lim_{k \rightarrow \infty} \tilde{v}_i(k) &= \tilde{v}_0; \\
 \lim_{k \rightarrow \infty} (x_i(k) + \tilde{x}_i(k)) &= \tilde{X}_0; \\
 \lim_{k \rightarrow \infty} (y_i(k) + \tilde{y}_i(k)) &= \tilde{Y}_0.
 \end{aligned} \tag{8.6}$$

for all  $i = 1, 2, \dots, n$ . Moreover, the convergence in (8.6) is exponentially fast.

The statement of Lemma 8.2.1 immediately follows from the main result of [48].

Since the consensus update rules in (8.5) is based on the averaging of the consensus variables of neighbouring robots, the consensus variables in (8.6) should be converged to the same constants  $\tilde{\theta}_0$ ,  $\tilde{X}_0$ ,  $\tilde{Y}_0$  and  $\tilde{v}_0$  for any robot  $i$ .

Assume that  $X_1, X_2, \dots, X_n, Y_1, Y_2, \dots, Y_n$  are given numbers. We define a navigation law that is globally stabilizing with initial conditions  $(x_i(0), y_i(0), \theta_i(0))$ ,  $i = 1, 2, \dots, n$  and the configuration  $\mathcal{C} = \{X_1, X_2, \dots, X_n, Y_1, Y_2, \dots, Y_n\}$ , if there exist a Cartesian coordinate system and  $\tilde{v}_0$  such that the solution of the closed-loop system (8.1) with these initial conditions and the proposed navigation law in this Cartesian coordinate system satisfies:

$$\begin{aligned} \lim_{t \rightarrow \infty} (x_i(t) - x_j(t)) &= X_i - X_j, \\ \lim_{t \rightarrow \infty} (y_i(t) - y_j(t)) &= Y_i - Y_j, \end{aligned} \quad (8.7)$$

$$\begin{aligned} \lim_{t \rightarrow \infty} \theta_i(t) &= 0, \\ \lim_{t \rightarrow \infty} v_i(t) &= \tilde{v}_0, \end{aligned} \quad (8.8)$$

for all  $1 \leq i \neq j \leq n$ .

Equation (8.7) and (8.8) defines the final convergence values for the consensus variables. (8.7) means that all the robots will move in the same direction (along x-axis of the global Cartesian coordinate system) with the same speed defined by  $\tilde{v}_0$ . (8.8) means that the robots will move in the desired geometric configuration defined by  $\mathcal{C} = \{X_1, X_2, \dots, X_n, Y_1, Y_2, \dots, Y_n\}$ . Both (8.7) and (8.8) require a global Cartesian coordinate system. They define the final goal for formation building of multi-robot system.

An simple example of formation building scenario for the robots to form a square of side 1 is shown in Fig. 8.3. In this case, for the geometric configuration  $\mathcal{C}$ , we can take  $X_1 = X_2 = 0, X_3 = X_4 = 1, Y_1 = Y_3 = 0, Y_2 = Y_4 = 1$ .

The objective of this section is to present a globally stabilizing control law for the multi-vehicle formation under consideration.

In our globally stabilizing law, we will use the consensus variables  $\tilde{\theta}_i(k)$ ,  $\tilde{x}_i(k)$ ,  $\tilde{y}_i(k)$  and  $\tilde{v}_i(k)$  updated according to (8.5). Introduce the corresponding piecewise

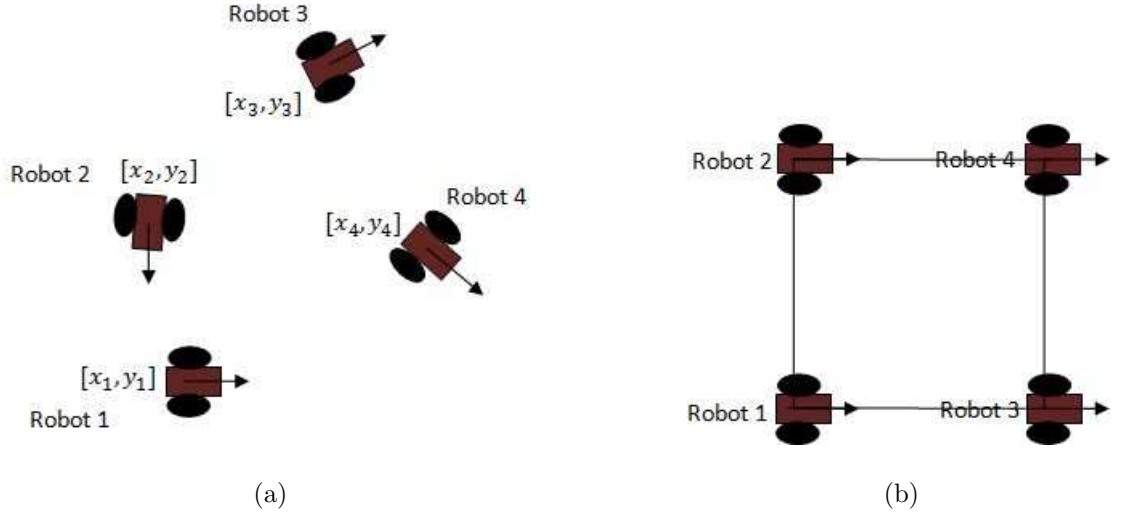


Figure 8.3: (a) Initial state (robots with arbitrary  $\tilde{\theta}_i(0)$ ,  $\tilde{x}_i(0)$ ,  $\tilde{y}_i(0)$  and  $\tilde{v}_i(0)$ ) (b) Final state (robots move in the same speed and direction with a desired square formation)

constant continuous time variables as

$$\begin{aligned}
 \tilde{\theta}_i(t) &:= \tilde{\theta}_i(k) \quad \forall t \in (k, k+1); \\
 \tilde{x}_i(t) &:= \tilde{x}_i(k) \quad \forall t \in (k, k+1); \\
 \tilde{y}_i(t) &:= \tilde{y}_i(k) \quad \forall t \in (k, k+1); \\
 \tilde{v}_i(t) &:= \tilde{v}_i(k) \quad \forall t \in (k, k+1).
 \end{aligned} \tag{8.9}$$

Let  $c > 0$  be any constant such that

$$c > \frac{2V^M}{\omega^{max}}. \tag{8.10}$$

Furthermore, let  $h_1$  and  $h_2$  be non-zero two-dimensional vectors, and let  $\alpha$  be the angle between the vectors  $h_1$  and  $h_2$  measured from  $h_1$  in the counter-clockwise direction,  $-\pi < \alpha \leq \pi$ , i.e.  $\alpha = 0$  if  $h_1 = h_2$ . Now introduce the following function:

$$f(h_1, h_2) := \text{sign}(\alpha) \tag{8.11}$$

where  $\text{sign}(\cdot)$  is defined by

$$\text{sign}(\alpha) := \begin{cases} -1 & \text{if } \alpha < 0 \\ 0 & \text{if } \alpha = 0 \\ 1 & \text{if } \alpha > 0 \end{cases} \quad (8.12)$$

For any time  $t$  and any robot  $i$ , we consider a Cartesian coordinate system with the  $x$ -axis in the direction  $\tilde{\theta}_i(t)$  (according to the definition (8.9),  $\tilde{\theta}_i(t)$  is piecewise constant). In other words, in this coordinate system  $\tilde{\theta}_i(t) = 0$ ,  $x_i(t), y_i(t)$  are now coordinates of the robot  $i$  in this system. Notice that we now formulate our decentralized control law for each robot in its own coordinate system. Since according to Lemma 8.2.1,  $\tilde{\theta}_i(k)$  converges to the same value for all  $i$ , all these robots' coordinate systems converge to the same coordinate system in which (8.7) holds.

Introduce the functions  $h_i(t)$  as

$$h(t) := (x_i(t) + \tilde{x}_i(t)) + X_i + t\tilde{v}_i(t) \quad (8.13)$$

for all  $i$ . Also, for all  $i = 1, 2, \dots, n$  introduce two-dimensional vectors  $g_i(t)$  as

$$\begin{aligned} g_i^x(t) &: = \begin{cases} h_i(t) + c & \text{if } x_i(t) \leq h_i(t) \\ x_i(t) + c & \text{if } x_i(t) > h_i(t) \end{cases} \\ g_i^y(t) &: = (y_i(t) + \tilde{y}_i(t)) + Y_i, \\ g_i(t) &: = \begin{pmatrix} g_i^x(t) \\ g_i^y(t) \end{pmatrix} \end{aligned} \quad (8.14)$$

and two-dimensional vectors  $d_i(t)$  as

$$d_i(t) := g_i(t) - z_i(t)$$

where  $z_i(t)$  is defined by (8.4).

**Assumption 8.2.1.** We assume that the configuration  $\mathcal{C} = \{X_1, X_2, \dots, X_n, Y_1, Y_2, \dots, Y_n\}$  and the constant  $c$  satisfying (8.10) are known to each robot  $i$ .

Now we introduce the following decentralized control law:

$$v_i(t) = \begin{cases} V^M & \text{if } x_i(t) \leq h_i(t) \\ V^m & \text{if } x_i(t) > h_i(t) \end{cases}$$

$$\omega_i(t) = \omega^{max} f(V_i(t), d_i(t)), \quad (8.15)$$

for all  $i = 1, 2, \dots, n$ . Here  $f(\cdot, \cdot)$ ,  $V_i(\cdot)$ ,  $d_i(\cdot)$  are defined by (8.4), (8.11).

We will need the following assumption.

**Assumption 8.2.2.** The initial robots' speeds satisfy

$$V^m < v_i(0) < V^M$$

for all  $i = 1, 2, \dots, n$ .

Notice that Assumption 8.2.2 is just slightly stronger the requirement (8.3) for  $t = 0$  where non-strict inequalities are required.

**Theorem 8.2.1.** *Consider the autonomous robots described by the equations (8.1) and the constraints (8.2), (8.3). Let  $\mathcal{C} = \{X_1, X_2, \dots, X_n, Y_1, Y_2, \dots, Y_n\}$  be a given configuration. Suppose that Assumptions 8.1.1, 8.1.2, 8.2.1 and 8.2.2 hold, and  $c$  is a constant satisfying (8.10). Then, the decentralized control law (8.5), (8.15) is globally stabilizing with any initial conditions and the configuration  $\mathcal{C}$ .*

The proof of this theorem is presented in [157]

The main idea of the navigation law (8.15) can be explained as follows. Each vehicle  $i$  is guided towards a fictitious target  $T_i$  that is always located "ahead" of the desired vehicle's position relative to its neighbours. The reason why we guide the vehicle towards a fictitious target but not the desired relative vehicle's position itself is that if we guided the vehicle towards the desired relative position, we would have  $\|d_i(t)\| \rightarrow 0$ , therefore,  $\omega_i(t) \rightarrow \infty$  and the constraint (8.2) would be violated. Notice that our method for guidance towards a fictitious target  $T_i$  is a pure pursuit type guidance law [154].

### 8.3 Formation Building with Anonymous Robots

In this section, we consider a more challenging problem: formation building with anonymous robots. It is more challenging than general formation building problem in the sense that each robots does not know its position in the configuration  $\mathcal{C} = \{X_1, X_2, \dots, X_n, Y_1, Y_2, \dots, Y_n\}$  in advance, the robots should reach a consensus on their position. In the area of robotics, it is common to use the multi-robot task allocation approach to similar problems. However, most work on multi-robot task allocation has been ad hoc and empirical especially in the case of an arbitrarily large number of robots; see e.g. [37, 74]. In this section, we propose a randomised algorithm to handle this problem. The randomised algorithm for anonymous robots is a modification of the algorithm from [150].

We first state our definition of navigation law with anonymous robots. A navigation law is said to be globally stabilizing with anonymous robots and the configuration  $\mathcal{C} = \{X_1, X_2, \dots, X_n, Y_1, Y_2, \dots, Y_n\}$  if for any initial conditions  $(x_i(0), y_i(0), \theta_i(0))$ , there exists a permutation  $r(i)$  of the index set  $\{1, 2, \dots, n\}$  such that for any  $i = 1, 2, \dots, n$ , there exist a Cartesian coordinate system and  $\tilde{v}_0$  such that the solution of the closed-loop system (8.1) with the proposed navigation law in this Cartesian coordinate system satisfies (8.8) and

$$\begin{aligned} \lim_{t \rightarrow \infty} (x_i(t) - x_j(t)) &= X_{r(i)} - X_{r(j)}, \\ \lim_{t \rightarrow \infty} (y_i(t) - y_j(t)) &= Y_{r(i)} - Y_{r(j)}, \end{aligned} \quad (8.16)$$

for all  $1 \leq i \neq j \leq n$ .

Let  $R > 0$  be the detection range of the robots, i.e, each robot  $i$  is able to detect all other robots inside the circle of radius  $R$  at the current position of robot  $i$ . Furthermore, let  $0 < \epsilon < \frac{R}{2}$  be a given constant. For any configuration  $\mathcal{C} = \{X_1, X_2, \dots, X_n, Y_1, Y_2, \dots, Y_n\}$  introduce a undirected graph  $\mathcal{P}$  consisting of  $n$  vertices. Vertices  $i$  and  $j$  of the graph  $\mathcal{P}$  are connected by an edge if and only if  $\sqrt{(X_i - X_j)^2 + (Y_i - Y_j)^2} \leq R - 2\epsilon$ , see Fig. 8.4 for example. We will need the following assumption.

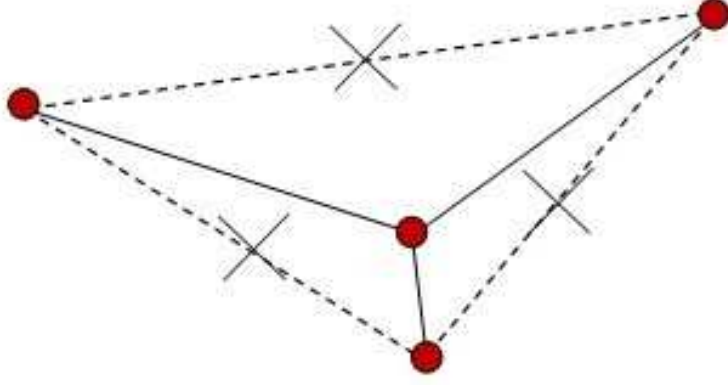


Figure 8.4: Graph  $\mathcal{P}$

**Assumption 8.3.1.** The graph  $\mathcal{P}$  is connected.

We present a randomised algorithm to build an index permutation function  $r(i)$ . Let  $N \geq 1$  be a given integer. Let  $r(0, i) \in \{1, 2, \dots, n\}$  be any initial index values where  $i = 1, 2, \dots, n$ .

As in the navigation law (8.5), (8.15), for any time  $t$  and any robot  $i$ , we consider a Cartesian coordinate system with the  $x$ -axis in the direction  $\tilde{\theta}_i(t)$  (according to the definition (8.9),  $\tilde{\theta}_i(t)$  is piecewise constant). In other words, in this coordinate system  $\tilde{\theta}_i(t) = 0$ ,  $x_i(t), y_i(t)$  are now coordinates of the robot  $i$  in this system. Furthermore, we say that a vertex  $j$  of the graph  $\mathcal{P}$  is vacant at time  $kN$  for robot  $i$  if there is no any robot inside the circle of radius  $\epsilon$  centred at the point

$$\begin{pmatrix} (x_i(kN) + \tilde{x}_i(kN)) + X_j + kN\tilde{v}_i(kN) \\ (y_i(kN) + \tilde{y}_i(kN)) + Y_j \end{pmatrix}$$

Let  $\mathcal{S}(kN, i)$  denote the set of vertices of  $\mathcal{P}$  consisting of  $r(kN, i)$  and those of vertices of  $\mathcal{P}$  that are connected to  $r(kN, i)$  and vacant at time  $kN$  for robot  $i$ . Let  $|\mathcal{S}(kN, i)|$  be the number of elements in  $\mathcal{S}(kN, i)$ . It is clear that  $1 \leq |\mathcal{S}(kN, i)|$  because  $r(kN, i) \in \mathcal{S}(kN, i)$ . Moreover, introduce the Boolean variable  $b_i(kN)$  such that  $b_i(kN) := 1$  if there exists another robot  $j \neq i$  that is inside of the circle of



radius  $\epsilon$  centred at

$$\begin{pmatrix} (x_i(kN) + \tilde{x}_i(kN)) + X_i + kN\tilde{v}_i(kN) \\ (y_i(kN) + \tilde{y}_i(kN)) + Y_i \end{pmatrix}$$

at time  $kN$ , and  $b_i(kN) := 0$  otherwise. We propose the following random algorithm:

$$\begin{aligned} r((k+1)N, i) &= r(kN, i) \quad \text{if} \\ &(b_i(kN) = 0 \text{ or } (b_i(kN) = 1 \text{ and } |\mathcal{S}(kN, i)| = 1)); \\ r((k+1)N, i) &= j \\ &\text{with probability } \frac{1}{|\mathcal{S}(kN, i)|} \quad \forall j \in \mathcal{S}(kN, i) \\ &\text{if } (b_i(kN) = 1 \text{ and } |\mathcal{S}(kN, i)| > 1). \end{aligned} \quad (8.17)$$

Now we are in a position to present the main result of this section.

**Theorem 8.3.1.** *Consider the autonomous robots described by the equations (8.1) and the constraints (8.2), (8.3). Let  $\mathcal{C} = \{X_1, X_2, \dots, X_n, Y_1, Y_2, \dots, Y_n\}$  be a given configuration. Suppose that Assumptions 8.1.1, 8.1.2, 8.2.2 and 8.3.1 hold, and  $c$  is a constant satisfying (8.10). Then, initial conditions  $(x_i(0), y_i(0), \theta_i(0))$ ,  $i = 1, 2, \dots, n$  there exists an integer  $N_0 > 0$  such that for any  $N \geq N_0$ , the decentralized control law (8.5), (8.15), (8.17) with probability 1 is globally stabilizing with these initial conditions and the configuration  $\mathcal{C}$ .*

The proof of this theorem is presented in [157].

## 8.4 Computer Simulation Results

### 8.4.1 General Formation Building

In this section, we present simulation results for the formation building algorithm in present in Section 8.2. In Fig. 8.5, the simulation result for straight line formation with four robots are presented. At the beginning of the simulation, the robots are randomly positioned and orientated, they also start with various speeds, i.e. The

robots start with different values of  $\tilde{\theta}_i(0)$ ,  $\tilde{x}_i(0)$ . The motions of the robots are governed by (8.1), (8.2) and (8.3) with decentralized law (8.5), (8.15) employed. The robots updates consensus information with the neighbouring robots and successfully form a straight line with equal distance between two consecutive robots. The formation is achieved at which the first straight line is drawn, and the robots are able to keep the formations for the rest of time, which demonstrates the consistency of the proposed formation building algorithm over time.

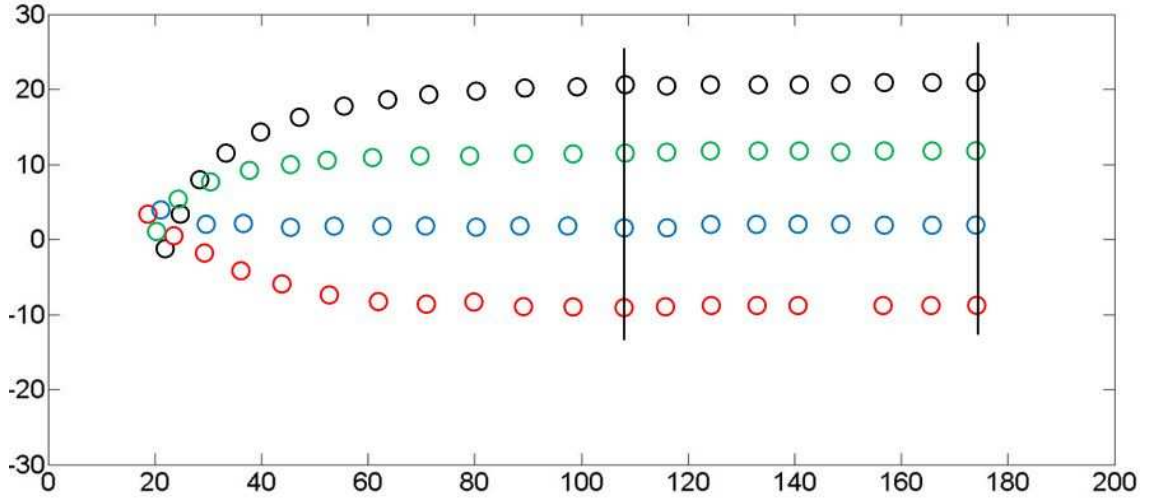


Figure 8.5: Straight line formation with equal separation between two consecutive robots

In Fig. 8.6, Fig. 8.7, Fig. 8.8 and Fig. 8.9, we present more complicated formation simulation results. From these results, we show that with any initial conditions and various configuration  $\mathcal{C}$ , the robots are always able to achieve global stability.

The following tables 8.1 and 8.2 show the detailed results over several experiment runs (performed in simulation) for four robots (square formation) .

The average error in x-coordinate is  $-0.0309m$ ,  $-0.0107m$ ,  $-0.0012m$ ,  $-0.0201m$ . and the standard deviation is  $0.0521$ ,  $0.0609$ ,  $0.0652$ ,  $0.0465$ .

The average error in y-coordinate is  $0.0020m$ ,  $0.0161m$ ,  $0.0252m$ ,  $0.0008m$ , and the standard deviation is  $0.0556$ ,  $0.0643$ ,  $0.0483$ ,  $0.0595$ .

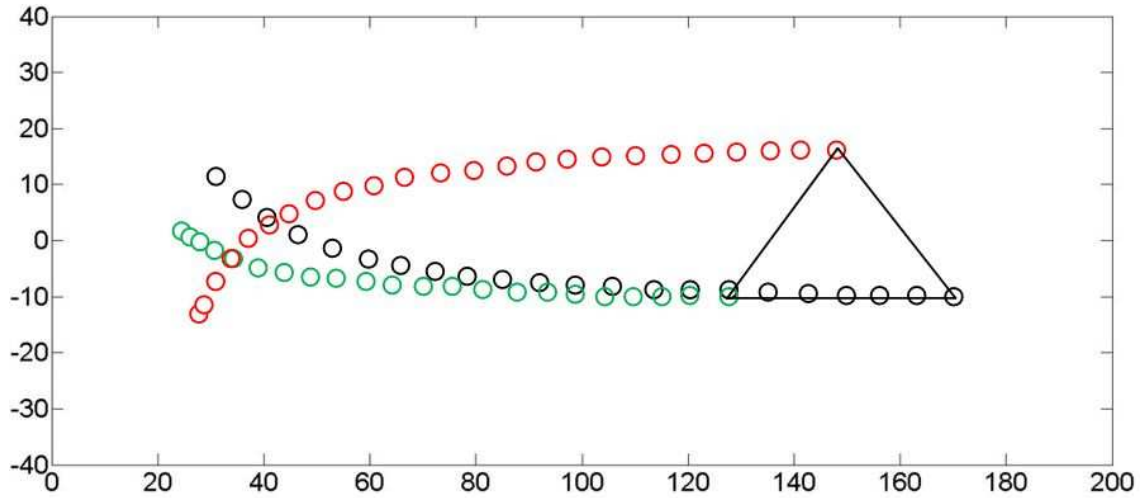


Figure 8.6: Equilateral Triangle formation

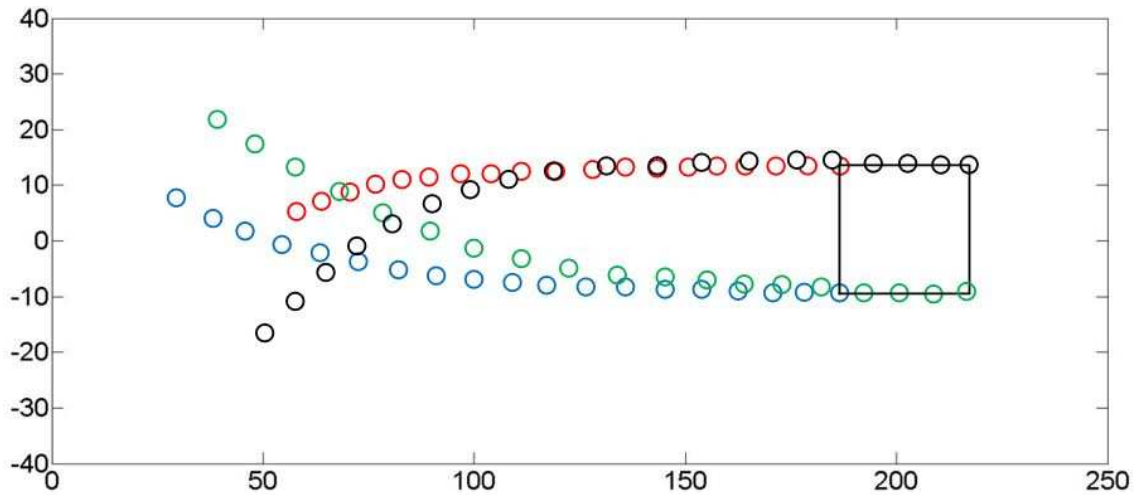


Figure 8.7: Robots form a square shape

### 8.4.2 Formation Building with Anonymous Robots

We present simulation results for formation building with anonymous robots. This randomised formation building algorithm is presented in Section 8.3. In Fig. 8.10, we present a similar simulation as in Fig. 8.5 with anonymous robots. The major difference is that the robots are not aware of their positions in the configuration  $\mathcal{C}$  and the motion and the motions of the robots are guided by the proposed randomised algorithm with index permutation. We can observe from Fig. 8.10, two robots may

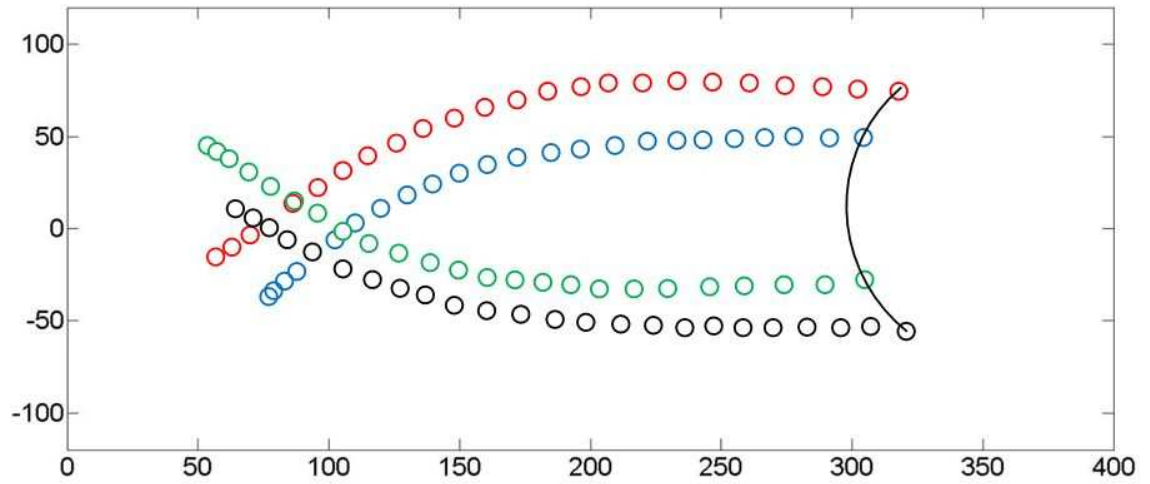


Figure 8.8: Robots form an arc

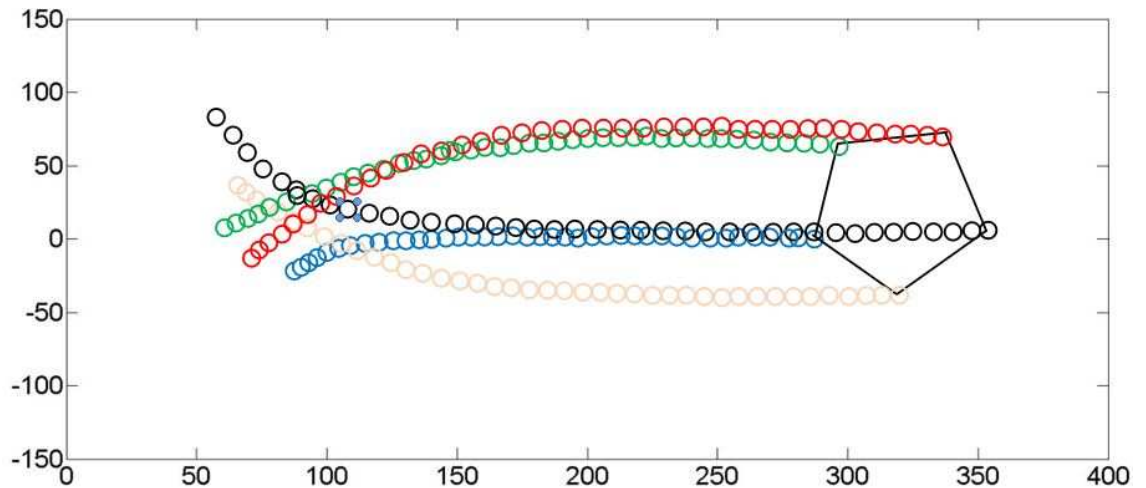


Figure 8.9: Robots form regular pentagon

aim for the same position in the configuration  $\mathcal{C}$  during the simulation. To resolve this situation, the index permutation assigns a new vertex to one of the two robots so that they do not "compete" for the same index. This permutation is likely to take place several time in one simulation. Table 8.3 shows the indices assigned to all the robots during simulation presented in Fig. 8.10, each index corresponds one vertex depicted in Fig. 8.10.

. More complicated formation building with anonymous robots are presented in Fig. 8.11, Fig. 8.12 and Fig. 8.13. The randomised algorithm achieve global stability

Table 8.1: Experiment Results over ten experiment runs (x coordinate)

	$X_1 - X_2$	$X_2 - X_3$	$X_3 - X_4$	$X_4 - X_1$
Desired difference (X)	-5.000	0	5.000	0
Actual output 1	-4.9071	0.0698	5.0868	0.0357
Actual output 2	-5.0515	0.0486	4.9784	0.0311
Actual output 3	-4.9342	0.0412	4.9064	-0.0446
Actual output 4	-4.9092	-0.0806	5.0647	0.0390
Actual output 5	-4.9634	0.0900	4.9069	-0.0123
Actual output 6	-4.9763	0.0531	5.0590	-0.0626
Actual output 7	-4.9980	-0.0109	5.0293	0.0419
Actual output 8	-5.0509	-0.0448	5.0359	0.0310
Actual output 9	-4.9325	-0.0762	4.9997	0.0919
Actual output 10	-4.9681	0.0171	4.9448	0.0503

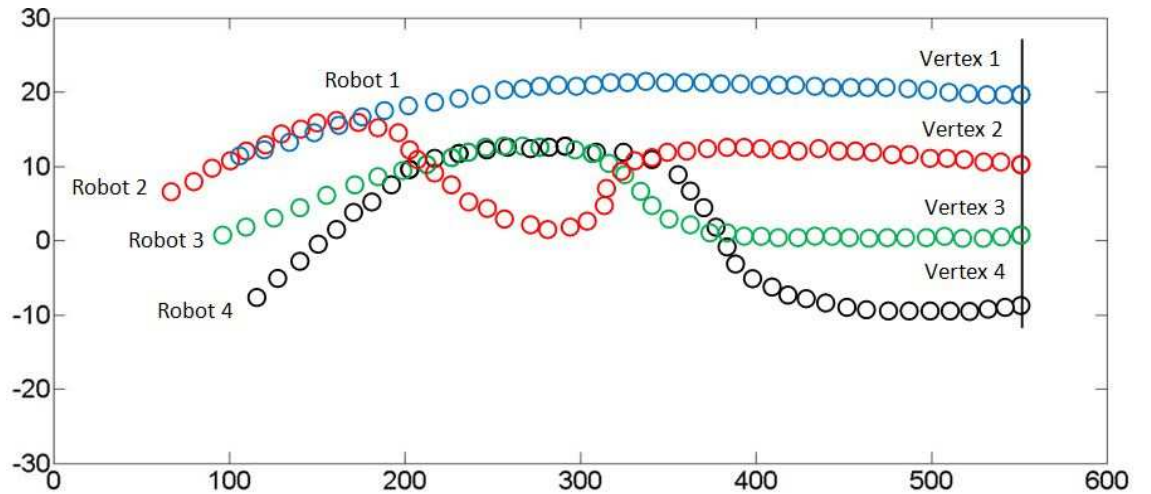


Figure 8.10: Straight line formation with anonymous robots, permutation applied

with any initial conditions and various configuration  $\mathcal{C}$ .

Table 8.2: Experiment Results over ten experiment runs (y coordinate)

	$Y_1 - Y_2$	$Y_2 - Y_3$	$Y_3 - Y_4$	$Y_4 - Y_1$
Desired difference (Y)	0	-5.000	0	5.000
Actual output 1	-0.0490	-5.0012	0.0398	5.0782
Actual output 2	0.0919	-5.0094	-0.0723	4.9299
Actual output 3	-0.0485	-5.0681	-0.0491	5.0629
Actual output 4	-0.0513	-5.0859	-0.0300	4.9393
Actual output 5	-0.0498	-5.0232	-0.0053	4.9703
Actual output 6	0.0662	-5.0171	0.0099	5.0834
Actual output 7	-0.0428	-5.0514	0.0507	4.9761
Actual output 8	0.0136	-4.9152	-0.0892	5.0062
Actual output 9	0.0558	-5.0868	-0.0740	5.0138
Actual output 10	-0.0061	-4.9024	-0.0326	4.9324

Table 8.3: Indices assigned to all the robots

Simulation time	Index of robot 1	Index of robot 2	Index of robot 3	Index of robot 4
1-12	1	1	2	2
13- 29	1	3	2	2
29-53	1	2	3	4

## 8.5 Experiments with Group of Real Robots

In this section, we present our experiments with real robots guided by the algorithm proposed in Section 8.2. In these experiments, the proposed algorithm is implemented on the TurtleBot and Pioneer 3-DX. The encoders are available for both type of the robots, thus all the necessary information for the proposed algorithm (positions, orientations and the velocities) can be easily accessed. We have done experiments with three and four wheeled robots.

The experiment snapshots in Fig. 8.14 and 8.15 show the performance of the

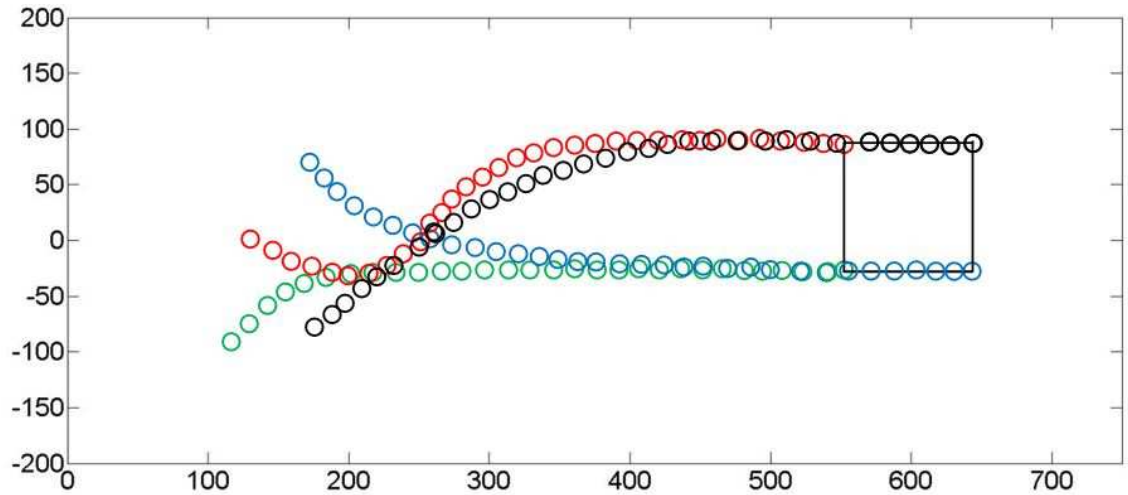


Figure 8.11: Square formation with anonymous robots, permutation applied

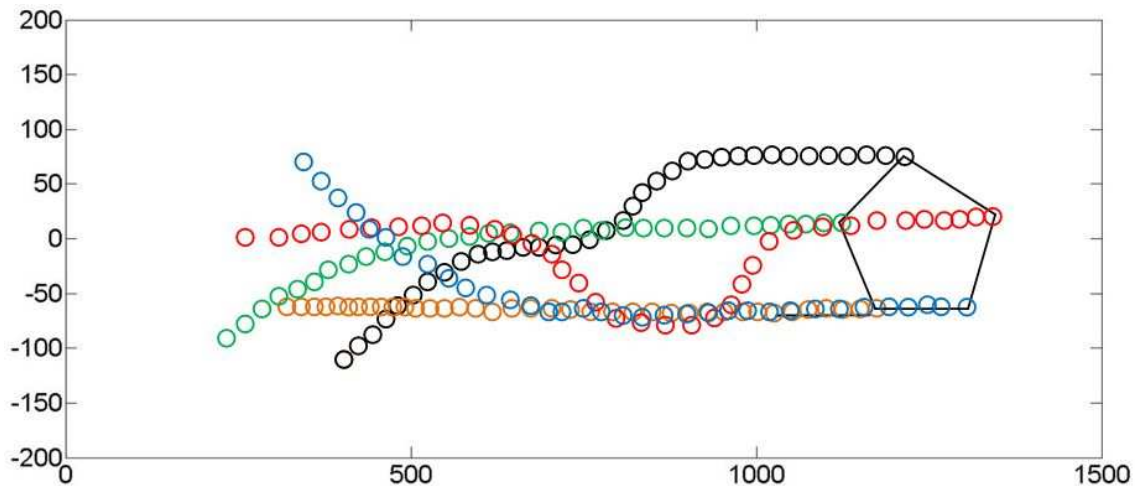


Figure 8.12: Regular pentagon formation with anonymous robots, permutation applied

algorithm with three robots. At the start of each experiment, the robots are placed in random positions with random orientations, see Fig. 8.14(a) and 8.15(a). In Fig. 8.14(b) and 8.15(b), the robots are converging to their final configurations, during this convergence process. The real time position and orientation information are obtained from encoders which are attached to both wheels of the robots. The final formation configurations for these two experiments, which are regular triangle and straight line, are shown in Fig. 8.14(c) and Fig. 8.15(c), respectively. The overall

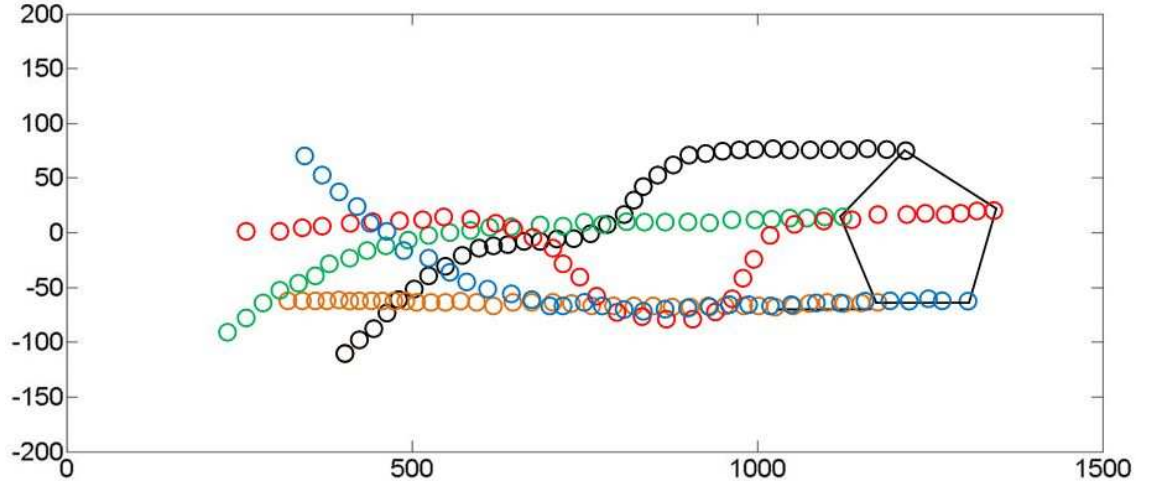


Figure 8.13: Random shape formation with anonymous robots, permutation applied path taken by the robots during these experiments are shown in Fig. 8.14(d) and 8.15(d).

In the next two experiments, one additional robot is added into the group. It is shown in Fig. 8.16 and Fig. 8.17 that, the formation of four robots (rectangle in Fig. 8.16 and kite in Fig. 8.17) is achievable under the guidance of the proposed algorithm. Notice that the figures of this section show illustrative schematic trajectories of the robots. The convergence time varies in different scenarios, normally, formations with three mobile robots take approximately 40 sec to converge and formations with four mobile robots take approximately 55 sec to converge. It can be seen that more complicated formation can be achieved as more robots are added into the group.

## 8.6 Summary

In this chapter, we propose a decentralised formation building algorithm for a group of mobile robots to collectively move with the same speed in a desired geometric formation from any initial positions. Furthermore, we consider the problem of formation with anonymous robots. The robots does not aware of their position in the desired formation in advance and they should reach a consensus on their position.



The multi-robot network considered in this chapter is an example of a network control system as in [90, 98–100, 146, 147]. The proposed algorithms are constructive and easy-to-implement. The performance of the proposed algorithms are confirmed by the computer simulations and experiments with a group of real mobile robots.



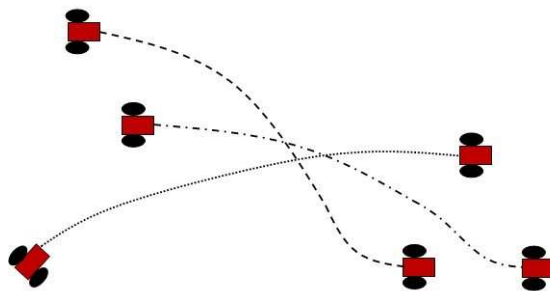
(a)



(b)



(c)



(d)

Figure 8.14: Robots form a regular triangle



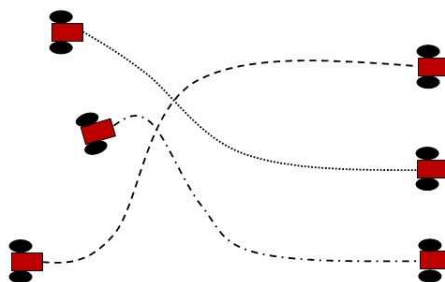
(a)



(b)



(c)



(d)

Figure 8.15: Robots form a straight line



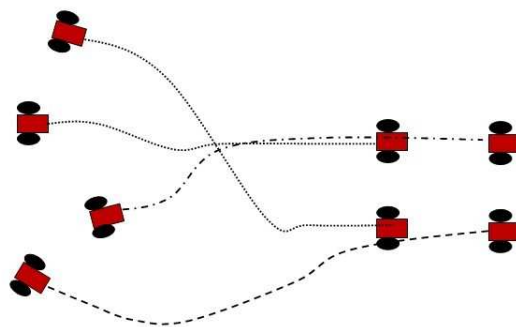
(a)



(b)



(c)



(d)

Figure 8.16: Robots form a rectangle



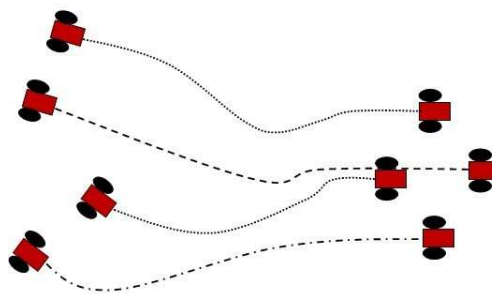
(a)



(b)



(c)



(d)

Figure 8.17: Robots form a kite



# Chapter 9

## Conclusion

The main focus of this report is to design control algorithms for collision free navigation of non-holonomic mobile robots. Unlike most of the existing navigation algorithms which focus on robot navigation in static environment, we present three different algorithms for safe navigation of mobile robots in dynamic environments with moving obstacles. We also consider a more realistic and complicated mobile robots of non-holonomic type whose motion is a better representation of a large number of control systems. Each of the proposed navigation algorithm employs different strategy to ensure the safety of the robot.

The biologically-inspired navigation algorithm (BINA) guides the robot so that there is always a constant avoiding angle between the instantaneous moving direction of the robot and one of boundaries of the enlarged vision cone. The equidistant navigation algorithm drive the robot to a  $d_0$ -equidistant curve around the obstacle. The navigation algorithm based on integrated environment representation ((NAIER) aims to seek a free path through the crowd of obstacles. These strategy are proven to able to accomplish navigation tasks in various scenarios. The features and merits of the proposed navigation algorithms are confirmed by simulation results and experiment results with real mobile robot Pioneer 3-Dx.

These obstacle avoidance strategies determine that one of these proposed navigation algorithms is more efficient in particular scenarios than the others. BINA

is the most efficient when the shapes of the obstacles are regular (circle or regular polygons) in both static and dynamic environments. The advantage of ENA is that applicable for a large variety of scenarios, especially when dealing with obstacles of irregular shapes or obstacles with time-varying shapes. Another advantage of ENA is that it is the most stable algorithm in terms of navigation time. NAIER is particularly efficient when the obstacles are extremely cluttered in the environments.

The successful implementations of BINA and ENA on intelligent wheelchair SAM and autonomous hospital bed Flexbed demonstrate their abilities to accomplish navigation tasks in real life scenarios. The experiment results show that these algorithms is able to solve complicated real life problem such as multiple moving obstacles in a narrow area, obstacles moving with non-linear velocities, obstacles with dynamically changing radii. They also indicates that these proposed navigation algorithms are applicable in many real control systems.

Finally, we investigate the problem of formation building for a group of mobile robots. A constructive and easy-to-implement decentralised controller formation building algorithm is proposed. The proposed controller allows the group of robots to not only move in the same direction but also in the desired geometric formation. This formation building is achieved without a leader robot which means that single point failure does not cause the whole system to fail. This design of formation building strategy enhances the robustness of the whole system. Furthermore, we consider a group of anonymous robots, each robot in this group are not aware of his position in the desired configuration and the robots have to reach a consensus on their positions. A randomised decentralised navigation algorithm is proposed to achieve formation building with anonymous robots. This algorithm achieves the convergence of final formation with probability 1. We present simulation results and experiments results with a group of robots to demonstrate the performance of the proposed algorithms.



## 9.1 Future Research Directions

The scope of this report can be possibly further extended by the following research directions.

- The problem of navigating mobile robots with complicated models can be considered. In such cases, it is not sufficient to solve the navigation problem by only considering the kinematic models of the mobile robots, the dynamics of the robots should also be studied. We will combine the proposed navigation ideas with advanced methods of modern robust control. see e.g. [126,151,182].
- It is interesting to investigate the performance of the proposed navigation algorithms against obstacles with even more complicated motions, such as those obstacles whose motions are not restricted by non-holonomic constraints.
- The proposed algorithm NAIER had not yet been implemented to any real control system. It is very suitable for systems such as wheelchairs which often find themselves involved in a crowded environments.
- The proposed navigation algorithms has been only implemented on ground robots/systems. It is possible to extend their applications to other underwater/aerial (e.g. [41]) systems with reasonable modifications of the algorithms.
- The proposed formation building strategies can be combined with the obstacle avoidance strategies so that the robots will not collide into each other during converging process.



# Bibliography

- [1] Acvtimedia pioneer 3-dx mobile robot data sheet. [Online]. Available: [www.mobilerobots.com/Libraries/Downloads/Pioneer3DX-P3DX-RevA.sflb.ashx](http://www.mobilerobots.com/Libraries/Downloads/Pioneer3DX-P3DX-RevA.sflb.ashx)
- [2] Adept mobile robots. [Online]. Available: <http://www.test.org/doe/>
- [3] T. Balch and R. C. Arkin, “Behavior-based formation control for multirobot teams,” *IEEE Transactions on Robotics and Automation*, vol. 14, no. 6, pp. 926–939, 1998.
- [4] U. Beckmann, D. M. Gillies, S. M. Berenholtz, A. W. Wu, and P. Pronovost, “Incidents relating to the intra-hospital transfer of critically ill patients,” *Intensive care medicine*, vol. 30, no. 8, pp. 1579–1585, 2004.
- [5] S. Belkhous, A. Azzouz, M. Saad, V. Nerguizian, and C. Nerguizian, “A novel approach for mobile robot navigation with dynamic obstacles avoidance,” *Journal of Intelligent and Robotic Systems*, vol. 44, pp. 187–201, 2005.
- [6] J. Borenstein and Y. Koren, “Histogramic in-motion mapping for mobile robot obstacle avoidance,” *IEEE Transactions on Robotics and Automation*, vol. 7, no. 4, pp. 535–539, 1991.
- [7] —, “The vector field histogram-fast obstacle avoidance for mobile robots,” *IEEE Transactions on Robotics and Automation*, vol. 7, no. 3, pp. 278–288, 1991.

- [8] A. Chakravarthy and D. Ghose, "Obstacle avoidance in a dynamic environment: a collision cone approach," *IEEE Transactions on Systems, Man, and Cybernetics*, vol. 28, no. 5, pp. 562–574, 1998.
- [9] —, "Obstacle avoidance in a dynamic environment: a collision cone approach," *IEEE Transactions on Systems, Man and Cybernetics, Part A: Systems and Humans*, vol. 28, no. 5, pp. 562–574, 1998.
- [10] Y. Q. Chen and Z. Wang, "Formation control: a review and a new consideration," in *IEEE/RSJ International Conference on Intelligent Robots and Systems*, Edmonton, Canada, Aug. 2005, pp. 3181–3186.
- [11] T. M. Cheng and A. V. Savkin, "A distributed self-deployment algorithm for the coverage of mobile wireless sensor networks," *IEEE Communications Letters*, vol. 13, no. 11, pp. 877–879, 2009.
- [12] —, "Self-deployment of mobile robotic sensor networks for multilevel barrier coverage," *Robotica*, vol. 30, no. 4, pp. 661–669, 2012.
- [13] —, "Decentralized control of mobile sensor networks for asymptotically optimal blanket coverage between two boundaries," *IEEE Transactions on Industrial Informatics*, vol. 9, no. 1, pp. 365–376, 2013.
- [14] T. M. Cheng, A. V. Savkin, and F. Javed, "Decentralized control of a group of mobile robots for deployment in sweep coverage," *Robotics and Autonomous Systems*, vol. 59, no. 7, pp. 497–507, 2011.
- [15] T. Cheng and A. V. Savkin, "Decentralized control for mobile robotic sensor network self-deployment: Barrier and sweep coverage problems," *Robotica*, vol. 29, pp. 283–294, 2011.
- [16] H. Choset, "Coverage for robotics—a survey of recent results," *Annals of mathematics and artificial intelligence*, vol. 31, no. 1-4, pp. 113–126, 2001.

- [17] J. Chunyu, Z. Qu, E. Pollak, and M. Falash, "Reactive target-tracking control with obstacle avoidance of unicycle-type mobile robots in a dynamic environment," in *American Control Conference*, Baltimore, USA, Jun. 2010, pp. 1190–1196.
- [18] J. Cortes, S. Martinez, T. Karatas, and F. Bullo, "Coverage control for mobile sensing networks," *IEEE Transactions on Robotics and Automation*, vol. 20, no. 2, pp. 243–255, 2004.
- [19] D. Craig and H. Nguyen, "Adaptive EEG thought pattern classifier for advanced wheelchair control," in *Proceedings of 29th IEEE/EMBS Annual International Conference*, Lyon, France, Aug. 2007, pp. 2544 –2547.
- [20] M. Deng, A. Inoue, Y. Shibata, K. Sekiguchi, and N. Ueki, "An obstacle avoidance method for two wheeled mobile robot," in *Proceedings of the IEEE International Conference on Networking, Sensing and Control*, London, UK.
- [21] J. P. Desai, J. Ostrowski, and V. Kumar, "Controlling formations of multiple mobile robots," in *IEEE International Conference on Robotics and Automation*, vol. 4, 1998, pp. 2864–2869.
- [22] J. Feddema, C. Lewis, and D. Schoenwald, "Decentralized control of cooperative robotic vehicles: theory and application," *IEEE Transactions on Robotics and Automation*, vol. 18, no. 5, pp. 852–864, 2002.
- [23] L. Fehr, W. Langbein, and S. B.Skaar, "Adequacy of power wheelchair control interfaces for persons with severe disabilities: A clinical survey," *Journal of Rehabilitation Research and Development*, vol. 37, no. 3, pp. 353 –360, 2000.
- [24] A. Ferrara and M. Rubagotti, "Sliding mode control of a mobile robot for dynamic obstacle avoidance based on a time-varying harmonic potential field," in *ICRA 2007 Workshop: Planning, Perception and Navigation for Intelligent Vehicles*, 2007.

- [25] M. Finlayson and T. van Denend, “Experiencing the loss of mobility: perspectives of older adults with ms,” *Disability and Rehabilitation*, vol. 25, no. 20, pp. 1168–1180, 2003.
- [26] P. Fiorini and Z. Shiller, “Motion planning in dynamic environments using velocity obstacles,” *International Journal of Robotics Research*, vol. 17, no. 7, pp. 760–772, July 1998.
- [27] —, “Motion planning in dynamic environments using the relative velocity paradigm,” in *IEEE International Conference on Robotics and Automation*, Atlanta, USA, May. 1993, pp. 560–565.
- [28] —, “Motion planning in dynamic environments using velocity obstacles,” *The International Journal of Robotics Research*, vol. 17, no. 7, pp. 760–772, 1998.
- [29] L. D. Foster and J. H. Breidenbach, “Hospital bed with collapsible side edges and laterally-movable side guards,” Patent US 5 083 332, Jan. 28, 1992.
- [30] D. Fox, W. Burgard, and S. Thrun, “The dynamic window approach to collision avoidance,” *IEEE Robotics and Automation Magazine*, vol. 4, pp. 23–33, 1997.
- [31] T. Fraichard, “Trajectory planning in a dynamic workspace: a state-time space approach,” *Advanced Robotics*, vol. 13, no. 1, pp. 75–94, 1999.
- [32] —, “A short paper about motion safety,” in *IEEE International Conference on Robotics and Automation*, Roma, Italy, Apr. 2007, pp. 1140–1145.
- [33] T. Fraichard and H. Asama, “Inevitable collision states. a step towards safer robots?” *Advanced Robotics*, vol. 18, no. 10, pp. 1001–1024, 2004.
- [34] J. Fredslund and M. Mataric, “A general algorithm for robot formations using local sensing and minimal communication,” *IEEE Transactions on Robotics and Automation*, vol. 18, no. 5, pp. 837–846, 2002.

- [35] C. Fulgenzi, A. Spalanzani, and C. Laugier, “Dynamic obstacle avoidance in uncertain environment combining PVOs and occupancy grid,” in *IEEE International Conference on Robotics and Automation*, Roma, Italy, Apr. 2007, pp. 1610–1616.
- [36] V. Gazi, “Formation control of a multi-agent system using decentralized nonlinear servomechanism,” in *Proceedings of 42nd IEEE Conference on Decision and Control*, vol. 3, Mani, USA, Dec. 2003, pp. 2531–2536.
- [37] B. P. Gerkey and M. J. Matarić, “A formal analysis and taxonomy of task allocation in multi-robot systems,” *The International Journal of Robotics Research*, vol. 23, no. 9, pp. 939–954, 2004.
- [38] A. Ghosh and S. K. Das, “Coverage and connectivity issues in wireless sensor networks: A survey,” *Pervasive and Mobile Computing*, vol. 4, no. 3, pp. 303–334, 2008.
- [39] I. Harmati and K. Skrzypezyk, “Robot team coordination for target tracking using fuzzy logic controller in game theoretic framework,” *Robotics and Autonomous Systems*, vol. 57, no. 1, pp. 75–86, 2009.
- [40] Y. G. Hong, H. P. Hu, and L. X. Gao, “Tracking control for multi-agent consensus with an active leader and variable topology,” *Automatica*, vol. 42, no. 7, pp. 1177–1182, 2006.
- [41] M. Hoy, A. S. Matveev, M. Garratt, and A. V. Savkin, “Collision-free navigation of an autonomous unmanned helicopter in unknown urban environments: sliding mode and mpc approaches,” *Robotica*, vol. 30, no. 4, pp. 537–550, 2012.
- [42] M. Hoy, A. S. Matveev, and A. V. Savkin, “Collision free cooperative navigation of multiple wheeled robots in unknown cluttered environments,” *Robotics and Autonomous Systems*, vol. 60, no. 10, pp. 1253–1266, 2012.

- [43] ———, “Algorithms for collision free navigation of mobile robots in complex cluttered environments: A survey,” *Robotica*, 2013, accepted.
- [44] H. Teimoori and A. V. Savkin, “A biologically inspired method for robot navigation in a cluttered environment,” *Robotica*, vol. 28, no. 5, pp. 637–648, 2010.
- [45] Z. Hu, L. Li, Y. Luo, Y. Zhang, and X. Wei, “A novel intelligent wheelchair control approach based on head gesture recognition,” in *Proceedings of International Conference on Computer Application and System Modeling (IC-CASM)*, vol. 6, Taiyuan, China, Oct. 2010, pp. 159–163.
- [46] W. V. Hunt, J. A. Coletta, R. J. Howling, and L. Higgs, “Support appliance for mounting on a standard hospital bed,” Patent US 4 525 885, Jun. 2, 1985.
- [47] L. Imsland, T. A. Johansen, T. I. Fossen, H. Fjær Grip, J. C. Kalkkuhl, and A. Suissa, “Vehicle velocity estimation using nonlinear observers,” *Automatica*, vol. 42, no. 12, pp. 2091–2103, 2006.
- [48] A. Jadbabaie, J. Lin, and A. Morse, “Coordination of groups of mobile autonomous agents using nearest neighbor rules,” *IEEE Transactions on Automatic Control*, vol. 48, no. 6, pp. 988–1001, Jun. 2003.
- [49] F. Janabi-Sharifi, V. Hayward, and C.-S. Chen, “Discrete-time adaptive windowing for velocity estimation,” *Control Systems Technology, IEEE Transactions on*, vol. 8, no. 6, pp. 1003–1009, 2000.
- [50] J. Jennings, G. Whelan, and W. Evans, “Cooperative search and rescue with a team of mobile robots,” in *8th International Conference on Advanced Robotics*, Monterey, USA, Jul. 1997, pp. 193–200.
- [51] M. L. Jones and J. A. Sanford, “People with mobility impairments in the united states today and in 2010,” *Assistive Technology*, vol. 8, pp. 43–53, 1996.



- [52] I. Kamon, E. Rimon, and E. Rivlin, "Tangentbug: A range-sensor-based navigation algorithm," *The International Journal of Robotics Research*, vol. 17, no. 9, pp. 934–953, 1998.
- [53] I. Kamon and E. Rivlin, "Sensory-based motion planning with global proofs," *IEEE Transactions on Robotics and Automation*, vol. 13, no. 6, pp. 814–822, 1997.
- [54] ———, "Sensory-based motion planning with global proofs," *IEEE Transactions on Robotics and Automation*, vol. 13, no. 6, pp. 814–822, 1997.
- [55] I. Kamon, E. Rimon, and E. Rivlin, "Tangentbug: A range-sensor-based navigation algorithm," *The International Journal of Robotics Research*, vol. 17, no. 9, pp. 934–953, 1998.
- [56] G. Kantor, S. Singh, R. Peterson, D. Rus, A. Das, V. Kumar, G. Pereira, and J. Spletzer, "Distributed search and rescue with robot and sensor teams," *Field and Service Robotics*, vol. 24, pp. 529–538, 2006.
- [57] O. Khatib, "Real-time obstacle avoidance for manipulators and mobile robots," *International Journal of Robotics Research*, vol. 5, no. 1, pp. 90–98, 1986.
- [58] S. Kinne, "Correlates of exercise maintenance among people with mobility impairments," *Disability and Rehabilitation*, vol. 21, no. 1, pp. 15–22, 1999.
- [59] F. Kobayashi, N. Tomita, and F. Kojima, "Re-formation of mobile robots using genetic algorithm and reinforcement learning," in *SICE Annual Conference*, vol. 3, Fukui, Japan, Aug. 2003, pp. 2902–2907.
- [60] K. Komiya, K. Morita, K. Kagekawa, and K. Kurosu, "Guidance of a wheelchair by voice," in *Proceedings of 26th IEEE Annual Conference on Industrial Electronics Society (IECON)*, vol. 1, Nagoya, Japan, Oct. 2000, pp. 102–107.

- [61] Y. Koren and J. Borenstein, "Potential field methods and their inherent limitations for mobile robot navigation," in *IEEE International Conference on Robotics and Automation*, vol. 2, Sacramento, USA, Apr. 1991, pp. 1398–1404.
- [62] L. Krick, M. E. Broucke, and B. A. Francis, "Stabilisation of infinitesimally rigid formations of multi-robot networks," *International Journal of Control*, vol. 82, no. 3, pp. 423–439, 2009.
- [63] R. Kulić and Z. Vukić, "Methodology of concept control synthesis to avoid unmoving and moving obstacles," *Journal of Intelligent and Robotic Systems*, vol. 45, pp. 267–294, 2006.
- [64] S. Kumar, T. H. Lai, and A. Arora, "Barrier coverage with wireless sensors," in *Proceedings of the 11th annual international conference on Mobile computing and networking*, vol. 13, no. 6. ACM, 2007, pp. 817–834.
- [65] Y. Kuwata, A. Richards, and J. How, "Robust receding horizon control using generalized constraint tightening," in *American Control Conference, 2007. ACC'07*, New York, USA, Jul. 2007, pp. 4482–4487.
- [66] W. Langson, I. Chrysoschoos, S. Raković, and D. Q. Mayne, "Robust model predictive control using tubes," *Automatica*, vol. 40, no. 1, pp. 125–133, 2004.
- [67] L. Lapierre, R. Zapata, and P. Lepinay, "Combined path-following and obstacle avoidance control of a wheeled robot," *The International Journal of Robotics Research*, vol. 26, no. 4, pp. 361–375, 2007.
- [68] F. Large, C. Laugier, and Z. Shiller, "Navigation among moving obstacles using the NLVO: Principles and applications to intelligent vehicles," *Autonomous Robots*, vol. 19, pp. 159–171, 2005.
- [69] F. Large, C. Laugier, and Z. Shiller, "Navigation among moving obstacles using the NLVO: Principles and applications to intelligent vehicles," *Autonomous Robots*, vol. 19, no. 2, pp. 159–171, 2005.

- [70] F. Large, S. Sekhavat, Z. Shiller, and C. Laugier, “Towards real-time global motion planning in a dynamic environment using the NLVO concept,” in *IEEE/RSJ International Conference on Intelligent Robots and Systems*, vol. 1, EPFL, Switichland, Sep. 2002, pp. 607–612.
- [71] S. L. Laubach and J. W. Burdick, “An autonomous sensor-based path-planner for planetary microrovers,” in *IEEE International Conference on Robotics and Automation*, vol. 1, Detroit, USA, May. 1999, pp. 347–354.
- [72] D. N. Lee, “Guiding movement by coupling taus,” *Ecological Phycology*, vol. 10, no. 3–4, pp. 221–250, 1998.
- [73] D. Lee and M. W. Spong, “Stable flocking of multiple inertial agents on balanced graphs,” *IEEE Transactions on Automatic Control*, vol. 52, no. 8, pp. 1469–1475, 2007.
- [74] K. Lerman, C. Jones, A. Galstyan, and M. J. Matarić, “Analysis of dynamic task allocation in multi-robot systems,” *The International Journal of Robotics Research*, vol. 25, no. 3, pp. 225–241, 2006.
- [75] L. I. Lezzoni, E. P. MaCarthy, R. B. Davis, and H. Siebens, “Mobility difficulties are not only a problem of old age,” *Journal of General Internal Medicine*, vol. 16, pp. 235–243, 2001.
- [76] S. Lindemann, I. Hussein, and S. M. LaValle, “Real time feedback control for nonholonomic mobile robots with obstacles,” in *45th IEEE Conference on Decision and Control*, San Diego, USA, Dec. 2006, pp. 2406–2411.
- [77] G. Liu, “On velocity estimation using position measurements,” in *Proceedings of the American Control Conference*, vol. 2, Anchorage, USA, May. 2002, pp. 1115–1120.

- [78] Y. H. Liu and S. Arimoto, "Path planning using a tangent graph for mobile robots among polygonal and curved obstacles," *The International Journal of Robotics Research*, vol. 11, no. 4, pp. 376–382, 1992.
- [79] E. M. P. Low, I. R. Manchester, and A. V. Savkin, "A biologically inspired method for vision-based docking of wheeled mobile robots," *Robotics and Autonomous Systems*, vol. 55, no. 10, pp. 769–784, 2007.
- [80] T. Luhandjula, K. Djouani, Y. Hamam, B. van Wyk, and Q. Williams, "A hand-based visual intent recognition algorithm for wheelchair motion," in *Proceedings of 3rd Conference on Human System Interactions (HSI)*, Rzeszow, Poland, May. 2010, pp. 749–756.
- [81] V. Lumelsky and A. Stepanov, "Dynamic path planning for a mobile automaton with limited information on the environment," *IEEE Transactions on Automatic Control*, vol. 31, no. 11, pp. 1058–1063, 1986.
- [82] V. J. Lumelsky and T. Skewis, "Incorporating range sensing in the robot navigation function," *IEEE Transactions on Systems, Man and Cybernetics*, vol. 20, no. 5, pp. 1058–1069, 1990.
- [83] I. R. Manchester and A. V. Savkin, "Circular navigation missile guidance with incomplete information and uncertain autopilot model," *Journal of guidance, control, and dynamics*, vol. 27, no. 6, pp. 1078–1083, 2004.
- [84] —, "Circular-navigation-guidance law for precision missile/target engagements," *Journal of guidance, control, and dynamics*, vol. 29, no. 2, pp. 314–320, 2006.
- [85] J. A. Marshall, T. Fung, M. E. Broucke, G. M. DEleuterio, and B. A. Francis, "Experiments in multirobot coordination," *Robotics and Autonomous Systems*, vol. 54, no. 3, pp. 265–275, 2006.

- [86] F. N. Martins, W. C. Celeste, R. Carelli, M. Sarcinelli-Filho, and T. F. Bastos-Filho, “An adaptive dynamic controller for autonomous mobile robot trajectory tracking,” *Control Engineering Practice*, vol. 16, no. 11, pp. 1354 – 1363, 2008.
- [87] A. Masoud, “Kinodynamic motion planning,” *IEEE Robotics and Automation Magazine*, vol. 17, no. 1, pp. 85–99, 2010.
- [88] —, “A harmonic potential approach for simultaneous planning and control of a generic uav platform,” *Journal of Intelligent and Robotic Systems*, vol. 65, no. 1-4, pp. 153–173, 2012.
- [89] G. M. Mathews, H. Durrant-Whyte, and M. Prokopenko, “Decentralised decision making in heterogeneous teams using anonymous optimisation,” *Robotics and Autonomous Systems*, vol. 57, no. 3, pp. 310–320, 2009.
- [90] A. S. Matveev and A. V. Savkin, “Optimal control of networked systems via asynchronous communication channels with irregular delays,” in *Proceedings of the 40th IEEE Conference on Decision and Control*, vol. 3, Orlando, FL, USA, 2001, pp. 2327–2332.
- [91] A. S. Matveev, H. Teimoori, and A. V. Savkin, “A method for guidance and control of an autonomous vehicle in problems of border patrolling and obstacle avoidance,” *Automatica*, vol. 47, pp. 515–524, 2011.
- [92] —, “Navigation of a unicycle-like mobile robot for environmental extremum seeking,” *Automatica*, vol. 47, no. 1, pp. 85–91, 2011.
- [93] —, “Range-only measurements based target following for wheeled mobile robots,” *Automatica*, vol. 47, no. 6, pp. 177–184, 2011.
- [94] A. S. Matveev, M. Hoy, and A. V. Savkin, “A method for reactive navigation of nonholonomic under-actuated robots in maze-like environments,” *Automatica*, vol. 49, no. 5, pp. 1268–1274, 2013.

- 
- [95] A. S. Matveev, M. Hoy, J. Katupitiya, and A. V. Savkin, “Nonlinear sliding mode control of an unmanned agricultural tractor in the presence of sliding and control saturation,” *Robotics and Autonomous Systems*, vol. 61, no. 9, pp. 973–987, 2013.
- [96] A. S. Matveev, M. Hoy, and A. V. Savkin, “The problem of boundary following by a unicycle-like robot with rigidly mounted sensors,” *Robotics and Autonomous Systems*, vol. 61, no. 3, pp. 312–327, 2013.
- [97] A. S. Matveev and A. V. Savkin, *Qualitative Theory of Hybrid Dynamical Systems*. Birkhauser, Boston, 2000.
- [98] —, “The problem of state estimation via asynchronous communication channels with irregular transmission times,” *IEEE Transactions on Automatic Control*, vol. 48, no. 4, pp. 670–676, 2003.
- [99] —, “An analogue of Shannon information theory for detection and stabilization via noisy discrete communication channels,” *SIAM Journal on Control and Optimization*, vol. 46, no. 4, pp. 1323–1367, 2007.
- [100] —, *Estimation and control over communication networks*. Birkhauser, Boston, 2009.
- [101] A. S. Matveev, H. Teimoori, and A. V. Savkin, “Method for tracking of environmental level sets by a unicycle-like vehicle,” *Automatica*, vol. 48, no. 9, pp. 2252 – 2261, 2012.
- [102] A. S. Matveev, C. Wang, and A. V. Savkin, “Real-time navigation of mobile robots in problems of border patrolling and avoiding collisions with moving and deforming obstacles,” *Robotics and Autonomous Systems*, vol. 60, no. 6, pp. 769 – 788, 2012.

- 
- [103] H. Mehrjerdi, J. Ghommam, and M. Saad, “Nonlinear coordination control for a group of mobile robots using a virtual structure,” *Mechatronics*, vol. 21, no. 7, pp. 1147 – 1155, 2011.
- [104] J. Minguez and L. Montano, “Nearness diagram (ND) navigation: collision avoidance in troublesome scenarios,” *Robotics and Automation, IEEE Transactions on*, vol. 20, no. 1, pp. 45–59, 2004.
- [105] M. Moussaïd, D. Helbing, and G. Theraulaz, “How simple rules determine pedestrian behavior and crowd disasters,” *Proceedings of the National Academy of Sciences*, vol. 108, no. 17, pp. 6884–6888, 2011.
- [106] K. Nak, Y. and R. Simmons, “The lane-curvature method for local obstacle avoidance,” in *IEEE International Conference on Robotics and Automation*, vol. 3, Leuven, Belgium, Nov. 1998, pp. 1615–1621.
- [107] J. Ng and T. Brunl, “Performance comparison of bug navigation algorithms,” *Journal of Intelligent and Robotic Systems*, vol. 50, no. 1, pp. 73–84, 2007.
- [108] N. Nguyen, H. T. Nguyen, and S. Su, “Optimal path-following control of a smart powered wheelchair,” in *Proceedings of 30th IEEE/EMBS Annual International Conference*, Buenos, Argentina, Aug. 2008, pp. 5025–5028.
- [109] S. Nguyen, H. Nguyen, P. Taylor, and J. Middleton, “Improved head direction command classification using an optimised bayesian neural network,” in *Proceedings of 28th Annual IEEE/EMBS International Conference*, New York, USA, Sep. 2006, pp. 5679–5682.
- [110] T. N. Nguyen, S. Su, and H. Nguyen, “Robust neuro-sliding mode multivariable control strategy for powered wheelchairs,” *IEEE Transactions on Neural Systems and Rehabilitation Engineering*, vol. 19, no. 1, pp. 105 –111, Feb. 2011.

- [111] H. Noborio, K. Fujimura, and Y. Horiuchi, "A comparative study of sensor-based path-planning algorithms in an unknown maze," in *IEEE/RSJ International Conference on Intelligent Robots and Systems*, vol. 2, Takamatsu, Japan, Oct. 2000, pp. 909–916.
- [112] H. Noborio, Y. Maeda, and K. Urakawa, "Three or more dimensional sensor-based path-planning algorithm HD-I," in *IEEE/RSJ International Conference on Intelligent Robots and Systems*, vol. 3, Kyongju, South Korea, Oct. 1999, pp. 1699–1706.
- [113] P. Ogren, E. Fiorelli, and N. Leonard, "Cooperative control of mobile sensor networks: Adaptive gradient climbing in a distributed environment," *IEEE Transactions on Automatic Control*, vol. 49, no. 8, pp. 1292–1302, 2004.
- [114] R. Olfati-Saber and R. Murray, "Consensus problems in networks of agents with switching topology and time-delays," *IEEE Transactions on Automatic Control*, vol. 49, no. 9, pp. 1520–1533, 2004.
- [115] J. G. Ortega and E. F. Camacho, "Mobile robot navigation in a partially structured static environment, using neural predictive control," *Control Engineering Practice*, vol. 4, no. 12, pp. 1669–1679, 1996.
- [116] E. Owen and L. Montano, "Motion planning in dynamic environments using the velocity space," in *IEEE/RSJ International Conference on Intelligent Robots and Systems*, Edmonton, Canada, Aug. 2005, pp. 2833–2838.
- [117] ———, "A robocentric motion planner for dynamic environments using the velocity space," in *IEEE/RSJ International Conference on Intelligent Robots and Systems*, Beijing, China, Oct. 2006, pp. 4368–4374.
- [118] S. Panzieri, F. Pascucci, and G. Ulivi, "An outdoor navigation system using gps and inertial platform," *IEEE/ASME Transactions on Mechatronics*, vol. 7, no. 2, pp. 134–142, 2002.



- [119] J. P. Papson, K. L. Russell, and D. M. Taylor, "Unexpected events during the intrahospital transport of critically ill patients," *Academic Emergency Medicine*, vol. 14, no. 6, pp. 574–577, 2007.
- [120] L. Parker, B. Kannan, F. Tang, and M. Bailey, "Tightly-coupled navigation assistance in heterogeneous multi-robot teams," in *IEEE/RSJ International Conference on Intelligent Robots and Systems*, vol. 1, Sendi, Japan, Sep. 2004, pp. 1016–1022.
- [121] E. Parssler, J. Scholz, and P. Fiorini, "A robotic wheelchair for crowded public environments," *IEEE Robotics and Automation Magazine*, vol. 8, pp. 38–45, 2001.
- [122] R. Parthasarathi and T. Fraichard, "An inevitable collision state-checker for a car-like vehicle," in *IEEE International Conference on Robotics and Automation*, Roma, Italy, Apr. 2007, pp. 3068–3073.
- [123] P. N. Pathirana, N. Bulusu, A. V. Savkin, and S. Jha, "Node localization using mobile robots in delay-tolerant sensor networks," *IEEE Transactions on Mobile Computing*, vol. 4, no. 3, pp. 285–296, 2005.
- [124] P. N. Pathirana, A. V. Savkin, and S. Jha, "Location estimation and trajectory prediction for cellular networks with mobile base stations," *IEEE Transactions on Vehicular Technology*, vol. 53, no. 6, pp. 1903–1913, 2004.
- [125] I. R. Petersen and A. V. Savkin, *Robust Kalman filtering for signals and systems with large uncertainties*. Birkhauser, Boston, 1999.
- [126] I. R. Petersen, V. A. Ugrinovskii, and A. V. Savkin, *Robust control design using H-infinity methods*. Springer-Verlag, London, 2000.
- [127] E. Prassler, J. Scholz, and P. Fiorini, "Navigating a robotic wheelchair in a railway station during rush hour," *The International Journal of Robotics Research*, vol. 18, no. 7, 1999.

- [128] M. Qadri and S. Ahmed, "Voice controlled wheelchair using DSK TMS320C6711," in *Proceedings of International Conference on Signal Acquisition and Processing (ICSAP)*, Kuala Lumpur, Malaysia, Apr. 2009, pp. 217–220.
- [129] Z. Qu, J. Wang, and C. Plaisted, "A new analytical solution to mobile robot trajectory generation in the presence of moving obstacles," *IEEE Transactions on Robotics*, vol. 20, no. 6, pp. 978–993, 2004.
- [130] S. Reahman, B. Raytchev, I. Yoda, and L. Liu, "Vibrotactile rendering of head gestures for controlling electric wheelchair," in *Proceedings of IEEE International Conference on Systems, Man Cybernetics*, San Antonio, USA, Oct. 2009, pp. 413–417.
- [131] B. Rebsamen, E. Burdet, C. Guan, H. Zhang, C. L. Teo, Q. Zeng, M. Ang, and C. Laugier, "A brain-controlled wheelchair based on P300 and path guidance," in *Proceedings of IEEE/RAS-EMBS International Conference on Biomedical Robotics and Biomechatronics*, Pisa, Italy, Feb. 2006, pp. 1101–1106.
- [132] J. Reif and M. Sharir, "Motion planning in the presence of moving obstacles," *Journal of the ACM*, vol. 41, pp. 764–790, 1994.
- [133] J. H. Reif and H. Wang, "Social potential fields: A distributed behavioral control for autonomous robots," *Robotics and Autonomous Systems*, vol. 27, no. 3, pp. 171–194, 1999.
- [134] J. Ren, K. A. McIsaac, and R. V. Patel, "Modified newton's method applied to potential field-based navigation for nonholonomic robots in dynamic environments," *Robotica*, vol. 26, no. 1, p. 117, 2008.
- [135] W. Ren and N. Sorensen, "Distributed coordination architecture for multi-robot formation control," *Robotics and Autonomous Systems*, vol. 56, no. 4, pp. 324–333, 2008.

- 
- [136] C. W. Reynolds, "Flocks, birds, and schools: a distributed behavioral model," *Computer Graphics*, vol. 21, pp. 25–34, 1986.
- [137] A. Richards and J. How, "Robust stable model predictive control with constraint tightening," in *American Control Conference, 2006*, Minneapolis, USA, Jun. 2006, pp. 1557–1562.
- [138] K. O. Rudolf and D. W. Williams, "Hospital bed castor control mechanism," Patent US 5 377 372, Jan. 3, 1995.
- [139] J. N. Russel, G. E. Hendershot, J. H. Felicia LeClere, and M. Adler, "Trends and differential use of assistive technology devices: United states, 1994," *Advanced Data*, no. 292, pp. 1–9, 1997.
- [140] T. Saitoh, N. Takahashi, and R. Konishi, "Oral motion controlled intelligent wheelchair," in *Proceedings of Society of Instrument and Control Engineers (SICE) Annual Conference*, Takamatsu, Japan, Sep. 2007, pp. 341–346.
- [141] A. Sankaranarayanan and M. Vidyasagar, "A new path planning algorithm for moving a point object amidst unknown obstacles in a plane," in *IEEE International Conference on Robotics and Automation*, vol. 3, Cincinnati, USA, May. 1990, pp. 1930–1936.
- [142] A. Sankaranarayanan and M. Vidyasagar, "Path planning for moving a point object amidst unknown obstacles in a plane: a new algorithm and a general theory for algorithm development," in *Proceedings of the 29th IEEE Conference on Decision and Control*, vol. 2, Honolulu, USA, Dec. 1990, pp. 1111–1119.
- [143] A. Satti, D. Coyle, and G. Prasad, "Self-paced brain-controlled wheelchair methodology with shared and automated assistive control," in *Proceedings of IEEE Symposium on Computational Intelligence, Cognitive Algorithms, Mind, and Brain (CCMB)*, Paris, France, Apr. 2011, pp. 1–8.

- [144] A. V. Savkin, “Coordinated collective motion of groups of autonomous mobile robots: analysis of Vicsek’s model,” *IEEE Transactions on Automatic Control*, vol. 49, no. 6, pp. 981–982, 2004.
- [145] A. V. Savkin and H. Teimoori, “Decentralized navigation of groups of wheeled mobile robots with limited communication,” *IEEE Transactions on Robotics*, vol. 26, no. 6, pp. 1099–1104, 2010.
- [146] A. V. Savkin, “Analysis and synthesis of networked control systems: Topological entropy, observability, robustness and optimal control,” *Automatica*, vol. 42, no. 1, pp. 51–62, 2006.
- [147] A. V. Savkin and T. M. Cheng, “Detectability and output feedback stabilizability of nonlinear networked control systems,” *IEEE Transactions on Automatic Control*, vol. 52, no. 4, pp. 730–735, 2007.
- [148] A. V. Savkin and R. J. Evans, *Hybrid dynamical systems: controller and sensor switching problems*. Birkhauser, Boston, 2002.
- [149] A. V. Savkin and M. Hoy, “Reactive and the shortest path navigation of a wheeled mobile robot in cluttered environments,” *Robotica*, vol. 31, no. 2, pp. 323–330, 2013.
- [150] A. V. Savkin, F. Javed, and A. S. Matveev, “Optimal distributed blanket coverage self-deployment of mobile wireless sensor networks,” *IEEE Communications Letters*, vol. 16, no. 6, pp. 949–951, 2012.
- [151] A. V. Savkin and I. R. Petersen, “Minimax optimal control of uncertain systems with structured uncertainty,” *International Journal of Robust and Nonlinear Control*, vol. 5, no. 2, pp. 119–137, 1995.
- [152] —, “Robust state estimation and model validation for discrete-time uncertain systems with a deterministic description of noise and uncertainty,” *Automatica*, vol. 34, no. 2, pp. 271–274, 1998.

- 
- [153] A. V. Savkin, E. Skafidas, and R. J. Evans, "Robust output feedback stabilizability via controller switching," *Automatica*, vol. 35, no. 1, pp. 69–74, 1999.
- [154] A. V. Savkin and H. Teimoori, "Bearings-only guidance of a unicycle-like vehicle following a moving target with a smaller minimum turning radius," *IEEE Transactions on Automatic Control*, vol. 55, no. 10, pp. 2390–2395, 2010.
- [155] A. V. Savkin and C. Wang, "A simple biologically inspired algorithm for collision-free navigation of a unicycle-like robot in dynamic environments with moving obstacles," *Robotica*, vol. 31, no. 6, pp. 993–1001, 2013.
- [156] —, "Seeking a path through the crowd: Robot navigation in unknown dynamic environments with moving obstacles based on an integrated environment representation," submitted.
- [157] A. V. Savkin, C. Wang, A. Baranzadeh, Z. Xi, and H. T. Nguyen, "Distributed formation building algorithms for groups of wheeled mobile robots," *Robotica*, accepted.
- [158] A. Savkin and I. Petersen, "Recursive state estimation for uncertain systems with an integral quadratic constraint," *IEEE Transactions on Automatic Control*, vol. 40, no. 6, pp. 1080–1083, 1995.
- [159] A. B. Schultz, "Mobility impairment in the elderly: Challenges for biomechanics research," *Journal of Biomechanics*, vol. 25, pp. 519–528, 1992.
- [160] P. O. Scokaert and D. Q. Mayne, "Min-max feedback model predictive control for constrained linear systems," *IEEE Transactions on Automatic Control*, vol. 43, no. 8, pp. 1136–1142, 1998.
- [161] M. Seder, K. Macek, and I. Petrovic, "An integrated approach to realtime mobile robot control in partially known indoor environments," in *31st An-*

- nual Conference of the IEEE Industrial Electronics Society*, Raleigh, USA, November 2005, pp. 1785–1790.
- [162] J. Serres, D. Dray, F. Ruffier, and N. Franceschini, “A vision-based autopilot for a miniature air vehicle: joint speed control and lateral obstacle avoidance,” *Autonomous Robots*, vol. 25, no. 1-2, pp. 103–122, 2008.
- [163] M. Shanmugavel, A. Tsourdos, and B. White, *Obstacle Avoidance: Static Obstacles*. John Wiley & Sons Ltd, 2010.
- [164] Z. Shiller, “Online suboptimal obstacle avoidance,” *The International Journal of Robotics Research*, vol. 19, no. 5, pp. 480–497, 2000.
- [165] Z. Shiller, F. Large, and S. Sekhavat, “Motion planning in dynamic environments: Obstacles moving along arbitrary trajectories,” in *IEEE International Conference on Robotics and Automation*, vol. 4, Seoul, South Korea, May. 2001, pp. 3716–3721.
- [166] B.-G. Shin, T. Kim, and S. Jo, “Non-invasive brain signal interface for a wheelchair navigation,” in *Proceedings of International Conference on Control Automation and Systems (ICCAS)*, Gyeonggi-do, Korea, Oct. 2010, pp. 2257–2260.
- [167] R. Simmons, “The curvature-velocity method for local obstacle avoidance,” in *IEEE International Conference on Robotics and Automation*, vol. 4, Minesota, USA, November 1996, pp. 3375–3382.
- [168] R. Simpson and S. Levine, “Voice control of a powered wheelchair,” *IEEE Transactions on Neural Systems and Rehabilitation Engineering*, vol. 10, no. 2, pp. 122–125, 2002.
- [169] R. C. Simpson, “Smart wheelchairs: A literature review,” *Journal of Rehabilitation Research and Development*, vol. 42, no. 4, pp. 423–436, 2005.

- 
- [170] R. C. Simpson, E. F. LoPresti, and R. A. Cooper, “How many people would benefit from a smart wheelchair?” *Journal of Rehabilitation Research and Development*, vol. 45, no. 1, pp. 53–72, 2008.
- [171] E. Skafidas, R. J. Evans, A. V. Savkin, and I. R. Petersen, “Stability results for switched controller systems,” *Automatica*, vol. 35, no. 4, pp. 553–564, 1999.
- [172] A. Solanas and M. Garcia, “Coordinated multi-robot exploration through unsupervised clustering of unknown space,” in *IEEE/RSJ International Conference on Intelligent Robots and Systems*, vol. 1, Sendi, Japan, Sep. 2004, pp. 717–721.
- [173] Y. Su, C. Zheng, D. Sun, and B. Duan, “A simple nonlinear velocity estimator for high-performance motion control,” *IEEE Transactions on Industrial Electronics*, vol. 52, no. 4, pp. 1161–1169, 2005.
- [174] H. Sugiyama, T. Tsujioka, and M. Murata, “Autonomous chain network formation by multi-robot rescue system with ad hoc networking,” in *IEEE International Workshop on Safety Security and Rescue Robotics (SSRR)*, Bremen, Germany, Jul. 2010, pp. 1–6.
- [175] H. Tanner, A. Jadbabaie, and G. Pappas, “Stable flocking of mobile agents, part I: fixed topology,” in *Proceedings of the 42nd IEEE Conference on Decision and Control*, vol. 2, Maui, USA, Dec. 2003, pp. 2010–2015.
- [176] —, “Stable flocking of mobile agents part II: dynamic topology,” in *Proceedings of the 42nd IEEE Conference on Decision and Control, 2003*, vol. 2, Maui, USA, Dec. 2003, pp. 2016–2021.
- [177] N. Ted, “Adjustable seat length hospital bed,” Patent US 3 220 021, Nov. 30, 1965.
- [178] H. Teimoori and A. V. Savkin, “A biologically inspired method for robot navigation in a cluttered environment,” *Robotica*, vol. 5, pp. 637–648, 2010.

- [179] ———, “Equiangular navigation and guidance of a wheeled mobile robot based on range-only measurements,” *Robotics and Autonomous Systems*, vol. 58, pp. 203–215, 2010.
- [180] H. T. Trieu, H. T. Nguyen, and K. Willey, “Advanced obstacle avoidance for a laser based wheelchair using optimised bayesian neural networks,” in *Proceedings of 30th IEEE/EMBS Annual International Conference*, British Columbia, Canada, Aug. 2008, pp. 3463–3466.
- [181] ———, “Shared control strategies for obstacle avoidance tasks in an intelligent wheelchair,” in *Proceedings of 30th IEEE/EMBS Annual International Conference*, British Columbia, Canada, Aug. 2008, pp. 4254–4257.
- [182] V. A. Ugrinovskii, I. R. Petersen, A. V. Savkin, and E. Y. Ugrinovskaya, “Decentralized state-feedback stabilization and robust control of uncertain large-scale systems with integrally constrained interconnections,” *Systems & Control Letters*, vol. 40, no. 2, pp. 107–119, 2000.
- [183] V. I. Utkin, *Sliding Modes in Control Optimization*. Berlin: Springer-Verlag, 1992.
- [184] J. Van den Berg, M. Lin, and D. Manocha, “Reciprocal velocity obstacles for real-time multi-agent navigation,” in *IEEE International Conference on Robotics and Automation*, Pasadena, USA, May. 2008, pp. 1928–1935.
- [185] T. Vicsek, A. Czirok, E. B. Jacob, I. Cohen, and O. Schochet, “Novel type of phase transitions in a system of self-driven particles,” *Physical Review Letters*, vol. 75, pp. 1226–1229, 1995.
- [186] N. Vlassis, N. Sgouros, G. Efthivolidis, and G. Papakonstantinou, “Global path planning for autonomous navigation,” in *Proceedings of the 8th IEEE International Conference on Tools with AI*, Toulouse, France, Nov. 1996, pp. 354–359.



- [187] P. K. C. Wang, "Navigation strategies for multiple autonomous mobile robots moving in formation," *Journal of Robotic Systems*, vol. 8, no. 2, pp. 177–195, 1991.
- [188] P. K. C. Wang and F. Y. Hadaegh, "The journal of the astronautical sciences," *The Journal of the Astronautical Sciences*, vol. 44, no. 3, pp. 315–355, 1996.
- [189] Q. Wang and Y.-P. Tian, "Minimally rigid formations control for multiple non-holonomic mobile agents," in *31st Chinese Control Conference*, Hefei, China, Jul. 2012, pp. 6171–6176.
- [190] L. Wei, H. Hu, and K. Yuan, "Use of forehead bio-signals for controlling an intelligent wheelchair," in *Proceedings of IEEE International Conference on Robotics and Biomimetics*, Bangkok, Thailand, Feb. 2009, pp. 108–113.
- [191] D. Wilkie, J. van den Berg, and D. Manocha, "Generalized velocity obstacles," in *IEEE/RSJ International Conference on Intelligent Robots and Systems*, St. Louis, USA, Oct. 2009, pp. 5573–5578.
- [192] T. N. Williams and G. R. Parrish, "Bedside control unit for a hospital bed," Patent US 5 542 138, Aug. 6, 1996.
- [193] J. Yan and R. R. Bitmead, "Coordinated control and information architecture," in *Proceedings of 42nd IEEE Conference on Decision and Control*, vol. 4. Maui, USA: IEEE, Dec. 2003, pp. 3919–3923.
- [194] H. Yu and Y. Wang, "Coordinated collective motion of groups of autonomous mobile robots with directed interconnected topology," *Journal of Intelligent and Robotic Systems*, vol. 53, pp. 87–98, 2008.
- [195] A. Zelinsky, "A mobile robot exploration algorithm," *IEEE Transactions on Robotics and Automation*, vol. 8, no. 6, pp. 707–717, 1992.

- [196] Y. Zhang, J. Zhang, and Y. Luo, “A novel intelligent wheelchair control system based on hand gesture recognition,” in *Proceedings of IEEE/ICME International Conference on Complex Medical Engineering (CME)*, Harbin, China, May. 2011, pp. 334–339.
- [197] L.-H. Zhao, Z.-Y. Liu, and H. Chen, “Design of a nonlinear observer for vehicle velocity estimation and experiments,” *IEEE Transactions on Control Systems Technology*, vol. 19, no. 3, pp. 664–672, 2011.